

School of Electrical and Computer Engineering  
Chalmers University of Technology  
Göteborg, Sweden

Technical Report No. 288

**PERMANENT MAGNET MACHINES WITH AIR GAP WINDINGS  
AND INTEGRATED TEETH WINDINGS**

by

**Mikael Alatalo**

Submitted to the School of Electrical and Computer Engineering  
Chalmers University of Technology  
in partial fulfilment of the requirements  
for the degree of  
Doctor of Philosophy



Department of Electric Power Engineering  
May 1996

PERMANENT MAGNET MACHINES WITH AIR GAP WINDINGS  
AND INTEGRATED TEETH WINDINGS

by

**Mikael Alatalo**

Technical Report No. 288



Akademisk avhandling  
som för avläggande av teknisk doktorsavhandling  
vid Chalmers Tekniska Högskola  
försvaras vid offentlig disputation  
i Henry Wallmans rum  
Hörsalsvägen 11, 4tr, Göteborg

Fredagen den 7 Juni 1996 kl. 10.15

Fakultetsopponent: Professor Chandur Sadarangani  
Kungliga Tekniska Högskolan Stockholm

ISBN 91-7197-312-5

*Chalmers Bibliotek*

Reproservice

Göteborg 1996

## **Abstract**

The thesis deals with axial and radial flux permanent magnet machines with air gap windings and an integrated teeth winding. The aim is to develop a machine that produces a high torque per unit volume with as low losses as possible. The hypothesis is that an advanced three-phase winding, magnetized by a permanent magnet rotor should be better than other machine topologies. The finite element method is used to find favourable dimensions of the slotless winding, the integrated teeth winding and the permanent magnet rotor. Three machines were built and tested in order to verify calculations. It can be concluded that the analysis method shows good agreement with the calculated and the measured values of induced voltage and torque. The experiments showed that the slotless machine with NdFeB-magnets performs approximately the same as the slotted machine. A theoretical comparison of axial flux topology to radial flux topology showed that the torque production of the inner rotor radial flux machine is superior to that of the axial flux machine. An integrated teeth winding based on iron powder teeth glued to the winding was studied. The force density of a pole with integrated teeth is around three times the force density of a slotless pole. A direct driven wind power generator of 6.4 kW with integrated teeth can have the same power losses and magnet weight as a transversal flux machine. Compared to a standard induction machine the integrated teeth machine has approximately 2.5 times the power capacity of the induction machine with the same power losses and outer volume.

## **Keywords**

synchronous machines, permanent magnets, iron powder, NdFeB, special windings.

## Acknowledgements

The work presented in this thesis was partly carried out at the Department of Electrical Machines and Power Electronics, Chalmers University of Technology, as a part of the wind energy project. NUTEK financed the work on the bigger axial flux machine, which resulted in a Licentiate degree. NUTEK also financed the work on the high-speed axial flux machine, and the experiment on the iron powder stator presented in Chapter 6. The thesis focuses on the machine with integrated teeth, i.e. Chapters 6 and 7. The material concerning these machines was compiled after that I have finished working at the Department.

I have had the opportunity to participate in the efforts of IRO AB in developing an alternative motor to their induction machines.

I would like to thank Tore Svensson who was my supervisor until 1994. This work would not have been possible without him. Karl Erik Hallenius was my examiner until the summer of 1994, when he retired. I wish to express my gratitude to Professor Jorma Luomi. His valuable advice has been a prerequisite for finishing the work.

I would also like to thank all the helpful and interested people at Chalmers Teknikpark, Höganäs AB, Anker-Zemer AB and VACTEK.

I am obliged to Deborah Fronko for revision of the language.

Thanks to all personnel at the Department who participated in the work.

## Contents

List of symbols	7
1. Introduction	9
1.1 Aim of the Thesis	10
2. Overview of Permanent Magnet Machines	13
2.1 Different Topologies of Permanent Magnet Machines	13
2.1.1 Radial Flux Machines	13
2.1.2 Axial Flux Machines	15
2.1.3 Transversal Flux Machine	16
2.2 Applications	17
2.2.1 Generator and Motor for Hybrid Cars	17
2.2.2 Medium-speed Servo Motor	19
2.2.3 Direct-driven Wind Power Generator	21
2.3 Magnetic Materials	22
2.3.1 Permanent Magnets	22
2.3.2 Iron Core Material	24
2.4 Equivalent Model of the Permanent Magnet Machine	27
2.5 Power Electronic Control	29
3. Investigation of a Slotless Pole	33
3.1. Flat Pole	34
3.1.1 Variation of Magnet Width	37
3.1.2 Varied Winding Thickness	40
3.1.3 Induced Voltage	43
3.1.4 The Influence of Permeability in the Stator Yoke	45
3.2. Radial Flux Rotors	46
3.3. Discussion	52
4. Experimental machines	55
4.1 Medium-speed Radial Flux Machine	55
4.2 12-pole Axial Flux Machine	60
4.2.1 Design Calculations	63
4.2.2 Measurements of Machine Parameters	66
4.2.3 Test with Resistive Load	69
4.2.4 Test with Diode Rectifier	70
4.3 6-pole machine for High Speed	73
4.3.1 Magnetisation	75
4.3.2 Calculations	76
4.3.3 Measurements	77
4.4 Discussion	77
5. Comparison of Radial and Axial Flux Machines.	79
5.1 High Torque Machine	83
5.2 High-speed Machine	85

6. Investigation of a Pole with Integrated Teeth	87
6.1. Stator with Integrated Teeth	88
6.1.1 Flux Density at Varied Permeability	89
6.1.2 Varied Air Gap Length	91
6.2 Further Investigations of a Pole with $q=2$	94
6.3 Minimized Power Losses	101
6.4 Measurements on Iron Powder Parts	105
6.4.1 Measurement of Power Losses	105
6.4.2 Measurements on Iron Powder as Teeth Material	107
6.5 Discussion	109
7. Calculated machines with integrated teeth	111
7.1 Direct-driven wind power generator	111
7.2 High-speed machine with slotted stator	117
7.3 PM machine compared to a standard induction machine	123
8. Conclusion	129
References	131
Appendices	135
A. Torque and Force in a PM-machine	135
B. Winding Factors	137
C. Representation of Magnets in the FEM-program	139
D. Measuring Instruments	141

## List of Symbols

$a$	area ( $m^2$ )
$A$	magnetic vector potential $B = \text{rot}(A)$
$B(x, y, z)$	flux density (T)
$B_n$	RMS-value of the $n^{\text{th}}$ order space harmonic (T)
$B_r$	remanent flux density (T)
$b_s$	slot width (m)
$c$	cost (SEK)
$d$	diameter (m)
$e_f$	induced voltage (emf) instantaneous value (V)
$E$	induced voltage RMS-value (V)
$f$	frequency (Hz)
$F$	force (N)
$F_A$	force density ( $N/m^2$ )
$H(x, y, z)$	magnetic field intensity (A/m)
$h$	thickness in axial and radial direction (m)
$h_\delta$	thickness of air gap (m)
$h_l$	winding thickness (m)
$h_{fe}$	iron yoke thickness (m)
$h_m$	thickness of magnet material (m)
$i$	current (A)
$J(x, y, z)$	current density ( $A/m^2$ )
$k_{cu}$	fill factor of copper in the winding region
$k_{po}$	fill factor of iron powder in the winding region
$k_w$	winding factor
$l$	length in axial direction (m)
$l_{st}$	stator length, i.e. active length (m)
$L$	inductance (H)
$L_\lambda$	inductance associated with leakage flux (H)
$L_h$	inductance associated with main flux (H)
$n$	rotational speed (rpm)
$N_p$	number of turns per pole-pair and phase
$p$	No. of pole-pair
$q$	number of slots per phase and pole
$P$	power (W)
$P_{fe}$	power losses in iron parts (W)
$P_{fe50}$	power loss factor at 50 Hz, 1 T ( $W/m^3$ )
$P_{cu}$	power losses in copper conductors, ohmic losses (W)
$P_{Ft}$	power losses due to eddy currents (W)
$P_{yoke}$	power losses in the yoke material (W)
$P_{teeth}$	power losses in teeth material (W)
$P''$	heat flow density ( $W/m^2$ )
$Q$	reactive power (VA <sub>r</sub> )
$r$	radius (m)
$r_r$	rotor radius (m)
$r_m$	radius of magnetic material (m)
$r_l$	inner radius of winding radial flux machine (m)

$r_2$	outer radius of winding radial flux machine (m)
$r_i$	inner radius of winding axial flux machine (m)
$r_y$	outer radius of winding axial flux machine (m)
$R$	resistance ( $\Omega$ )
$s$	current loading (A/m)
$t$	time (s)
$T$	torque (Nm)
$u$	voltage (V)
$V$	volume ( $m^3$ )
$W$	energy (Ws)
$X$	reactance ( $\Omega$ )
$\Delta x_{cu}$	width of rectangular conductor in x-direction (m)
$\Delta y_{cu}$	width of rectangular conductor in y-direction (m)
$\alpha$	heat transfer coefficient ( $W/m^2K$ )
$\beta$	electric angle between flux density and current density waves (rad, $^\circ$ )
$\gamma$	mass density ( $kg/m^3$ )
$\mu_r$	relative permeability
$\mu_0$	permeability of vacuum (Vs/Am)
$\mu_m$	permeability of magnet material (Vs/Am)
$\Delta\mu$	differential permeability (Vs/Am)
$\Phi$	flux (Wb)
$\omega$	electric rotational speed (rad/s)
$\rho$	resistivity ( $\Omega m$ )
$\theta$	electrical angle (rad, $^\circ$ )
$\vartheta$	temperature (K)
$\eta$	efficiency
$\psi$	flux linkage (Wb)
$\tau_m$	magnet width (m)
$\tau_p$	pole pitch (m)
$\tau_s$	slot pitch (m)

#### Indexes

a,b,c	three phases
al	aluminium
cu	copper
d	direct axis
el	electric
f	phase-to-zero
fe	iron (transformer sheet)
h	phase-to-phase
k	order of time harmonic
mech	mechanical
m	permanent magnet material
n	order of space harmonic
Nd	NdFeB material
p	peak value or amplitude
po	powder material
q	quadrature axis

## 1. Introduction

Variable-speed drives have developed quickly in recent decades. Microprocessors, power electronics, control theory, new magnetic materials and design tools make it possible to build compact drive systems with high efficiency. It is possible to integrate the motor and the controller to an integrated device with the same cooling arrangement. The induction machine is commonly used but the permanent magnet machine has higher efficiency and power factor, which reduces the power rating of the power electronic control also the cooling arrangement of a permanent magnet machine solution will be smaller. If a control method that does not require extra sensors can be utilized the cost of the permanent magnet machine system may decrease.

Using ordinary machine construction, the permanent magnet machine can be improved with new materials. The power losses in the teeth and the yoke may be decreased by using better material. In order to further increase the performance of the machines, new ways of constructing the machine have to be utilized. For instance, the power losses in the teeth can be completely avoided by using an air gap winding fixed to the stator yoke without any slots. The air gap winding is possible by using new magnets of reasonable sizes, based on rare earth materials. Cogging torque and noise due to the slots are avoided. Furthermore, the power losses due to varying flux density on the rotor surface are avoided, which is important in high frequency machines.

Radial flux topology is dominant in traditional electric machines. An example of recent work on radial flux topology is the 18 kW/100 000 rpm generator studied by Chudi and Malmquist [1]. Another interesting experiment is reported on by Debruzzi, Huang and Riso [2]. The electric machine is an electric car motor composed of an iron powder stator and an NdFeB excitation. The machine has a high torque to weight ratio.

Other topologies of permanent magnet machines have been studied in different applications. Axial flux and transversal flux machines have been studied as alternatives to the radial flux machine. The axial flux machine has the advantage of an ironless rotor which can be used between two stator parts. The low weight of this rotor has been utilized in servo-motor applications. Some simplifications in the construction in contrast to the radial flux machine can also be made. The axial flux machine is suggested for high-speed operation [3-6], and with toroidal winding for low speed [7]. The transversal flux machine has in recent decades been developed by Weh et al. [8-12]. The flux is closed in the transverse direction, and current loading can be increased, compared with the radial and axial flux machines, i.e. the force per unit area of the pole is increased.

In applications which demand a machine with low weight, machines with high torque to weight ratio are discussed. An example is a wind power mill drive train, which normally consists of a gear box and a normal speed generator. This drive train can be replaced by a low-speed generator.

In this application Weh [11, 12] has suggested the transversal flux machine, because of its high force density. Spooner, Caricchi et al. [13-14] have studied a particular axial flux machine as an alternative in wind power applications. The latter machine type has a toroidal winding without slots and is magnetized by NdFeB-magnets.

Another application, where the weight and efficiency of the machine is important, is the motor to an electric car. In traction applications the machine works over a wide range of rotational speeds and normally the produced power must be constant over a major part of the speed range. This constant speed range is not a problem when the flux and the machine voltage can be controlled. If permanent magnet machines are to be used in traction applications, the air gap flux must be controlled, although the magnet mmf is constant. Andersson and Cambier [15] report on a motor for electric cars. A special technique to produce the stator which makes it possible to manufacture machines with small pole pitches, is used. The machine is intended for an electric car drive and the speed is in the medium range, 7000 rpm. Selecting a machine with many poles and an increased radius lowers the weight of the active material.

In high-speed applications, other restrictions limit the available power. The machine rotor will be exposed to high tensions due to centrifugal force. Centrifugal force depends on radius and speed and, therefore, the rotor radius must be limited. In high-speed machines the power losses are low in terms of the percentage of nominal power, but the power losses per unit volume are high and, consequently, there are problems with heat transfer.

### 1.1 Aim of the Thesis

The thesis deals with axial and radial flux machines with air gap windings as well as a new type of winding comprising integrated teeth. In the latter winding, the teeth are fixed to the winding instead of being a part of the stator yoke. In this way, the fill factor of active material is increased.

The aim is to find a machine that produces a high torque per unit volume with as low losses as possible. As a hypothesis an advanced three-phase winding in the stator, magnetized by a permanent magnet rotor, is presented as better than other machine topologies. Another aim is to study how the slotless winding, the integrated teeth winding and the permanent magnet rotor should be constructed. The resulting constructions are compared with each other, as well as with the transversal flux machine and ordinary slotted constructions.

Chapter 2 is a brief overview of permanent magnet machines. Different ways of constructing the machine and different applications are presented. The chapter also describes various permanent magnet materials and soft magnetic materials. A mathematical model of the machine is presented, and, finally, two frequency convertors, which can be used to control the machine, are described.

Chapter 3 deals with air gap windings. The magnet size and winding thickness are studied in

machines with a small pole pitch in relation to the radius. In addition three different four-pole radial flux machines are compared with each other and with a two-pole machine with a cylindrical rotor magnet. Chapter 4 describes three experimental radial and axial flux machines with air gap windings as well as test results. In the first section, a medium speed radial flux machine is compared with a commercial permanent magnet machine. The second section describes a 4.7 kW axial flux machine and the third describes a machine element that is to be used in a high speed axial flux machine.

Chapter 5 compares radial and axial flux topologies. The torque production of the two types of machines is investigated both for low speed machines and for high speed machines.

The force producing parts of the integrated teeth machine are studied in Chapter 6. Iron powder material is investigated as a material that lowers the reluctance of the winding and makes it possible to decrease the slot pitch and increase the thickness of the active region. A special winding technique which is necessary in producing the integrated teeth winding is discussed. The influence of the dimensions of the pole and material data is investigated.

Chapter 7 deals with examples of machines with integrated teeth. The integrated teeth machine is studied theoretically in a low speed machine application, a high speed machine application and in comparison with a standard induction machine.

## 2. Overview of Permanent Magnet Machines

This chapter is an overview of machine topologies, applications and materials of permanent magnet synchronous machines. The machines that are studied are only intended for use in connection with power electronics, and consequently some types of converters are also discussed.

### 2.1. Different Topologies of Permanent Magnet Machines

Various ways to construct permanent magnet machines are described below. There are many possibilities but the thesis mainly deals with three-phase machines having stators without salient poles. The transversal flux machine, which is equipped with salient poles, is, however, used as a reference object.

#### 2.1.1 Radial Flux Machines

The most common machine type is the radial flux machine. In the radial flux machine the conductors are directed in the axial direction and the air gap magnetic flux is directed in the radial direction. Two types of rotors are shown in Figure 2.1. A rotor with surface-mounted magnets and a rotor with a cylindrical magnet surrounded by a high-strength shell excite an air gap wound stator. The different winding parts are indicated as six areas. In a three-phase machine, two of the areas are associated with each phase.

A simple way to construct a machine is with surface-mounted magnets. The draw-back is that an arrangement is required to fix the magnet to the rotor core. A thin layer of epoxy-impregnated fibre glass, kevlar or fiber carbon can be applied to the outside of the magnet. This method is applicable at moderate speed, but at high speed the layer must be thick and the amount of active material in the magnetic air gap will be low.

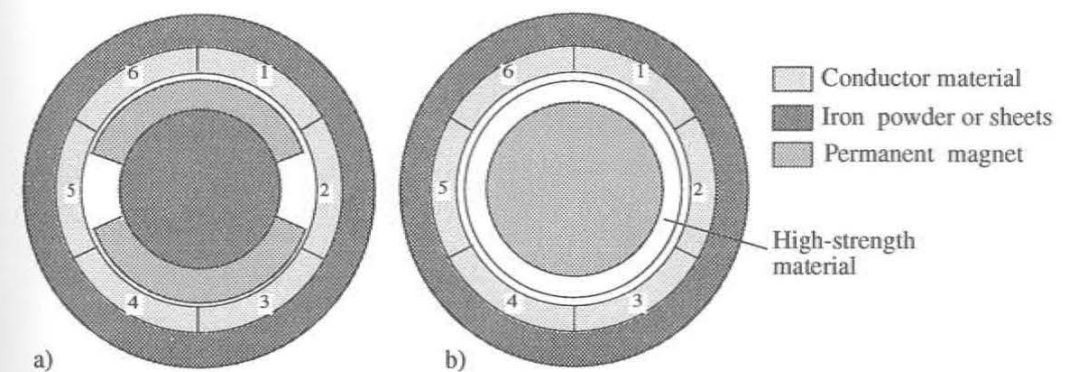


Figure 2.1 Cross section of the active parts of a two-pole radial flux air gap wound machine.  
a) Surface-mounted magnets. b) Cylindrical magnet with high-strength shell.

The machine in Figure 2.1b) has the same principle as the machine in [1] and is preferably used at high speed or very high speed. The high strength shell provides the necessary strength to the permanent magnet material and also serves as a shaft. This machine type has been studied for speeds up to 500 000 rpm [16] and, in this case, the rotor is able to produce 17 kW.

In many cases, slotted stator constructions are used. In order to avoid heating the magnets due to slot space harmonics and in order to fix the magnets to the rotor, the magnets are buried beneath the surface of a rotor core made of laminated sheets. With this construction, the rotor has a different reluctance in the direct and quadrature directions. The direct direction is defined as coinciding with the direction of the magnet flux and the coordinate system is fixed to the rotor. Some examples of machines having different inductance in the q- and d-directions are highlighted in Figure 2.2.

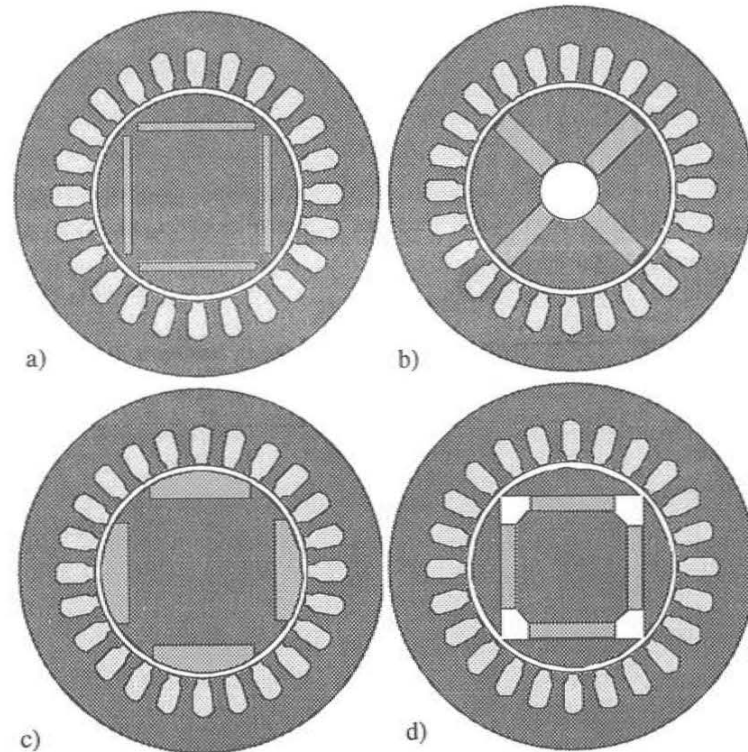


Figure 2.2. Different rotor constructions of a 4-pole permanent magnet machine.

- a) Interior magnets.
- b) Flux concentrating magnets.
- c) Inset magnets.
- d) Pole shoes.

In many variable speed drives it is of interest to use the converter at maximum voltage with a large speed register. In this case, the current to the machine has to be directed so that the flux from the magnets is lowered [17,18,19]. Machines suited for this control method have been studied by Schiferl [20] who has optimized both a surface-mounted magnet and an interior-magnet machine. The described machines usually have higher inductance in the q-direction, which is utilized in field weakening. A current in the negative d-direction (field weakening of the magnet) produces a positive torque together with the flux in the q-direction.

### 2.1.2 Axial Flux Machines

The axial flux machine has been used in applications where the axial length is limited and in applications where the low inertia of an ironless rotor between two stators is needed. The principle of the axial flux machine is displayed in Figure 2.3.

The axial flux machine has some constructional advantages, which can make the topology an economical alternative. The stator core is easily made of a wound generator sheet with the desired inner and outer active diameters. In the case of a slotless construction, punching the stator core is not necessary. Further, the magnet pieces in a permanent magnet machine have a rectangular cross-section, which is, according to the manufacturer, the cheapest way to construct permanent magnets. In a high-speed operation, the material supporting the magnet is placed around the rotor and does not occupy the space of the winding. The drawback of this machine is that if slots are to be used the slot pitch varies with the radius, hence the slots must be punched in a special way. To avoid this problem, stators made of iron powder material have been proposed [21, 6, 22].

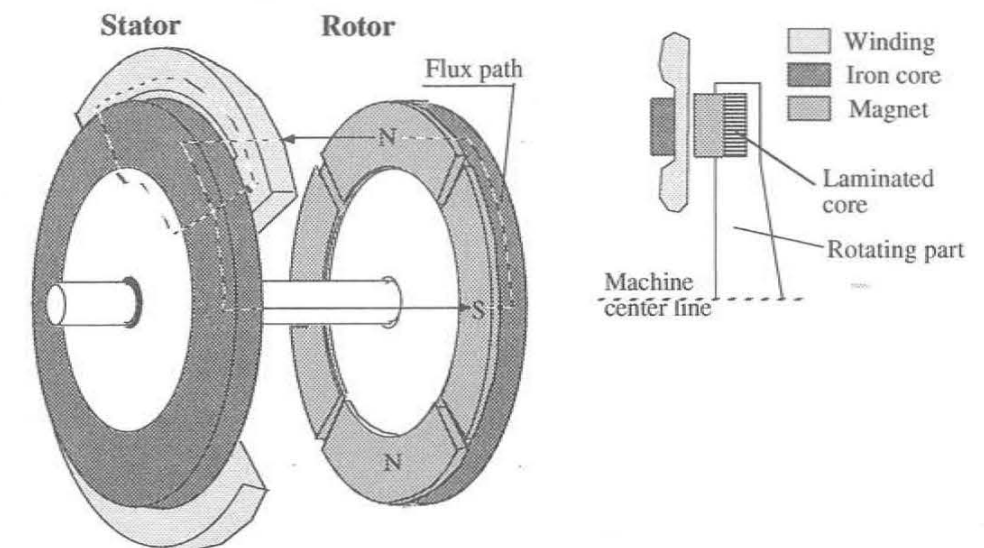


Figure 2.3. 4-pole axial flux permanent magnet machine.

At high-speed, the rotor radius must be restricted due to high centrifugal stresses on the rotor. In this case, it may be necessary to use stators and rotors that are stacked according to Figure 2.4. The winding between the rotor parts must be constructed in a special way due to the fact that the space for end windings is limited, especially at the inner radius of the machine.

A machine type that has been studied recent years is the axial flux machine with a toroidal air-gap winding [12,13,14,8]. The end turns of this winding are very short due to the special winding technique. The short end turn implies low material weight and low ohmic losses of the winding, which is used to increase the power rating. Toroidal winding is displayed in Figure 2.5. Toroidal winding and easily produced iron core have been utilized in a machine with amorphous iron as the core material [23]. Punching slots in amorphous material is difficult due to the brittle material, and in this case, the slotless axial flux machine is an alternative.

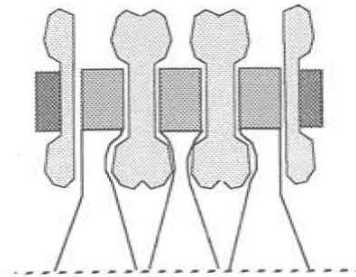


Figure 2.4. Axial flux machine with several stators and rotors.

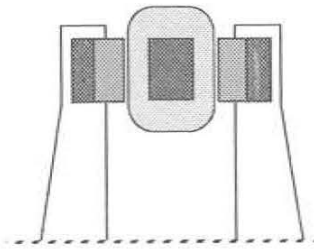


Figure 2.5. Axial flux machine with toroidal winding.

### 2.1.3 Transversal Flux Machine

The transversal flux machine has, in the 1980s, been further developed by Weh et al. [9-11]. In the transversal flux machine the flux is closed perpendicular to the direction of movement. Defining this as the transverse direction contrary to the longitudinal direction in normal machines explains the name of the machine. It has been shown that the force density in this machine is higher than in a longitudinal machine. The transversal flux machine is an alternative in high-performance machines where the main demand is high torque per weight.

The main parts of the machine are shown in Figure 2.6. Several iron cores are mounted around a circular coil forming the stator. The distance between the iron cores corresponds to the pole pitch. The rotor is made of magnets mounted with alternating polarity. The flux flows round the conductor in opposite directions depending on which magnet is under the iron part. The main advantage of the machine is the long air gap between the two iron core ends and the easily produced conductor parts. The long air gap between the iron core ends leads to low leakage

inductance and high current loading, thus may be used.

An alternative machine design, where the number of stator parts is increased, hence, increasing the force density, has been invented by Zwegbergk [24]. No experimental data have been published.

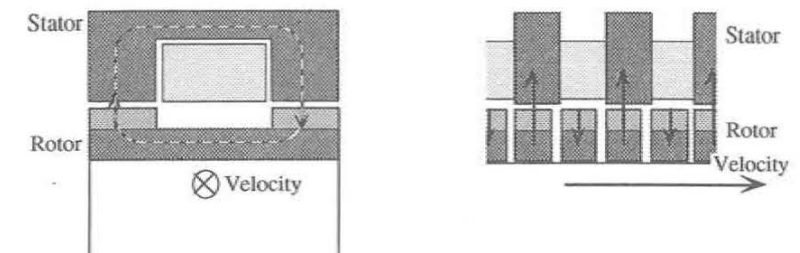


Figure 2.6. Transversal flux machine.

## 2.2 Applications

In this section, four applications are described in which the electrical and mechanical environments are quite different. The common features are the high-performance magnets, a new winding technique or an uncommon machine topology, which should improve the performance of the machine compared to other types of machines.

### 2.2.1 Generator and Motor for Hybrid Cars

To overcome the problem of the limited energy content of batteries, so called hybrid electric cars are being developed. A combustion machine propels a generator which charges the energy store from which traction energy is drawn; see Figure 2.7 in which a series hybrid system is out-lined. As the primary energy source the high speed gas turbine is an interesting alternative. The gas turbine works at very high speed, which reduces the size and weight of the machinery. The content of hazardous substances in the exhaust is lower in comparison with the Otto- and Diesel-motors, due to continuous combustion.

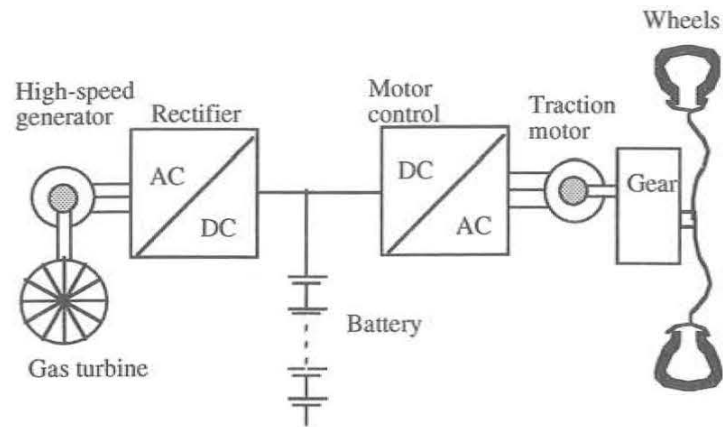


Figure 2.7. Hybrid system with gas turbine as primary energy source.

An example of this system is the Environmental Concept Car (ECC) designed by Volvo. In this car, the gas turbine propels a high-speed permanent magnet generator [1]. The generator power is distributed to the batteries and to the traction motor by means of power electronics. The generator is of the radial flux type with an air gap winding similar to the machine in Figure 2.1b). The power rating of the gas turbine is higher than that of the experimental machine reported on in [1]. The power rating is around 30 kW and the rotational speed is 90 000 rpm. The machine principle is displayed in Figure 2.8. Figure 2.8a) shows the distribution of the winding and the other materials. The winding is made of Litz-wire and wound in a toroidal way without any slots, as illustrated in Figure 2.8b). Electrically, this machine has worked well but the power losses due to leakage of flux and eddy currents from the end windings are high.

A group in Great Britain is working on a similar concept but the machine is of the axial flux type [3,5]. The generator consists of several rotor and stator discs on the same shaft. The rotor of this machine consists of several magnet pieces held together by a supporting ring made of reinforced carbon fibre.

To power the wheels of an electric car, a permanent magnet machine can be used instead of an induction motor. The operating range of an electric car strongly depends on vehicle weight. Therefore, there is a need to minimize the weight of the machinery. At the same time, the efficiency of the electric system must be high. Unique Mobility [15] reaches a high torque to weight ratio by using a medium-speed machine with a high number of poles. The motor produces 68 Nm and the weight is approximately 16 kg. The stator windings are manufactured in a special way that permits small pole pitches. The power rating is 50 kW at 8000 rpm with an efficiency of 96.5 %. Using a rather high stator radius and small pole pitch turns the active materials into a thin rim. The machine is outlined in Figure 2.9.

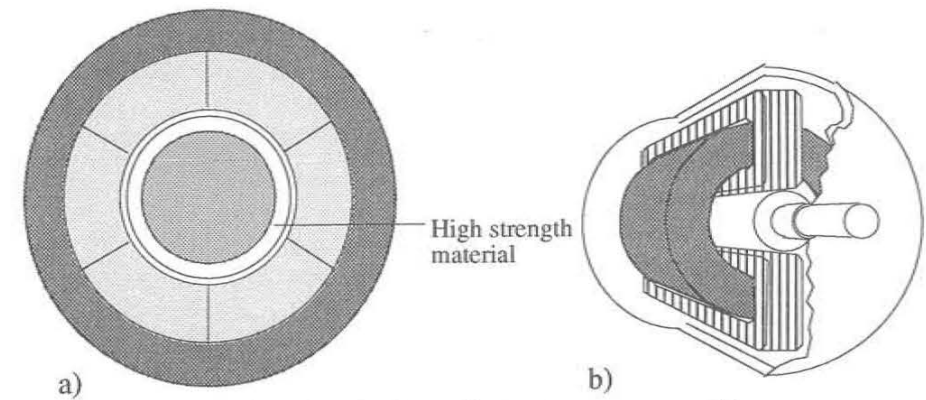


Figure 2.8. High-speed permanent magnet machine.

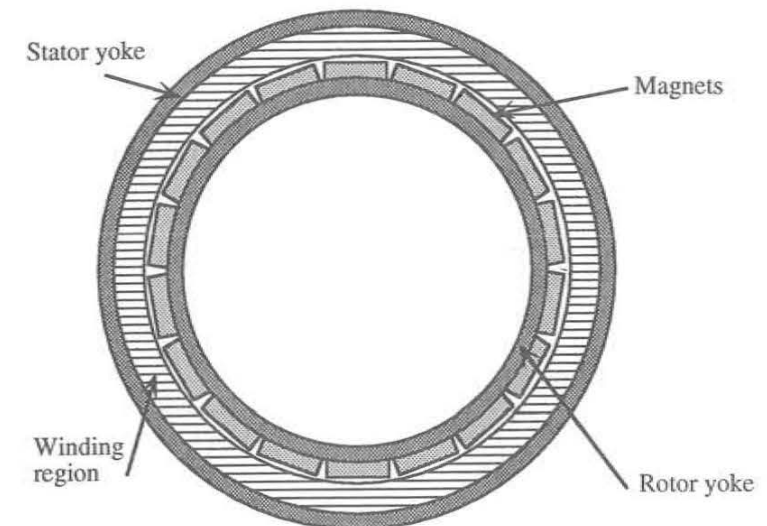


Figure 2.9. High-torque permanent magnet motor.

### 2.2.2 Medium-speed Servo Motor

In industrial variable speed drives, a converter often feeds an induction machine. The permanent magnet machine can, however, save weight and volume, and give a higher performance. Using modern control theory and the fact that the power rating of the converter for a permanent magnet machine is lower will probably increase the number of variable speed drives based on the permanent magnet machine. There are two main control methods: one uses sinusoidal emf and a vector control and the other the so called DC-brushless method where the emf is trapezoidal and a constant current is fed to two phases of the winding simultaneously while the third is resting.

The IRO company uses induction machines to power their yarn feeders. The machines are equipped with a hollow shaft, through which the yarn is drawn and wound on a drum. The yarn is then fed from the drum into a weaving machine. In this way, it is possible to avoid torn yarn caused by high acceleration. The drum is mounted on the shaft to the right in Figure 2.10, which shows a side view of the yarn feeder. The whole converter is mounted in an integrated design on top of the displayed construction. The machine and the electronics have a common cooling system, which implies that the losses and the temperature must be kept low, in order to avoid damaging the electronic circuits.

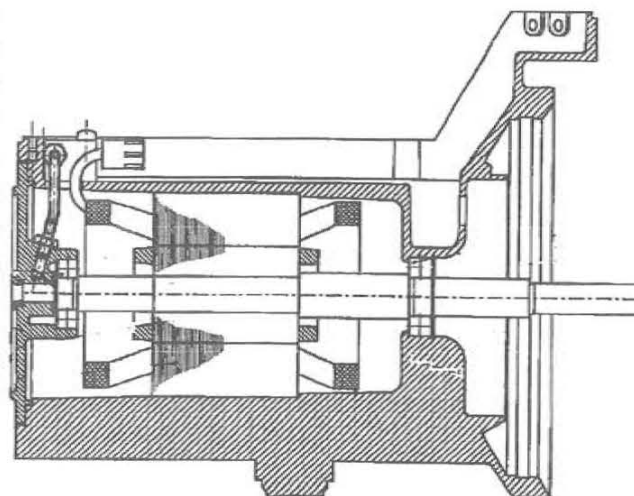


Figure 2.10. Cross section of yarn feeder with induction machine.

The intention of the manufacturer was to increase the capacity of the yarn feeder and, therefore, permanent magnet machines were tested. The data of the induction motor are displayed in Table 2.1 together with the data of a permanent magnet machine available on the market. The permanent magnet machine is made by GEC Alsthom and have the nominal torque of 1.0 Nm.

The torque of the permanent magnet machine is 2.5 times the torque of the induction machine and the volume is reduced to 66 % of the induction machine. This example shows that especially small machines with permanent magnet excitation have a higher torque to volume ratio than induction machines.

Table 2.1. Servo motor data

	Induction machine	Slotted permanent magnet machine Type LX310BF R3100
Rated torque	0.4 Nm	1.0 Nm
Stator core diameter	60 mm	60 mm
Stator core length	60 mm	40 mm
Volume	170 cm <sup>3</sup>	113 cm <sup>3</sup>

### 2.2.3 Direct-driven Wind Power Generator

Today most wind power mills are equipped with a drive train consisting of a step down gear and a normal speed induction or synchronous generator directly connected to the grid. A direct-driven generator is an alternative that minimizes the number of moving components and it may be economical in comparison with a system with a gear and normal-speed generator. Weh [11] has shown that the weight of the gear box and the normal speed generator can be decreased by one third by using a direct-driven transversal flux machine. Using permanent magnet excitation and a transversal flux topology it is possible to build machines with high force density, and the efficiency of a 6 kW machine may exceed 91 %. Ordinary radial and axial flux machines with permanent magnetization have also been studied [13,25]. The common problem is to build machines with small pole pitches. Punching stators sets the minimum distance between slots and, if the pole pitch is small, the number of slots per pole and phase will be low [25].

For smaller wind power plants, the axial flux machine with toroidal winding has been suggested [13], see Figure 2.5. Air gap winding implies high amounts of permanent magnet material which can be accepted in smaller plants where the material cost is low compared with production cost.

A permanent magnet machine that is connected directly to the grid must be equipped with damping windings and, consequently will be heavy. This weight can be avoided if a converter controls the speed of the generator. Controlled torque can also be useful in other ways. Normally, the speed of the turbine is fixed or within the slip variations of an induction generator. At high wind speed the wind power exceeds the rated power of the generator. Different methods to regulate the power are used but often torque pulsations occur and the peaks exceed the rated torque. The mechanical gear box and turbine wing roots must be designed for these peaks. The torque may be controlled by means of a frequency converter that controls the speed of the turbine. The electric system is outlined in Figure 2.11. A wind gust produces an increase of rotational speed instead of increased torque. By means of the variable speed it is possible to rotate the turbine at the speed that gives the optimal ratio between wind speed and the tip speed of the turbine. More energy can be produced than in a system with constant speed, but it is necessary to have a generator with high efficiency in order to compensate for increased power losses due to the converter.

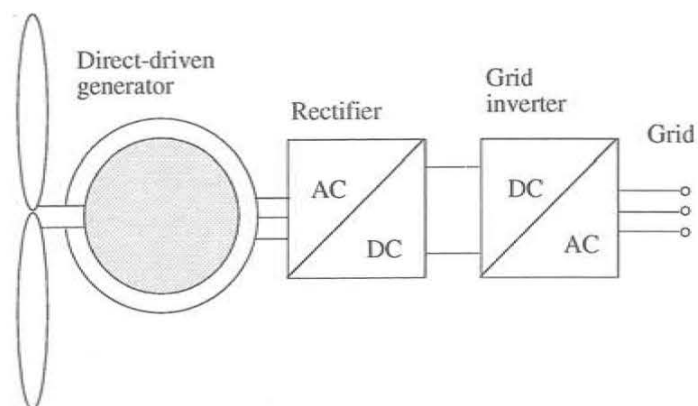


Figure 2.11. Direct-driven wind turbine generator system.

### 2.3. Magnetic Materials

The development of better machines strongly depends on new materials. New permanent magnet materials make the magnets smaller compared to AlNiCo- and Ferrite-magnets, due to higher energy content. The torque in an electric machine is produced by the force of the active region and the radius. The force is proportional to flux density and the available current. If ordinary machine design is to be used, higher flux density or current density must be used in order to increase the force density. The saturation flux density of new soft magnetic materials has not increased and until superconductors are developed, copper is the main conductor material. Until a major breakthrough (if possible) occurs the only possibility is to alter the machine design and to use the available material with as low losses as possible.

#### 2.3.1 Permanent Magnets

The development of permanent magnet materials has been remarkable in recent decades. New materials based on neodymium and samarium have increased the energy density in permanent magnets manifold. According to Parker [26] laboratory alloys of NdFeB have reached  $0.4 \text{ MJ/m}^3$ , see Figure 2.12, and development may present materials with  $0.8 \text{ MJ/m}^3$  in the coming decade. There are materials on the market with an energy density of  $385 \text{ kJ/m}^3$ , [27]. The remanent flux density, which is  $B_r=1.41 \text{ T}$  [27] today, may also increase and perhaps reach  $1.6 \text{ T}$ . Magnets based on neodymium and samarium-cobalt have almost linear demagnetizing characteristics, see Figure 2.13, where one of the best material made by VACUUMSCHMELZE is displayed.

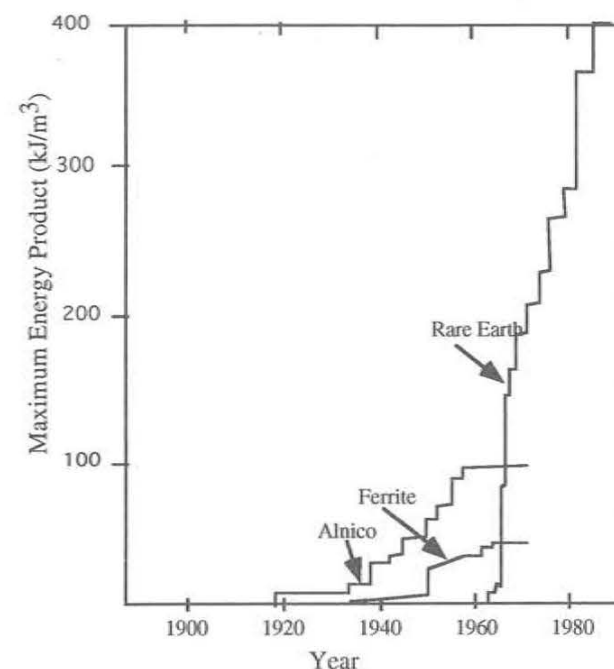


Figure 2.12. Development of permanent magnet material, according to Parker [26].

Figure 2.13 shows the flux density  $B$  at different temperatures and as a function of the magnetomotive force  $H$ . The magnetic materials from the NdFeB group have the disadvantage of a rather low Curie temperature:  $312 \text{ }^\circ\text{C}$ . At elevated temperatures, as indicated in Figure 2.13, the  $B$ - $H$  characteristics is lowered towards the origin of the coordinates and the material becomes irreversibly demagnetized if the flux density is too low. Other relevant data are listed in Table 2.2.

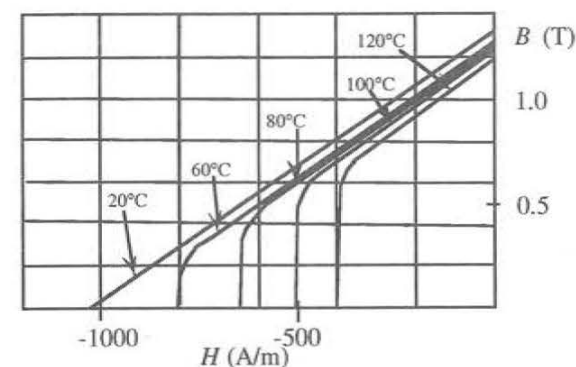


Figure 2.13.  $B$ - $H$  characteristics of VACODYM 362 HR.

Table 2.2. Common data of NdFeB material made by VACUUMSCHMELZE [27]

Tensile strength	270 MPa
Pressing strength	1050 MPa
Resistivity	$1.5 \cdot 10^{-6}$ ( $\Omega\text{m}$ )
Thermal conductivity	approx. 9 W/(Km)

### 2.3.2. Iron Core Material

Following the conductors and the permanent magnets, the core material is the third important material in permanent magnet machines. The main purpose of the core is to conduct magnetic flux through the winding and act as a return path. The magnetic flux is time-dependent, which means that the material cannot be homogeneous. The varying flux will induce a large eddy current in a homogeneous material. Core materials may be divided into two main groups: laminated sheets of soft magnetic material and powder materials. Generally, laminated sheets give a better performance than iron powder materials but the cost of a large punched stator core must be related to the cost of iron powder segments [2].

The iron powder material consists of small iron powder particles packed and electrically separated. The material has lower relative permeability than other types of core material, which is an important restriction when used as teeth material [6]. When the iron powder material is used as the iron core of an air gap wound construction, the reluctance of the winding is so high that the low permeability has little influence. The main advantage of iron powder material is that it can be formed arbitrarily, eddy current losses are low at high frequency and the material is isotropic. The flux may enter the material in any direction without causing any large eddy current loops. This quality can be used in machines with a toroidal winding by having the magnetisation entering the yoke from several directions. Since the iron powder material is almost homogeneous, the noise produced by this material is low. The material may be used up to several kHz.

In addition to different iron powder materials, carbonyl is also a material that is made of particles. The material is made of iron, nitrogen, carbon and oxygen, and the molecules are joined in a way that suppresses eddy currents. The hysteresis loop is very thin allowing low hysteresis losses. The material can be used in applications with a frequency up to several MHz.

Iron powder materials and especially carbonyl powder have lower thermal conductivity than other types of iron core material, which implies that special attention must be given to conducting heat from the winding to the ambient. The magnetic and electric characteristics of some typical materials are displayed in Table 2.3.

Compared to ordinary sheets, iron powder materials (EF6880 and Genalex SH) have rather high power losses at 50 Hz, but for higher frequency the power losses in iron powder material are comparable to generator sheets. Grade S and carbonyl iron powder have lower power losses but grade S cannot be used at high flux density and the carbonyl powder material has a relatively low permeability. Figure 2.14 shows power losses of Genalex 140 SH as a function of flux density amplitude,  $B_p$ . The power losses per unit volume,  $p_{Fe}$ , according to Figure 2.14 may be approximated as a second-order polynomial:

$$p_{Fe} = k_1 B_p + k_2 B_p^2$$

where

$$k_1 = 3.99 \cdot 10^6 \text{ W / m}^3\text{T}$$

$$k_2 = 60.52 \cdot 10^6 \text{ W / m}^3\text{T}^2 \quad (2.1)$$

The second-order term is dominant, and the power losses in this material can with good approximation be described as depending only on the flux density squared.

Table 2.3 Electric and magnetic characteristics.

Material	Supplier	Relative permeability	Saturation flux density (T)	Core losses (1T, 50 Hz) ( $\text{kW/m}^3$ )	Resistivity ( $\Omega\text{m}$ )	Thermal conductivity (W/Km)	Tensile strength (MPa)
EF6880 Iron powder	Vactek	175-300	1.95	55	$50 \cdot 10^6$	6-15	50-100
D25 carbonyl powder	Thomson	25	1.9	13		1.7	14
Genalex grade SH NiFe	SEI	140	1.3	64			
Genalex grade S (70-75 % Ni)	SEI	140	0.6	4.2 (0.4 T)			
CK30 (*) Generator sheet	Surahammar		1.9-2	7.6	$5 \cdot 10^{-3}$	70-80	400

(\*) CK30 is the name of a generator sheet manufactured by Surahammar, Sweden. The sheet thickness is 0.35 mm and the power losses at 1T and 50 Hz are 1 W/kg.

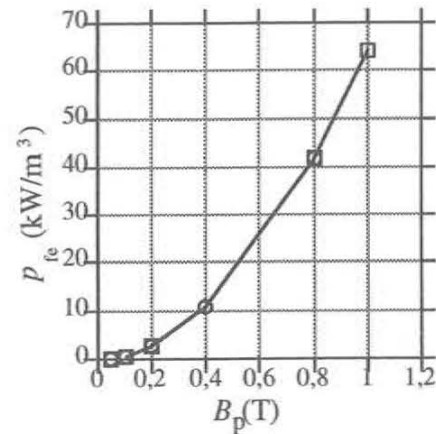


Figure 2.14. Power losses per unit volume of Genalex SH as a function of flux density.

The magnetizing curve and relative differential permeability of EF6880 are displayed in Figure 2.15a). The curve is a reprint of data sheets. The power losses of EF6880 and generator sheets as a function of frequency are displayed in Figure 2.15b). The power losses of EF6880 are almost linear with frequency up to approximately 4-5 kHz.

It can be concluded that iron powder materials have lower relative permeability than ordinary sheets and higher power losses in the frequency range of 0 to 1000 Hz. The power losses of the material can be considered as linear with frequency up to 4 kHz and the power losses are proportional to the flux density squared. The advantages of the iron powder material of today, are in the field of production and lower noise emission.

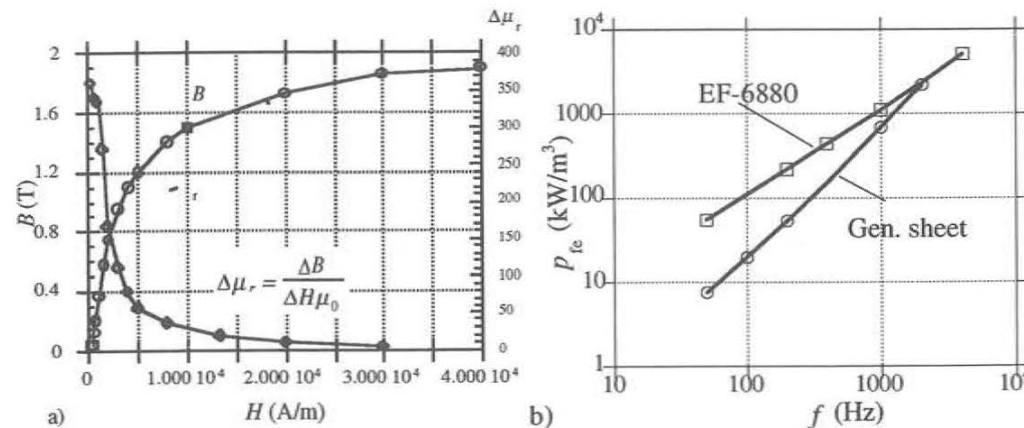


Figure 2.15a) Magnetizing curve of EF6880 and the relative differential permeability.  
b) Power losses of generator sheet CK30, 0.35 mm and EF6880.

## 2.4 Equivalent Model of the Permanent Magnet Machine

According to Kovacs [28] a permanent magnet machine with a smooth stator can be described by the two-phase rotor-fixed equations

$$\begin{aligned} u_{dq} &= u_d + j \cdot u_q \\ i_{dq} &= i_d + j \cdot i_q \\ u_d &= R i_d + \frac{d\psi_d}{dt} - \omega \psi_q \\ u_q &= R i_q + \frac{d\psi_q}{dt} + \omega \psi_d \\ \psi_d &= \psi_m + L_d i_d \\ \psi_q &= L_q i_q \end{aligned} \quad (2.2)$$

where  $u_d$  and  $u_q$  are the voltage components in the d- and q-direction respectively,  $i$  is the current,  $R$  is the resistance of the winding and  $\psi$  is the flux linkage.  $\psi_m$  is the flux linkage generated by the permanent magnet.

The inductances of the machine are

$$\begin{aligned} L_d &= L_{\lambda d} + \frac{3}{2} L_{hd} \\ L_q &= L_{\lambda q} + \frac{3}{2} L_{hq} \end{aligned} \quad (2.3)$$

where  $L_{\lambda}$  is the inductance associated with leakage flux and  $L_h$  is the main inductance of one winding phase.

The direct axis is directed in the same direction as the flux from the magnet, see Figure 2.16. The stator fixed system  $\alpha\beta$  is also displayed. The transformation between the stator fixed and rotor-fixed system is carried out by multiplication with  $e^{-j\theta}$  where  $\theta$  is the electric angle between the systems

$$\theta = \omega t + \theta_0 \quad (2.4)$$

$\omega$  is the electric angular velocity.

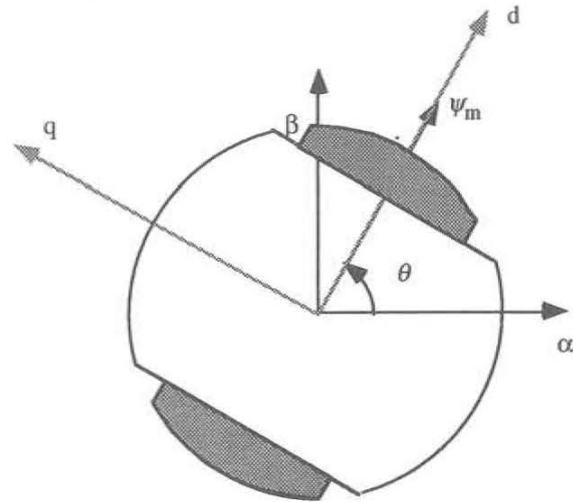


Figure 2.16. Rotor of a two pole permanent magnet machine and the coordinate systems.

In a special case where

$$\frac{di_d}{dt} = \frac{di_q}{dt} = 0$$

$$L_d = L_q = L \tag{2.5}$$

i.e. at steady state and a rotor without salient poles, the voltage equations may be written as

$$u_d = Ri_d - \omega Li_q$$

$$u_q = Ri_q + \omega Li_d + \omega \psi_m \tag{2.6}$$

The voltage equations can be visualized as vectors and they are displayed in Figure 2.17a). The vector diagram in this case is equivalent to the circuit of Figure 2.17b). The model is simply a voltage generator (emf), an inductance and a resistance.

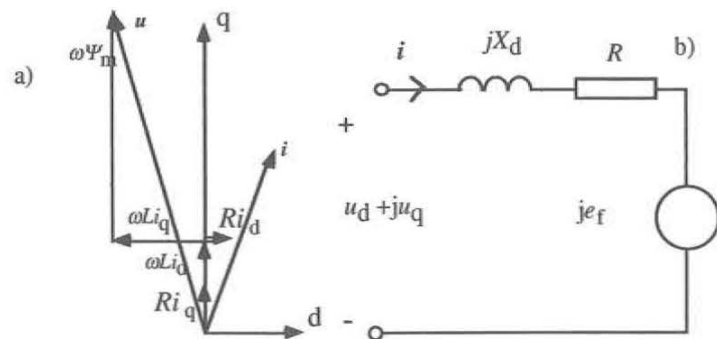


Figure 2.17a). Vector diagram of the machine at steady state and smooth rotor. b) Equivalent circuit of the permanent magnet machine.

The amplitude of the emf is

$$e_m = \omega \psi_m \tag{2.7}$$

and the impedance is

$$\omega L_d = \omega L_q = X_d \tag{2.8}$$

In other cases the Equations (2.2) of the permanent magnet machine should be used. In cases where high frequency is to be taken into account eddy currents in the rotor should also be considered.

2.5. Power Electronic Control

Depending on the application, permanent magnet machines can be controlled by various types of converters. In generator operation, a diode rectifier according to Figure 2.18 may be sufficient. A current source PWM converter can be used to feed the grid [29] and to control the torque.

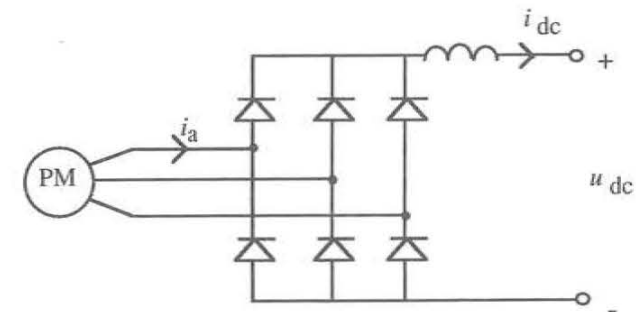


Figure 2.18. Diode rectifier.

The output voltage from the diode rectifier is [30]:

$$\bar{u}_{dc} = 1.35 E_n - 2R \bar{i}_{dc} - \frac{3}{\pi} X_d \bar{i}_{dc} \tag{2.9}$$

where  $\bar{u}_{dc}$  is the mean value of the DC-link voltage,  $\bar{i}_{dc}$  is the mean value of the DC-link current and the RMS-value of the line-to-line voltage  $E_n = \sqrt{3} E_f$ . The power is:

$$P_{dc} = (1.35 \sqrt{3} E_f - \frac{3}{\pi} X_d \bar{i}_{dc}) \bar{i}_{dc} \tag{2.10}$$

The RMS-value of the fundamental motor current is:

$$I_1 = \sqrt{\frac{3}{2}} \frac{2}{\pi} \bar{i}_{dc} \tag{2.11}$$

In the case of nominal machine operation, i.e.  $E_f = I_1 = 1.0$  (p.u.), the power of the DC-link is:

$$P_{dc} = 3 - \frac{\pi}{2} X_d \quad (2.12)$$

The voltage source PWM-converter can be used in motor operation as well as in generator operation, see Figure 2.19. This converter can feed the machine with the appropriate reactive power and lower current harmonics are cancelled with a proper modulation [31]. If the PWM-voltage is not filtered, a high-frequency voltage is added to the fundamental voltage. The high-frequency voltage produces a machine flux that rotates at high speed and induces currents and power losses in the rotor, machine housing and stator core.

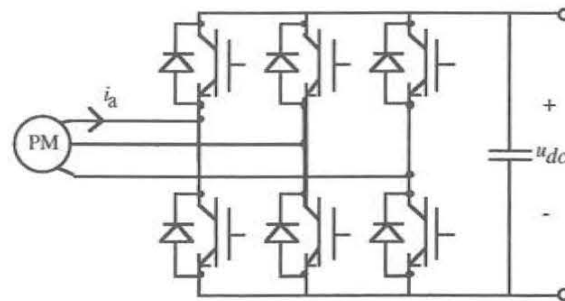


Figure 2.19. PWM-converter with IGBT-switches

If reactive power is fed to the machine, which can be the case if a PWM-converter is used, the induced voltage and the current have the same phase angle. The electric output from the machine is in this case:

$$P_{PWM} = 3E_f \cdot I_a \quad (2.13)$$

In the case of nominal operation the current and voltage are

$$I_a = I_1 = E_1 = E_f = 1 \text{ (p.u.)} \quad (2.14)$$

and the output power is

$$P_{PWM} = 3 \quad (2.15)$$

Compared to the case where a PWM converter controls the direction of the current, the output power from a machine connected to a diode rectifier is derated, due to the fact that the overlap angle directly lowers the output voltage of the rectifier. Inserting typical reactance values of a permanent magnet machine with slotted stator yields the nominal power of the systems:

$$X_d = 0.35 \text{ p.u.}$$

$$P_{PWM} = 3 \text{ p.u.}$$

$$P_{DC} = 2.45 \text{ p.u.}$$

The output power from the system with a diode rectifier is 82 % of the PWM system. This difference between the systems places different demands on the machine construction. If the machine is to be connected to a diode rectifier, the machine reactance should be low. In the case where the machine is to be connected to a PWM converter, the reactance of the machine is not critical but the machine should be built to minimize the power losses due to high-frequency current components.

### 3. Investigation of a Slotless Pole

An electric machine has several parameters that directly or indirectly influence the torque. Some of them are machine length, rotor radius, yoke thickness, number of poles, slot width, slot depth, magnet thickness and material data, current density and cooling arrangement. Finding the optimum value of all these parameters is a very difficult task. In order to optimize a construction, the cost for the parts must be summarized and the cost for power losses over machine lifetime should be added. For example, in the case of a generator, the power losses of the generator can be related to a loss of income. The influence of an altered machine design can be calculated in this way.

In order to find an approximative way to construct the pole, the parameters of the pole are studied. In this way, it will be easier to find a favourable machine construction.

Defining the winding region as the cross-section between the air gap and the stator core, see Figure 3.1, the fill factor of conductor material is

$$k_{cu} = \frac{3N_p a_{cu}}{h_1 \tau_p} \quad (3.1)$$

where  $N_p$  is the number of turns per pole-pair and phase,  $a_{cu}$  is the area of the conductor,  $h_1$  is the height of the winding region and  $\tau_p$  is the pole pitch.

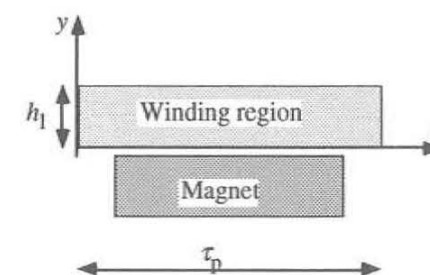


Figure 3.1. Magnet and winding region.

In a slotless machine, the winding region can theoretically be filled with 100 % conducting material. In practice a fill factor of 60–80 % can be utilized if rectangular conductors are used. This fill factor can be compared with the fill factor of a normal machine with round conductors where the teeth occupy approximately 50 % of the winding region. The slots are filled with approximately 50 % conductors, i.e. the total fill factor of copper is around 25 %.

It is assumed that the coils are wound on the outside of the machine and fixed to the stator core afterwards. In order to simplify the production and to make it possible to use rectangular

conductors, the coils are wound on a bobbin according to Figure 3.2 and after this formed to the right curvature and fixed to the stator. With this technique the different phases of a three-phase winding are distributed according to Figure 3.2. The electric angle of the pole is divided equally in three pieces.

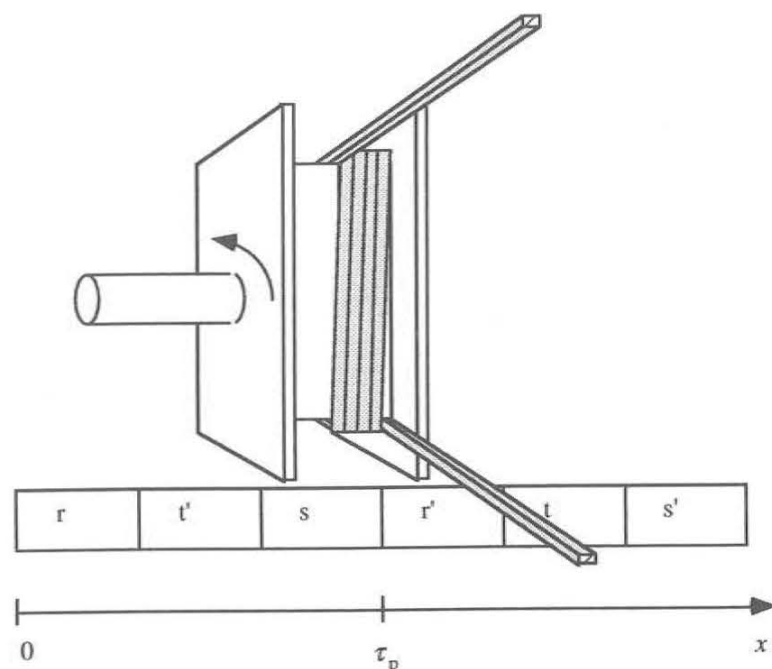


Figure 3.2. Winding production and the winding distribution.

### 3.1. Flat Pole

As a start, a flat structure is studied, which is relevant in the case of an axial flux machine. In addition, in a radial flux machine with a high number of poles, the pole can be approximated by a flat structure. If the radial flux machine has a low number of poles, then the surface is curved and the flux is distributed in a different way.

In this work an FEM program is used to analyse the constructions. The FEM program can handle two-dimensional problems and nonlinear material characteristics. In this way, relatively long constructions are treated correctly but short machines may be wrongly dimensioned. Earlier attempts to find the optimal winding thickness are based on a mix of analytical methods and the approximation of measured data [32]. The analysed machine in the mentioned reference is an axial flux machine which required a thin winding in order to avoid leakage of flux in the radial direction.

The permanent magnet material used is VACODYM 370 HR (60 °C), the remanent flux density of this material is  $B_r=1.15$  T and the coercive force  $H_c=870$  kA/m. As a start, it is assumed that the iron core material is linear with a relative permeability  $\mu_r=1000$ . A flat pole is displayed in Figure 3.3 and a Cartesian coordinate system is defined.

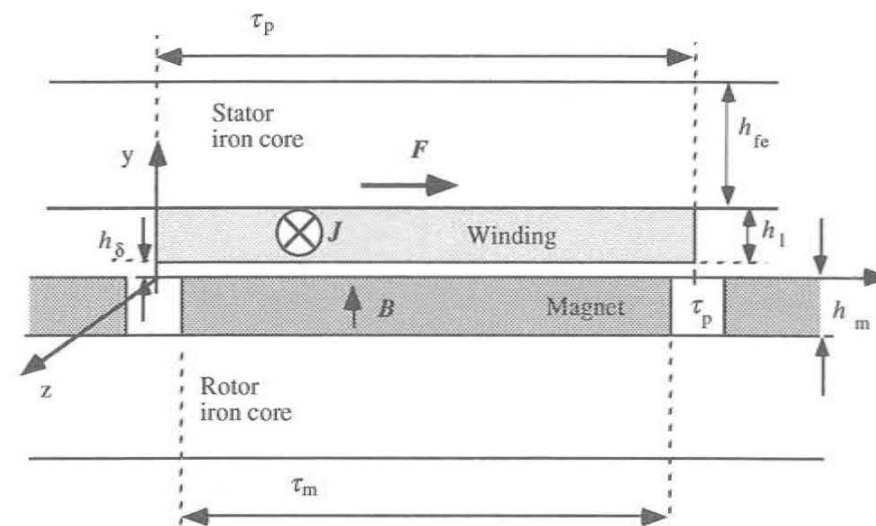


Figure 3.3. Cross-section of a flat pole. Cartesian coordinate system.

In order to make a comparison with the results from the FEM program, an idealized calculation is made, see Figure 3.4. Under idealized conditions, the flux density vector is directed only in the y-direction. The magnitude of the flux density is given by :

$$B(x) = \frac{B_r}{1 + \frac{h_l \mu_m}{h_m \mu_0}} = B_{id} ; \quad x \in \left[ \frac{\tau_p - \tau_m}{2}, \frac{\tau_p + \tau_m}{2} \right]$$

$$B(x) = 0 \quad ; \quad x \notin \left[ \frac{\tau_p - \tau_m}{2}, \frac{\tau_p + \tau_m}{2} \right] \quad (3.2)$$

where  $\mu_m$  is the permeability of the magnet and  $B_{id}$  is the ideal value of the magnet flux density in the air gap,  $h_l$  is the winding thickness and  $h_m$  is the thickness of the magnet.  $\tau_p$  and  $\tau_m$  are the pole pitch and magnet width, respectively.

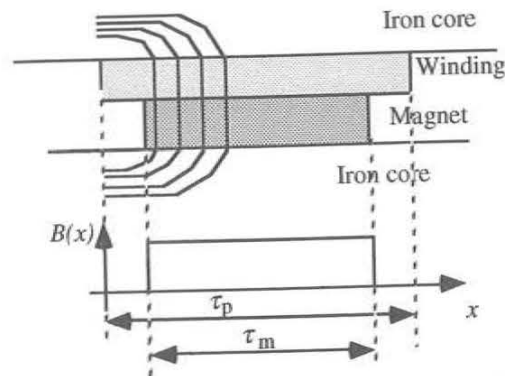


Figure 3.4. Idealized field. Equipotential lines cross the air gap without spreading in  $x$ -direction.

When  $\tau_m/\tau_p$  is known, the Fourier coefficients of the ideal flux density wave are calculated:

$$B_{sp-id} = \frac{4}{n\pi} B_{id} \cos \left[ n \frac{\pi}{2} \left( 1 - \frac{\tau_m}{\tau_p} \right) \right], \quad (n = 1, 3, 5, \dots) \quad (3.3)$$

When the flux density is known the force can be calculated. The force on the winding area with the length  $l_{st}$  is:

$$F = l_{st} \frac{\tau_p}{2} \cos(\beta) J_{1p} \int_0^{h_1} B_{1p}(y) \cdot dy \quad (3.4)$$

where  $\beta$  is the angle between the current density and flux density waves.  $J_{1p}$  is the peak value of the current density wave and  $l_{st}$  is the length of the active region. The derivation of this expression is given in Appendix A. The force depends on the phase shift, which from the beginning is assumed to be  $\beta=0$ . Often this is adequate, since the reactance of an air gap wound machine is low, then the phase shift is very low as long as the power factor of the machine is unity. In machines that have higher inductance, it is assumed that reactive power is fed to the machine. If Equation (3.4) is divided by magnet volume,  $V_m$  and the current density of the actual configuration, a figure of merit of the cross-section is obtained. The figure of merit is defined by:

$$g = \frac{F}{J_{1p} V_m} = \frac{B_{1p} h_1 \tau_p}{2 h_m \tau_m} \quad (3.5)$$

### 3.1.1 Variation of Magnet Width

In the first calculations, it is assumed that the magnet thickness is 20 % higher than the winding thickness,  $h_m/h_1=1.2$ . The winding thickness divided by the pole pitch ( $h_1/\tau_p$ ) and the magnet width divided by the pole pitch ( $\tau_m/\tau_p$ ) are varied. It is further assumed that  $h_m < h_1$ , i.e. the air gap length is much smaller than the winding thickness. This is not a problem in the case of a small machine with few poles, but in a big machine with the radius of one meter or more the air gap must be around 1-2 mm which is not negligible if the winding thickness is 10 mm.

Figure 3.5 shows the cross-section of the pole. Figure 3.5 also shows how the fundamental flux density amplitude varies with the winding thickness to the pole pitch ratio  $h_1/\tau_p$ . The displayed value of the flux density is the average over  $h_1$ .

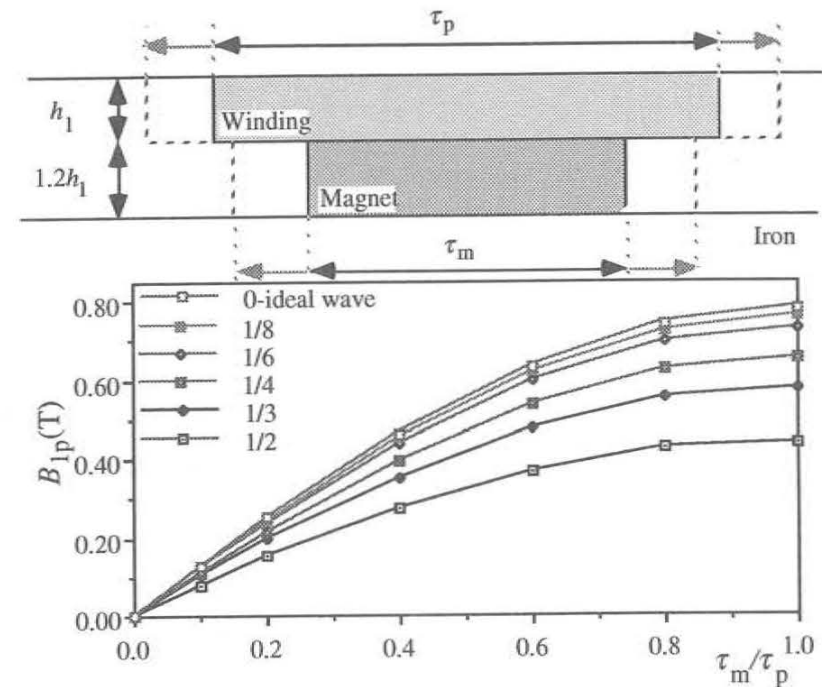


Figure 3.5. Peak value of fundamental flux density with  $h_1/\tau_p$  as a parameter. The flux density is averaged over  $h_1$ .

The curves indicate that flux density increases with increased magnet width and the increase is almost linear up to  $\tau_m/\tau_p=0.6$ . For values above this, the slope decreases and the increase of permanent magnetic material does not change the fundamental flux density to the corresponding degree. The curve signed with  $h_1/\tau_p=0$  corresponds to the ideal case where the flux goes straight

over the air gap, i.e.  $\tau_m, \tau_p \gg h_l, h_m$ , and the fundamental is calculated according to Equation (3.3).

The flux density decreases with an increase in the value of the winding thickness,  $h_l/\tau_p$ . This is due to the leakage of the magnetic flux as the flux does not pass the winding but goes around the edges of the magnet. The fundamental flux density when  $\tau_m/\tau_p = 0.7$ , as a function of  $h_l/\tau_p$ , is displayed in Figure 3.6.

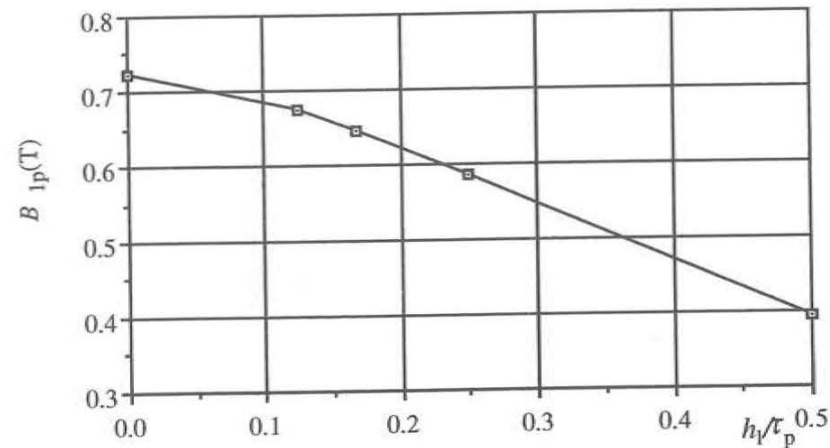


Figure 3.6. Amplitude of fundamental flux density as function of  $h_l/\tau_p$ . Magnet width to pole pitch ratio is fixed  $\tau_m/\tau_p = 0.7$ .

In order to minimize the leakage of the magnet flux, it is necessary to have a rather thin winding in relation to the pole pitch. This is a problem when a small pole pitch are a primary goal. If the pole pitch is small, the winding must be thin and the mechanical air gap cannot be considered as much smaller than the winding thickness.

The equipotential lines of the magnetic vector potential can be compared in Figure 3.7, which shows a case with a narrow magnet and a case where the magnet is wider. In the latter case, the relative flux that does not penetrate the winding is lower. Representing the permanent magnets in the FEM-program is done according to a method [33] which uses a current-carrying area at the edges of the magnet as indicated in Figure 3.7. The area carries a current corresponding to the coercive force  $H_c$  multiplied by the magnet height  $h_m$ .

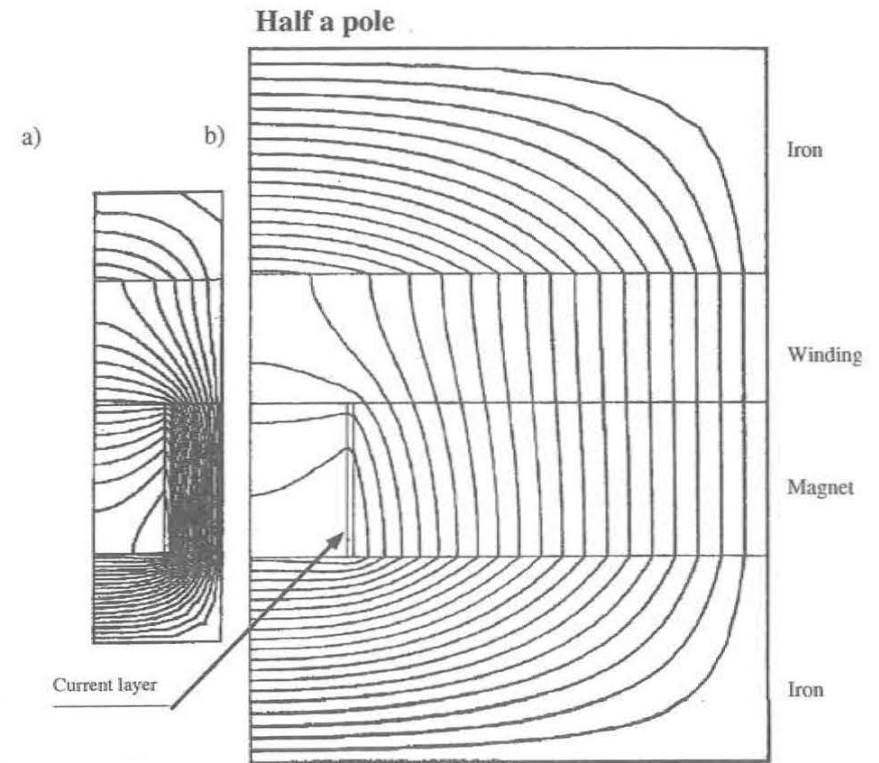


Figure 3.7. Equipotential lines of the magnetic vector potential. Without current loading.

a)  $\tau_m/\tau_p = 0.4$  and  $h_l/\tau_p = 0.5$ .

b)  $\tau_m/\tau_p = 0.8$  and  $h_l/\tau_p = 0.125$ .

Now we will study the function  $g$  defined by Eq. (3.5), i.e. force per length, current density and magnet volume. The result is displayed in Figure 3.8. The function  $g$  declines with an increase in the value of the magnet width divided by pole pitch. Nevertheless, the range  $0.6 < \tau_m/\tau_p < 0.8$  is a recommendable compromise. In this region, the fundamental of the flux density is rather high and the leakage at the ends of the magnet is moderate. The optimal pole shoe width has earlier been found to be 73 % of the pole pitch [34] and in the case of a DC-brushless construction the magnet width will be lower than 93 % of the pole pitch, [35]. In this study, we are not considering a DC-brushless motor and in the following calculations,  $\tau_m/\tau_p = 0.7$  is used and this value has also been tested in a laboratory machine. As stated earlier high values of  $h_l/\tau_p$  are not recommended. It is recommended that the value of the winding thickness is  $h_l/\tau_p < 0.2$ .

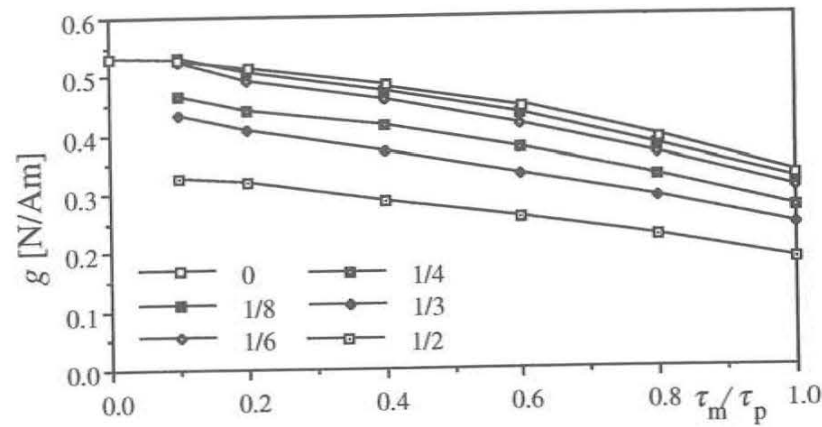


Figure 3.8. The function  $g$  with  $h_1/\tau_p$  as a parameter.

### 3.1.2 Varied Winding Thickness

The winding thickness is varied in order to find a favourable thickness. The magnet width and height are constant, see Figure 3.9. Calculations are performed with a constant magnet width divided by pole pitch  $\tau_m/\tau_p=0.7$ . The ratio between magnet height and pole pitch is  $h_m/\tau_p=0.2$ . The function  $g$  increases but the flux density decreases with increased winding thickness, see Figure 3.9. The winding thickness must be restricted since, otherwise, the power losses will be too high.

As the winding thickness is increased from  $h_1/\tau_p=0.1$  to  $h_1/\tau_p=0.5$ , approximately 100 % more force can be produced by the same magnet if the current density is constant. It is necessary, however, to increase the copper volume by a factor of 5, and this means that the power losses and the cost associated with the winding increase by the same factor.

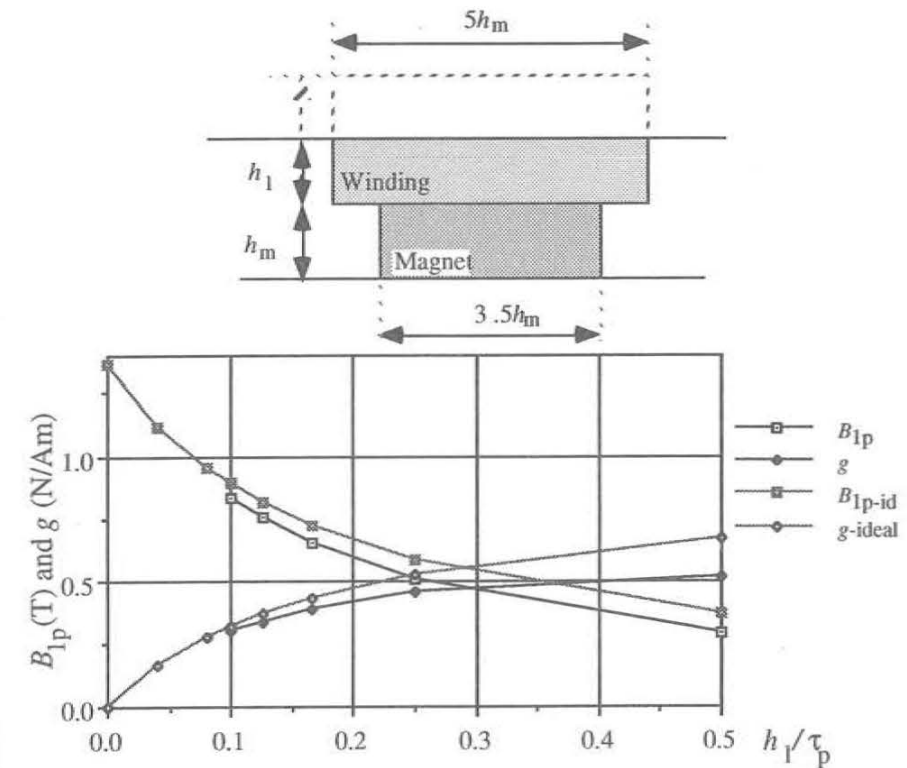


Figure 3.9. Flux density and  $g$  at varied winding thickness.

If the cooling capacity from the winding to ambient is limited, the current density may be varied so that the winding power losses and winding temperature are constant independent of winding thickness. It is here assumed that the heat transfer through the winding is much better than the heat transport to the ambient. This assumption is relevant if the winding thickness is lower than  $h_1=10$  mm and the heat transfer coefficient from the yoke surface to the ambient is  $\alpha < 50$  ( $\text{W}/\text{m}^2\text{K}$ ). In other cases the heat transfer of the winding must be taken into account. The copper losses of one pole are:

$$P_{cu} = \int_{V_w} \rho J^2 dV = k_{cu} \rho J_{1cu}^2 h_1 \tau_p l_{st} \quad (3.6)$$

where  $V_w$  is the volume of the winding. Assuming constant copper losses of the winding, the current density in the conductor is:

$$J_{1cu} = \sqrt{\frac{P_{cu}}{\rho k_{cu} l_{st} h_1 \tau_p}} \quad (3.7)$$

The current density is, thus, inversely proportional to the square root of the winding thickness. If the current density according to Eq. (3.7) is substituted into (3.4), the force is

$$F = \sqrt{\frac{l_{st} \tau_p P_{cu}}{8 \rho k_{cu} h_1}} \int_0^{h_1} B_{1p}(y) \cdot dy \approx \sqrt{\frac{h_1 l_{st} \tau_p P_{cu}}{8 \rho k_{cu}}} B_{1p} = k_1 \sqrt{h_1} B_{1p} \quad (3.8)$$

where  $k_1$  is a constant. The force is proportional to the square root of the winding thickness and proportional to the flux density  $B_{1p}$  as long as the pole pitch and length are constant. Normalizing the equation with the pole pitch and dividing by the constant yields

$$\frac{F}{k_1 \sqrt{\tau_p}} = \sqrt{\frac{h_1}{\tau_p}} B_{1p} \quad (3.9)$$

The flux density according to Figure 3.9 is used to evaluate the Equation (3.9). In Figure 3.10 the result from Eq. (3.9) is shown for a realistic flux density wave and for an idealized flux density.

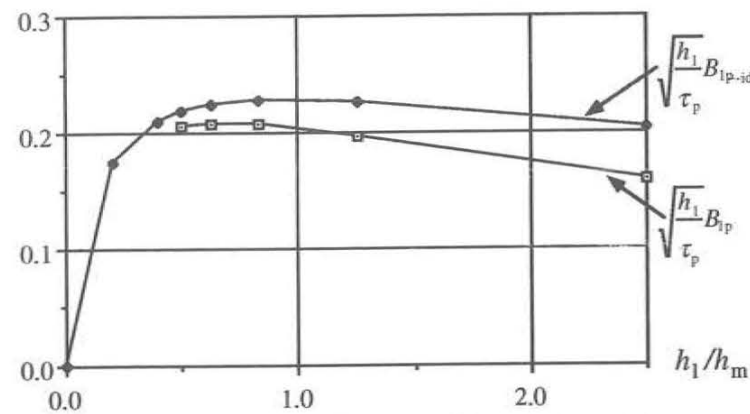


Figure 3.10. Normalized force when power losses in the winding are constant.

It is shown that depending on how much the flux leaks, the winding thickness should be in the range of  $h_1/h_m = 0.7-1.0$ . The upper limit is valid in an ideal case where the winding thickness is very small in relation to the pole pitch. In a more realistic case, the winding thickness should be approximately  $0.7h_m$ .

All calculations in this section are based on the assumption that the air gap is negligible. In cases where this is not true, the air gap will decrease the useful volume of the winding. The force density of the pole will decrease and the optimal winding thickness will be smaller than shown in Figure 3.10.

### 3.1.3 Induced Voltage

The width of one winding phase is one third of the pole pitch, as shown in Figure 3.2. The winding factor of the fundamental wave is:

$$k_w = \frac{3}{\pi} \quad (3.10)$$

which is more closely examined in Appendix B.

For calculating induced voltage, torque and armature reaction in air gap windings a program PERMASYNK was developed. The program uses the calculated flux density waveform in the air gap winding, which may be three-dimensional. With a time stepping method, the flux density wave is stepped through a period and the flux variations in each winding are calculated. In the same way the torque as a function of time can be evaluated. Feeding the program with a flux density wave from the winding, the flux density variation on the rotor surface can be calculated. The structure of the program is displayed in Figure 3.11. Assuming  $N_p$  turns per pole and phase the induced voltage in the winding may be evaluated as

$$e_p(t) = p \frac{d}{dt} l_{st} \left[ \sum_{l=1}^{N_y} \sum_{m=1}^{N_x} \int_{x_{1m}}^{x_{2m}} B(x, y_l) dx \right] \quad (3.11)$$

where  $e_p$  is the induced voltage of each phase and pole,  $N_x$  is the number of layers per pole and phase,  $N_y$  is the number of turns per layer and  $p$  is the number pole pairs.

To illustrate the influence of the magnet shape on the induced winding voltage, the flux density waves according to Figure 3.7a) are used to calculate the induced voltage in a winding according to Figure 3.2. The flux density waves at different positions in the winding are shown in Figure 3.12a) and the induced voltage in Figure 3.12 b).

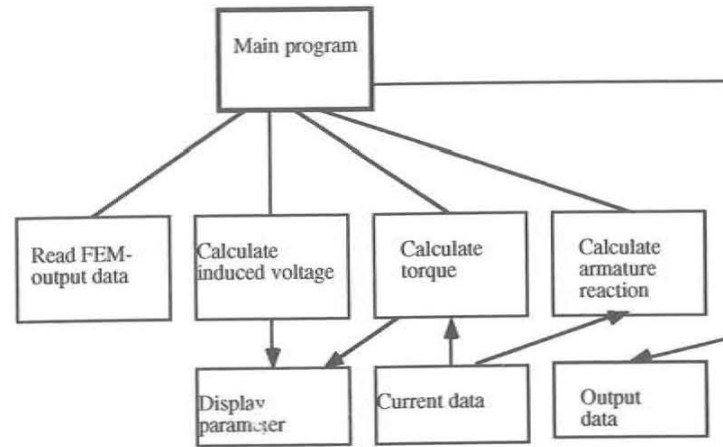
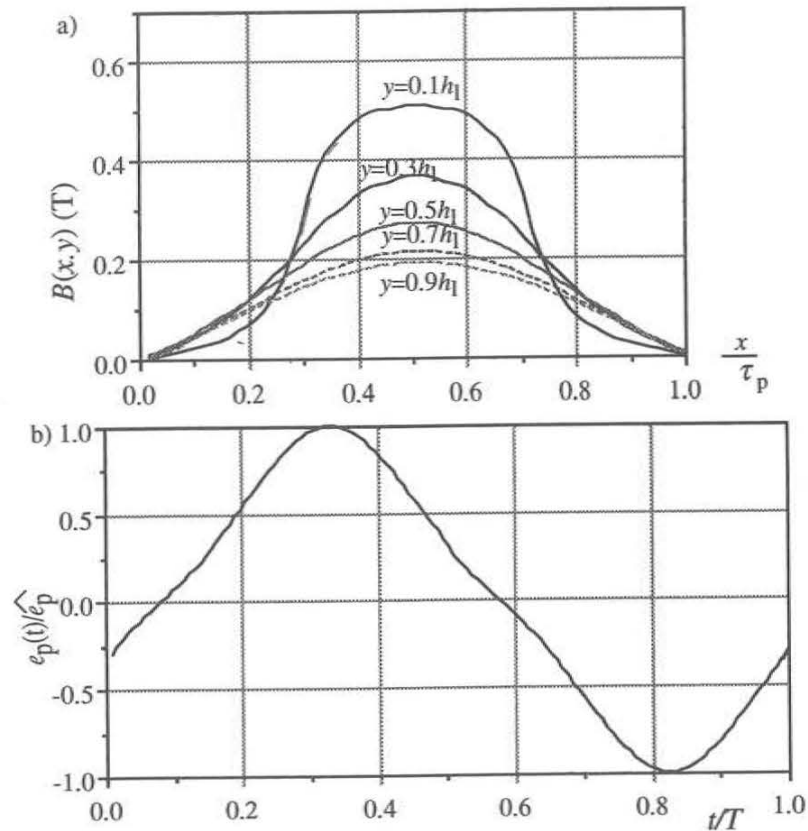
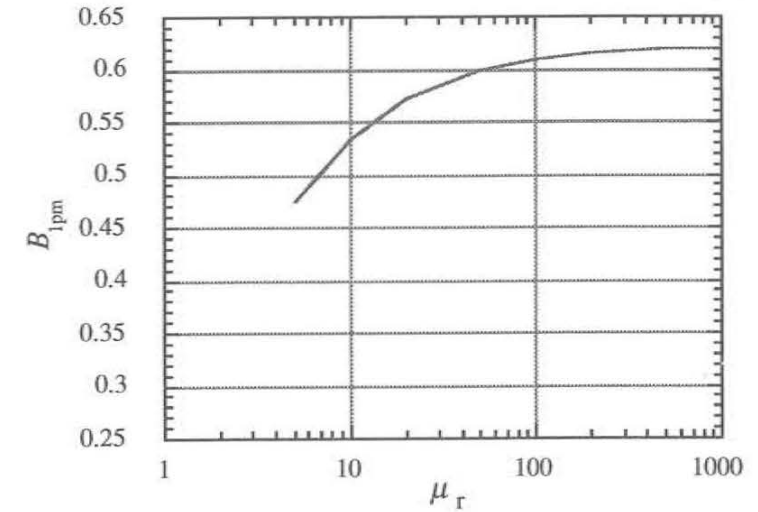


Figure 3.11. Program structure of PERMASYNK

Figure 3.12. a) Flux density waves at different positions in the winding. b). Induced voltage,  $\tau_m/\tau_p=0.4$  and  $h_1/\tau_p=0.5$ 

### 3.1.4 The Influence of Permeability in the Stator Yoke

In order to investigate if iron powder material may be used together with air gap windings, the permeability of the stator yoke is varied. The thickness of the core ( $h_{Fe}$ ) is 16.5 % of the pole pitch. The averaged value over  $h_1$  of the fundamental flux density in the winding region is displayed in Figure 3.13.

Figure 3.13. Mean value of fundamental flux density as a function of relative permeability in the stator core.  $h_1/\tau_p=0.2$ ,  $\tau_m/\tau_p=0.7$ .

In this case, where the reluctance of the winding region is high, the relative permeability can be low and the fundamental flux density will remain high. A relative permeability of 100 is enough to reach 98 % of the flux density of a machine equipped with a yoke made of laminated sheets.

### 3.2 Radial Flux Rotors

In a radial flux machine with a low number of poles, the surfaces are cylindrical and the magnetic field is distributed in a different way than in the flat pole. This chapter treats different types of rotors in radial flux machines. The examples examined are machines with the rotor inside the stator. The machines have four poles except for the high-speed machine which has two poles. The section does not intend to cover every design option but four different types are studied. Two of the constructions are made with surface mounted magnets which may be used at a moderate speed. If necessary, a thin layer of reinforced fiber glass may be enough to hold the magnets in place. At a very high speed, the magnet must be surrounded by a high-strength material and in this case a hollow shaft made of high strength steel is an alternative that is compared with the surface-mounted magnets. A machine with interior magnets is also described.

One conclusion from the previous chapter is that magnet width should be around 70 % of the pole pitch. This percentage is chosen in the following calculations. According to the previous chapter, the optimal winding thickness is 0.7–1 times the magnet thickness. As we will see below, the winding thickness can be increased when the geometry is cylindrical.

The different rotor constructions of the four-pole machines are displayed in Figures 3.14–3.16. The equipotential lines of the vector potential are shown for each construction. There is quite a difference between the three rotor constructions. The first one with radially magnetized magnets, outlined in Figure 3.14 and called C.1, spreads the magnet flux evenly along the magnet surface. This construction is recommended for a DC-brushless operation where a trapezoidal emf is desired [35].

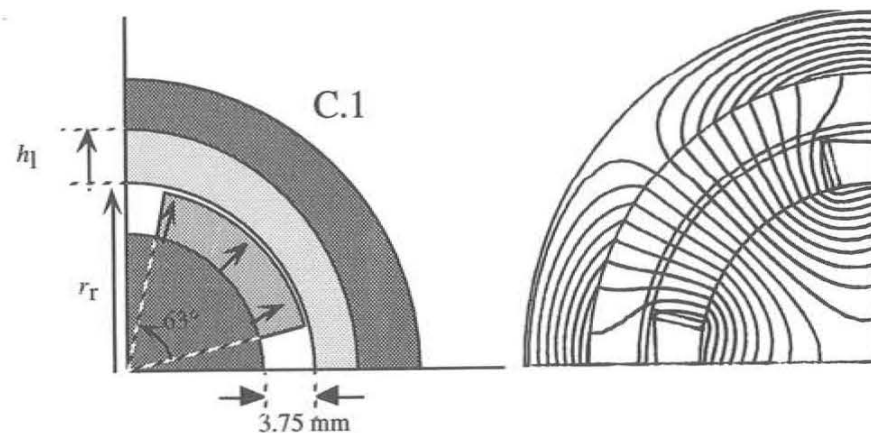


Figure 3.14 Radially magnetized magnets. One pole of a four-pole machine. Construction No. C.1.

The semi-radial magnet construction, C.2, according to Figure 3.15, is simpler to manufacture owing to a flat bottom. The curved surfaces have to be ground to the right shape which makes construction C.1 a more expensive construction. Construction C.2 concentrates the flux in the direction of the d-axis.

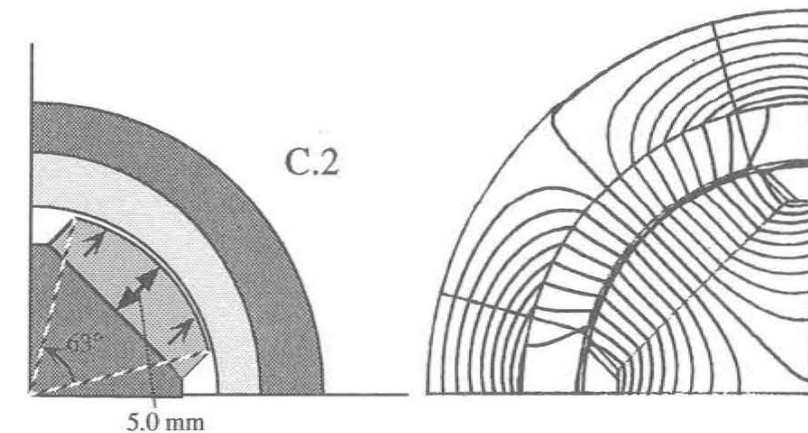


Figure 3.15. Semi-radial magnets with diametrical magnetization. Construction No. C.2.

The flux concentrating magnets, C.3, shown in Figure 3.16, are not recommended when slotless constructions are used. In this case, the reluctance of the winding is high and a large part of the flux flows through the centre of the machine. This flow can be observed from the equipotential lines of the construction in Figure 3.16.

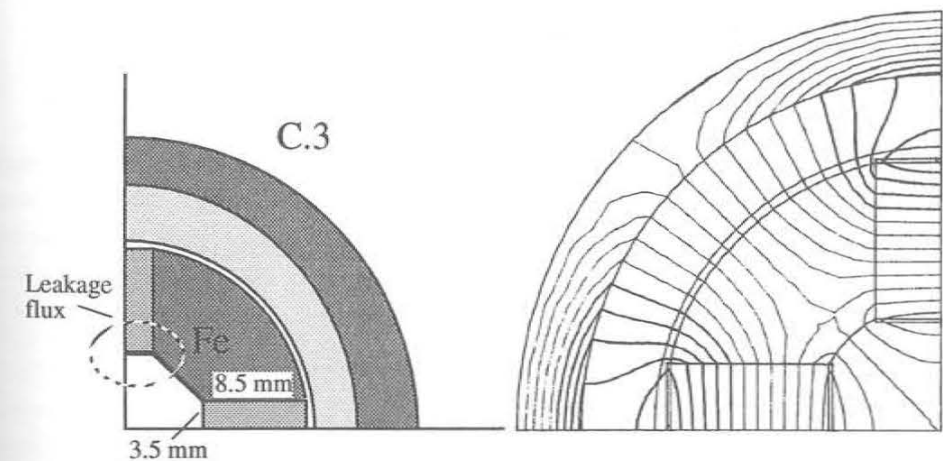


Figure 3.16. Concentrating magnets. Construction No. C.3.

The machines are analysed under the conditions described in Table 3.1. The permeability of the yoke-material is relatively high  $\mu_r=1000$ .

Table 3.1. Conditions used when analysing radial flux machines.

Rotor radius, $r_r$	15 mm
Air gap length, $h_g$	0.5 mm
Magnet type	VACODYM 370 HR (20 °C)
Remanent flux density, $B_r$	1.2 T
Coercive force, $H_c$	920 kA/m
Mass density of magnets, $\gamma_m$	7400 kg/m <sup>3</sup>
Fundamental current density, $J_{1cu}$	6 A/mm <sup>2</sup>
Fill factor of copper, $k_{cu}$	50 %.
Magnet weight C.1.	1.6 kg/m
Magnet weight C.2.	2.0 kg/m
Magnet weight C.3.	1.8 kg/m
Magnet weight C.4.	2.0 kg/m

The four-pole machines are compared in terms of torque production and copper losses. The FEM-program is used to calculate the flux density at three different radii in the winding. The torque is derived from Equation (A.5) in Appendix A and then is numerically integrated:

$$T = 3k_{cu} J_{1pcu} l_{st} \cos(\beta) \int_{r_1}^{r_2} r^2 \cdot B_{1p}(r) dr \quad (3.12)$$

where  $r_1$  is the inner radius of the winding and  $r_2$  is the outer radius of the winding. It is assumed that  $\beta=0$ . The torque produced by the different rotors is displayed in Figure 3.17. Construction C.2 clearly has a higher torque than the other two. The magnet weight of C.2 is higher, but we must consider that the C.1 construction must be ground and the magnet is probably ground from a rhomboid. If that is the case, the original weight of the rhomboids to be ground to magnets C.1 and C.2 are approximately the same.

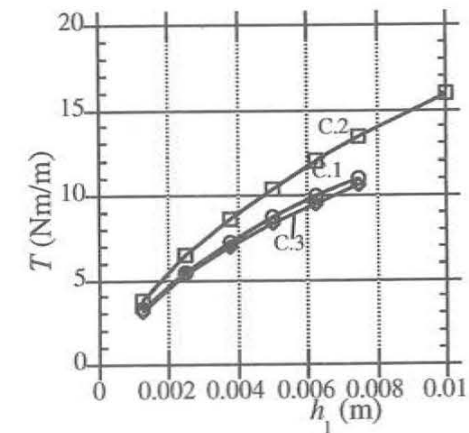


Figure 3.17. Torque per unit length as a function of winding thickness of the different rotors.

Assuming that the rotors are to produce 10 Nm/m, the ohmic power losses may be evaluated. Naturally, the C.2 construction has lower copper losses at constant torque than the other two. The power losses are displayed in Figure 3.18.

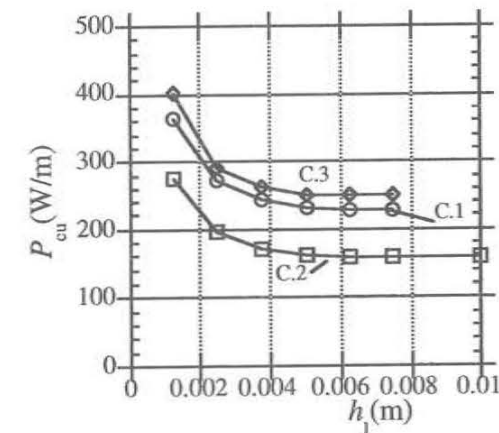


Figure 3.18. Ohmic losses per unit length at constant torque.

The semi-radial magnet machine is used as an example of a medium-speed machine and it is compared with the shaft-magnet rotor according to Figure 3.19. This machine has been tested in high-speed operation [1] and it has shown good performance. The shaft-magnet rotor has a thick shell of material that is not magnetic and the influence of this material is investigated. Will an increase in the magnetic air-gap make the performance of this machine lower than that of a surface-mounted magnet construction?

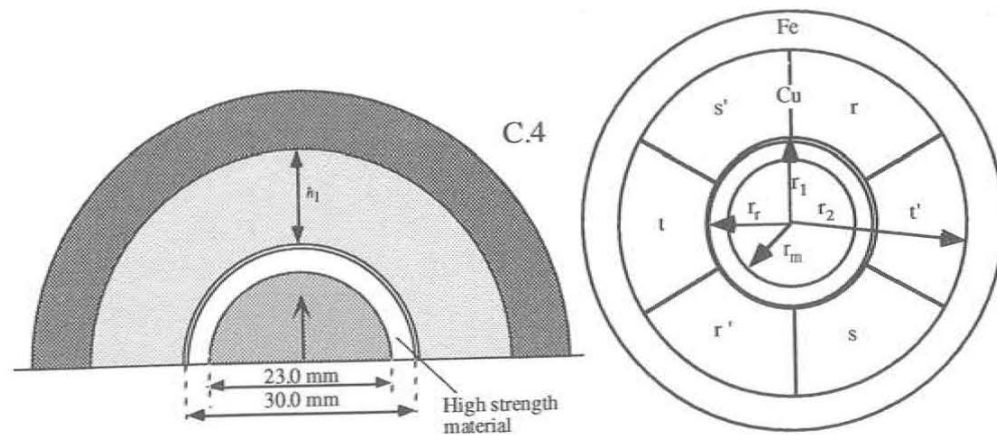


Figure 3.19. Shaft magnet rotor. Construction No. C.4.

The torque per unit length is displayed in Figure 3.20 at varied winding thicknesses. Although the magnet radius of the shaft magnet rotor is lower than that of the surface mounted magnet rotors, the torque of the shaft magnet rotor is higher. The shaft magnet rotor can be used with a higher winding thickness, which is partly due to the two-pole design. The pole pitch is wider and, therefore, the winding thickness may be higher, when compared with the flat pole, where the recommended value is  $h_1/\tau_p=0.2$ . As can be seen from Figure 3.20, the torque increases almost linearly, which is not the case for the four-pole semi-radial construction.

The torque to magnet weight ratio of the surface-mounted magnet is better, see Figure 3.21. This high torque to magnet weight ratio means that the material cost is lower for the surface-mounted magnets, which is preferable if high rotor speed does not limit the construction.

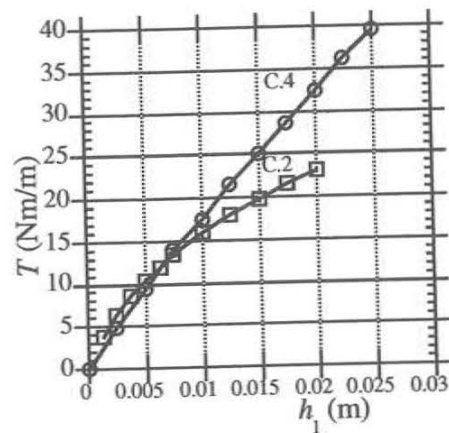


Figure 3.20. Torque per unit length of constructions C.2. and C.4.

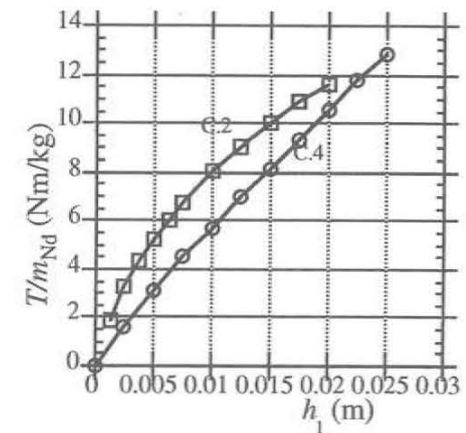


Figure 3.21. Torque to magnet weight of constructions C.2. and C.4.

The copper losses at constant torque  $T=10 \text{ Nm/m}$  are evaluated based on the necessary current density. The copper losses are

$$P_{cu} = \rho_{cu} J_{rms}^2 V_{cu} = \rho_{cu} k_{cu} J_{1cu}^2 \pi (r_2^2 - r_1^2) l_{st} \quad (3.13)$$

where  $\rho_{cu}$  is the resistivity of copper. The copper losses are displayed in Figure 3.22.

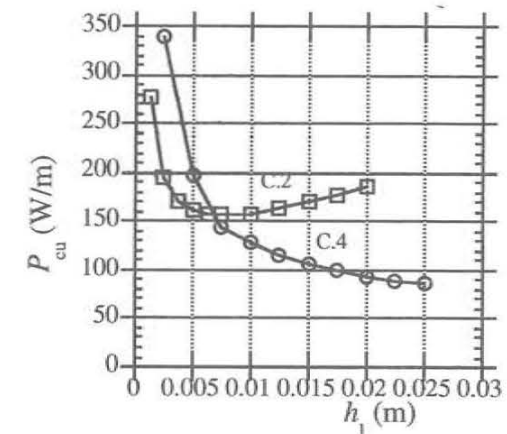


Figure 3.22. Copper losses per unit length of constructions C.2. and C.4. Constant torque  $T=10 \text{ Nm/m}$ .

The shaft magnet rotor shows a very good performance for high winding thickness, and it seems ideal when used at extremely high rotational speed. As can be seen in Figure 3.22, copper losses decrease with an increase in winding thickness without indicating any particular optimal winding thickness. The rotor radius can be low and the radius of the conductors may remain high, which

implies high torque from a small rotor size, which is essential at high speed.

3.3 Discussion

In an axial flux machine the pole structure is flat but the pole pitch varies with radius. The non-constant pole pitch means that an optimal pole construction may be difficult to find. If the number of poles is high, the pole pitch is as an approximation equal to the pole pitch at the mean active radius. Radial flux machines can also be approximated by the flat pole if the number of poles is high. The width of a rectangular magnet in a flat pole should be approximately 70 % of the pole pitch, the magnet should be 20 % thicker than the winding and the winding should be thinner than one fifth of the pole pitch. The recommended pole is shown in Figure 3.23.

The optimal pole may, however, have a thinner winding, such as in the case where the machine is short in comparison with the winding thickness, i.e. there is a significant amount of leakage in the third direction. For instance, Takano et.al. [32] found that the optimal magnet thickness of an axial flux machine with a high amount of flux in the radial direction should be twice the winding thickness.

The force density is proportional to the fill factor of copper, which will vary due to different conductors and constructions. The force density may be written as:

$$F_A = \frac{F}{\tau_p l_{st}} = \frac{1}{2} k_w h_l k_{cu} J_{1pcu} B_{1p} = k_{fl} \tau_p J_{1pcu} \tag{3.14}$$

where  $k_{fl}$  is constant which is evaluated assuming a fill factor of  $k_{cu}=0.6$  and a better magnetic material which will increase the remanent flux density from 1.15 to 1.3:

$$k_{fl} = \frac{3}{2\pi} \frac{h_l}{\tau_p} k_{cu} B_{1p} = 40 \cdot 10^{-3} \text{ (N / Am}^3\text{)}$$

Depending on the fill factor of copper and the remanent flux density of the magnetic material, the force density may be enhanced some 10-20 % for the time being.

The weight per unit length of the pole is shown in Table 3.2.

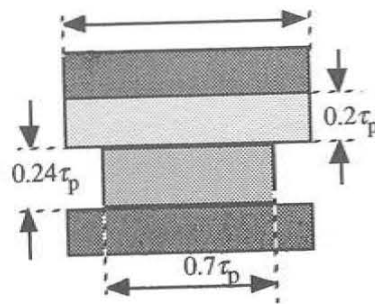


Figure 3.23. Recommended flat pole

Table 3.2. Weight per unit length of the slotless pole

Magnet weight	$1243\tau_p^2$
Copper weight	$1078\tau_p^2$
Iron core weight	$1350\tau_p^2 (h_{fe}=0.18\tau_p)$
Total weight	$3671\tau_p^2$
Force/weight	$10.9 \cdot 10^{-6} J_{1cu}/\tau_p$

The poles with curved surfaces differ from the flat structure. Higher winding thickness can be used, especially with the shaft magnet rotor. A four-pole machine with semi-radial magnets, see Figure 3.24, is recommended for medium speed due to good performance and because only one surface is curved. The torque to magnet weight ratio of the semi-radial magnet rotor is higher than that of the shaft magnet rotor. The ohmic power losses of the machine are at a minimum when the winding thickness divided by rotor radius is:

$$\frac{h_l}{r} = 0.53 \tag{3.15}$$

The torque from the four-pole, semi-radial magnet machine can, then, be expressed as:

$$T = 0.815 r_r^3 B_r J_{1pcu} k_{cu} l_{st} \text{ (Nm)} \tag{3.16}$$

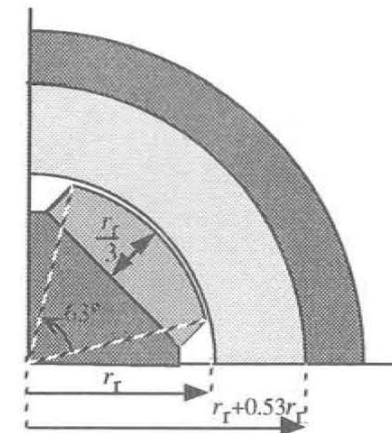


Figure 3.24. One pole of the semi-radial machine.

As with the flat pole, the length of the machine must be considered. The machine must be long if a high winding thickness is to be used. Otherwise, the amount of leakage in the third direction will be high and the optimal winding thickness must be found using three-dimensional methods.

The shaft magnet rotor shows good performance at high torque and the mechanical solution is suitable for high-speed operation. The amount of magnetic material is higher compared to the semi-radial magnet rotor but the construction is mechanically rigid.

In machines with slotless windings, the reluctance of the winding region is high and in such a case an iron powder material can be used as a stator yoke. A relative permeability of 100 is enough to achieve 98 % of the flux density of a laminated stator material.

#### 4. Experimental Machines

This chapter describes three experimental machines with air-gap windings. One of the machines is of the radial flux type and this machine is compared to a slotted machine. The other two machines are of the axial flux type. The first axial flux machine with a power rating of 4.7 kW-machine was built and tested as part of the wind-power research program. The full scale machine will be used as a direct-driven generator. The third machine was built in order to investigate the possibilities of using the axial flux machine as a high-speed generator.

##### 4.1 Medium-speed Radial Flux Machine

This section describes a medium speed servo machine with air gap winding. The machine is intended to be used to increase the capacity of a yarn feeder, see Section 2.2. The cross section of the machine is shown in Figure 4.1. The magnets are of the semi-radial type and a slotless winding was chosen. It was anticipated that the winding production should be more rational and the volume of the machine should be lower with the slotless winding. The calculation of the machine was done based on the result from section 3.2 and by approximating the loss of flux in the third direction. The mechanical production of the machine was made by IRO. The machine was tested and compared with a slotted machine built by GEC Alsthom, according to Table 2.1.

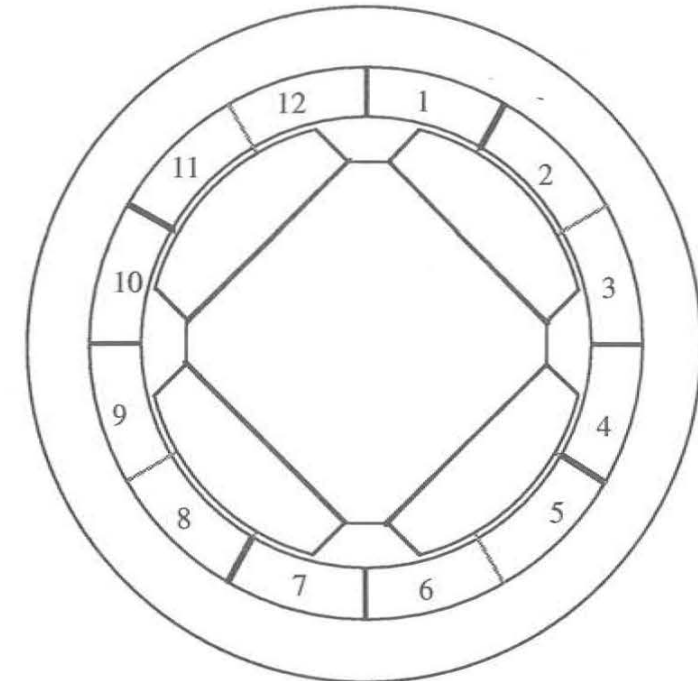


Figure 4.1. Slotless permanent magnet machine.

The calculated data of the slotless machine are listed in Table 4.1. Observe that the iron core material DK70 was used in the test machine, although it is recommended that the production machine should have the better material CK30.

Table 4.1. Calculated data of the slotless permanent magnet machine

Nominal speed	8000 rpm
Remanent flux density	$B_r=1.12$ T
Coercive force	$H_c=850$ kA/m
Rotor radius	$r_r=18$ mm
Magnet width	$\tau_m/\tau_p=0.7$
Magnet height	$h_m=6.3$ mm
Winding thickness	$h_1=4.2$ mm
Iron core length	$l_{st}=40$ mm
Outer diameter	$d=55.4$ mm
Current density	$k_{cu}J_{cu}=6.9$ A/mm <sup>2</sup>
Torque	$T=1.2$ Nm
Ohmic losses	$P_{cu}=123$ W
Eddy current losses in the winding	$P_{Fe}=10$ W
Iron core losses CK30	$P_{Fe}=7.5$ W
Iron core losses DK70	$P_{Fe}=45$ W

The manufacturer's intention is to produce a machine with the torque rate of 1.2 Nm, and with the ability to accelerate the yarn feeder from zero to 8000 rpm in 300 ms.

Figure 4.2 shows the machine and the drive equipment during the tests. The loading machine is a DC-machine which is loaded by means of a variable resistance. The permanent magnet machine is fed with a servo-control converter that produces a sinusoidal current. A resolver is used to measure the angular position of the rotor. The permanent magnet machine can also be rotated by the DC-machine in order to measure no-load losses and induced voltage.

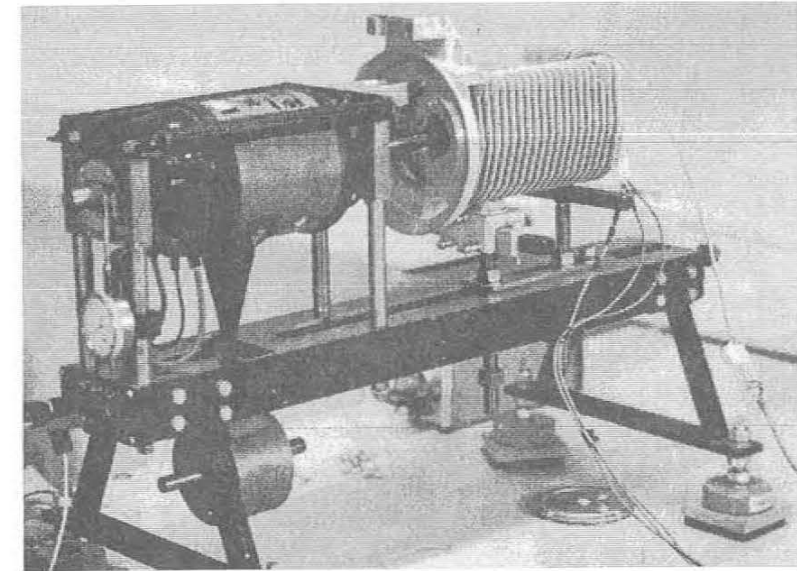


Figure 4.2. Machine during tests.

The induced voltage from the machine is shown in Figure 4.3. The measured voltage is 6 % lower than the calculated value.

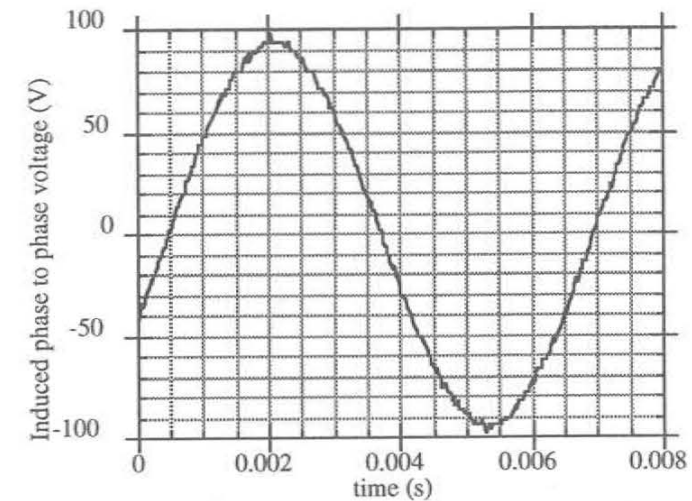


Figure 4.3. Measured phase to phase voltage,  $f=150$  Hz,  $n=4500$  rpm and no load.

The slotted machine was also tested in order to compare the two machines. The slotted machine

has the same rotor dimensions as the slotless construction, but the stator dimensions are larger than those of the slotless machine. The rotor magnets of this machine are mounted in a flux concentrating arrangement and the magnets are made of SmCo. The measured data at nominal current of the machines are summarized in Table 4.2.

Table 4.2. Data of the permanent magnet machine at rated speed

	Slotless machine 8000 rpm	Slotted machine 7000 rpm
Torque	1.08 Nm (4.6 A)	1.04 Nm (4.0 A)
Resistance 20 °C	1.07 Ω	1.43 Ω
Inductance	$L_d=L_q=1.6$ mH	$L_d=3.7$ mH $L_q=6.5$ mH
Induced voltage phase to phase	117 V	111 V
Copper losses warm machine	95 W	82 W
No load losses	64 W	36 W
Additional losses	0	8 W
Total losses	159 W	126 W
Efficiency	0.82	0.84

The measured torque of the slotless machine is 10 % lower than predicted, which can partly be explained by a loss of flux in the axial direction. According to measured voltage, 6 % of the flux is lost. The calculated value of the losses is 178 W (DK70) and the measured value is 159 W. The losses can be lowered to approximately 120 W if the better iron core material CK30 is used. The power losses will, in this case, be in the same range as those of the slotted machine. The additional losses are losses that could not be classified as ohmic losses or no-load losses. These were very low in the slotless machine but clearly measurable in the slotted machine. This discrepancy does not mean that the additional losses are zero in the slotless machine, but that the accuracy of the loss model is not high enough to separate this power loss source.

Figure 4.4 shows the speed response of the slotted machine when running the machine from 0 to 7000 rpm in 340 ms; the desired acceleration performance was not met. In this test the current limit of the controller was set at the nominal current of the machines. During the accelerations the

converter was not able to position the current vector at the correct angle which resulted in a lower torque during dynamic periods. This loss of torque can be concluded after measuring the acceleration capacity and the inertia of the rotating parts. The mean torque during the acceleration was only 0.8 Nm.

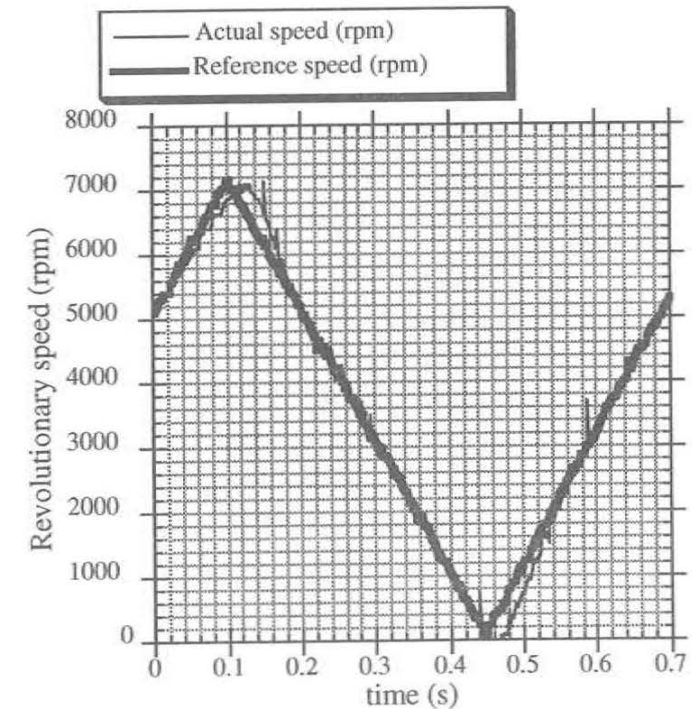


Figure 4.4. Speed response with the slotted machine

The test showed that it is possible to reach nearly the same performance with the air gap stator as with the slotted stator. The permanent magnets used are not the best, which means that there is potential to increase the torque of the slotless machine if a material with higher energy density is used. If a better yoke material is used, the power losses of the machines will be almost the same.

#### 4.2 12-pole axial flux machine

A direct driven generator for wind power mills must have high efficiency, low price and low weight. For smaller wind power plants, the air gap winding and the axial design may be an alternative. In order to verify calculations and to get experience of the NdFeB-material a test machine was constructed, built and tested. The experimental machine is displayed in Figure 4.5.

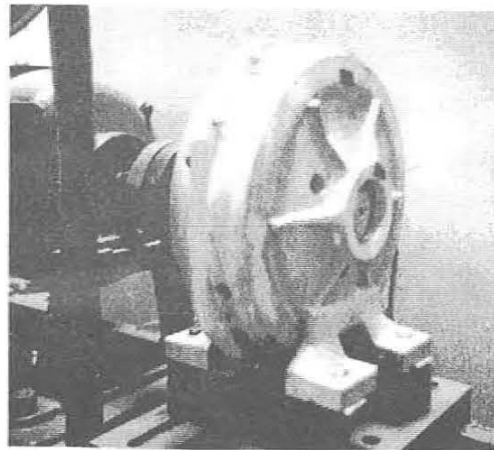


Figure 4.5. Test machine.

The housing of the machine is made of aluminium. The iron core is made of a rim of generator sheet that is wound to the right dimensions and glued to the housing. A cross-section of the machine is shown in Figure 4.6. The permanent magnets are glued to an aluminium disc, which is fixed to the shaft. A glass fibre bandage, that is impregnated with epoxy resin is wound around the periphery of the rotor. The winding is fixed to the stator iron core and impregnated with epoxy resin, see Figure 4.7.

The coils are made of a  $0.8 \times 2$  mm rectangular copper conductor. The coil shape is displayed in Figure 4.8. The number of coils per pole and phase is one.

The magnets are 15 mm thick, see Figure 4.9, i.e. the magnet thickness for each air gap is  $h_m = 7.5$  mm. The optimal winding thickness should be approximately  $h_1 = 6.5$  mm. With a mechanical air gap  $h_g = 1.5$  mm, the winding thickness should be 5 mm on each side of the magnet. Due to the conductor dimension of 2 mm there are two layers of conductors on one side, i.e. 4 mm and, three layers of conductors on the other side, i.e. 6 mm. The final winding thickness is  $h_1 = 8$  mm on each side, depending on problems with insulation and production. This winding thickness results in the winding to magnet ratio  $h_1/h_m = 1.07$ , which is not optimal according to Figure 3.10. The fill factor in the winding volume is only 40 % which can be enhanced. The mechanical dimensions of the machine are summarized in Table 4.3.

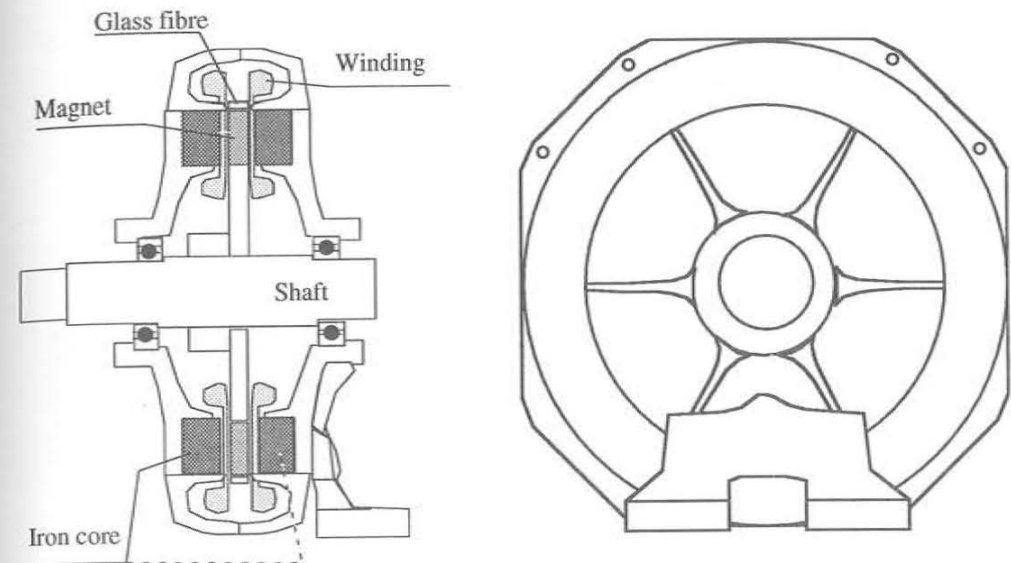


Figure 4.6. 4.7 kW machine. Cross section and axial view.

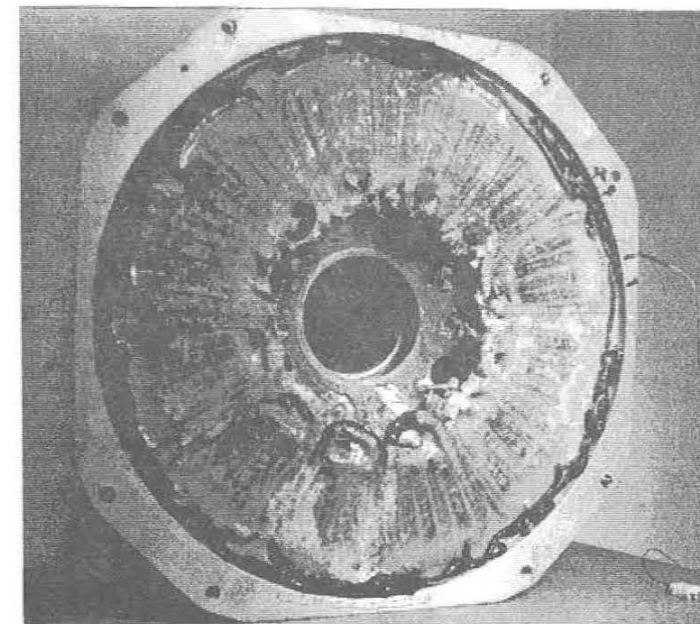


Figure 4.7. Stator impregnated with epoxy resin.

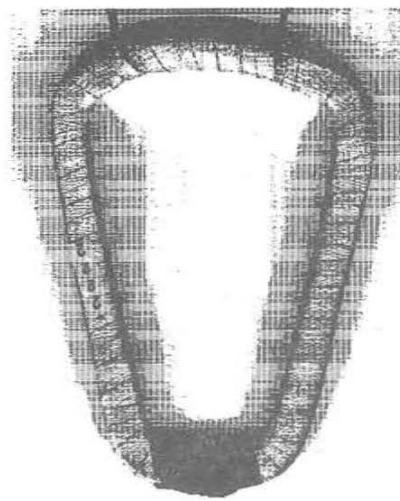


Figure 4.8. One coil to the axial flux machine

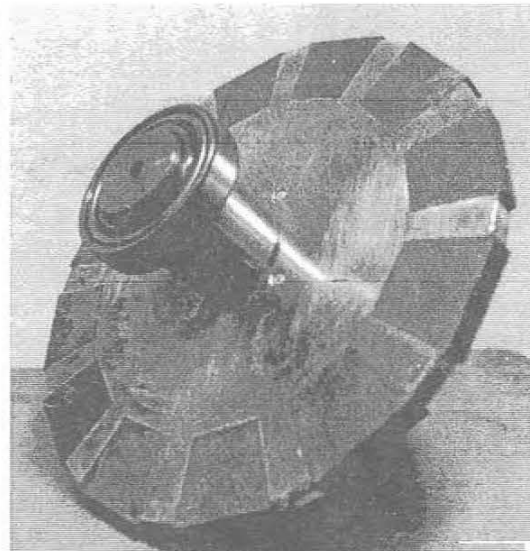


Figure 4.9. Rotor with magnets.

Table 4.3 Summary of mechanical data

Number of phases	3
Connection	Star
Outer radius $r_y$	0.148 m
Inner radius $r_i$	0.104 m
$r_i/r_y$	0.7
Number of pole pairs $p$	6
$\tau_m/\tau_p$	0.7
Thickness of magnet	15 mm
Number of turns per phase	540
Conductor area	1.6 mm <sup>2</sup>
Winding thickness $h_l$	8 mm/stator
Fill factor of copper $k_{cu}$	0.50 (at the inner radius)
Nominal speed	1000 rpm
Outer dimensions	400×400×270 mm (length between feet)
Copper weight $m_{cu}$	8.5 kg
Iron weight $m_{fe}$	18 kg
Magnet weight $m_{Nd}$	3.2 kg
Total weight active material $m_{tot}$	30 kg
Weight other parts	23 kg
Total weight	53 kg

### 4.2.1 Design Calculations

This section deals with the calculations that the construction of the machine is based on. The two-dimensional FEM analysis is used to calculate the flux density in the machine. The flux density is calculated at the mean radius  $r_m=0.126$  m, with  $h_l=8$  mm and  $h_m=7.5$  mm. The axial component of the flux density at different locations in the winding is displayed in Figure 4.10.

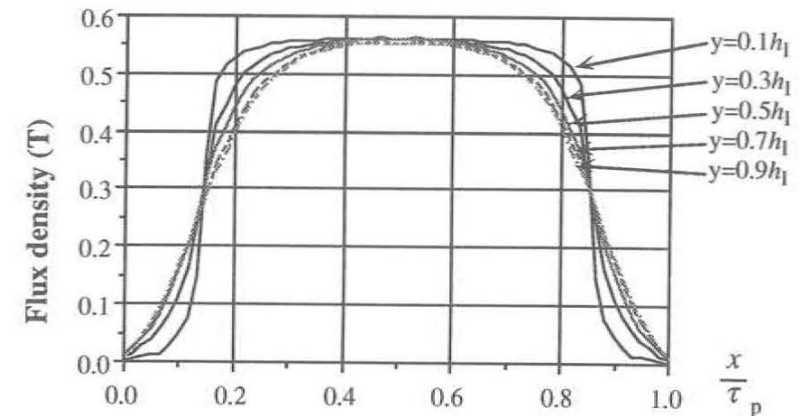


Figure 4.10. Calculated flux density at different axial locations in the winding.

The two-dimensional flux density data according to Figure 4.10 is used as input into the PERMASYNK-program. The average fundamental amplitude of the flux density is calculated at  $B_1=0.62$  T and the induced voltage is calculated at 1000 rpm. The calculated phase-to-neutral voltage is shown in Figure 4.11. It is assumed here that the flux density wave does not change with the radius. The resulting calculated fundamental phase to phase voltage is 450 V at nominal speed.

The iron core losses are evaluated based on the data sheets of the SURAHAMMAR quality CK30, 0.35 mm. The peak flux density in the iron core is 0.43 T according to the FEM-program. The power losses in the iron are 1 W/kg at 100 Hz and 0.5 T, according to the data sheets.

The inductance of the winding is calculated using the two-dimensional FEM-program. The main inductance,  $L_h$ , and leakage inductance of the active region,  $L_{\lambda a}$ , are:

$$L_h=2.4 \text{ mH}$$

$$L_{\lambda a}=0.46 \text{ mH}$$

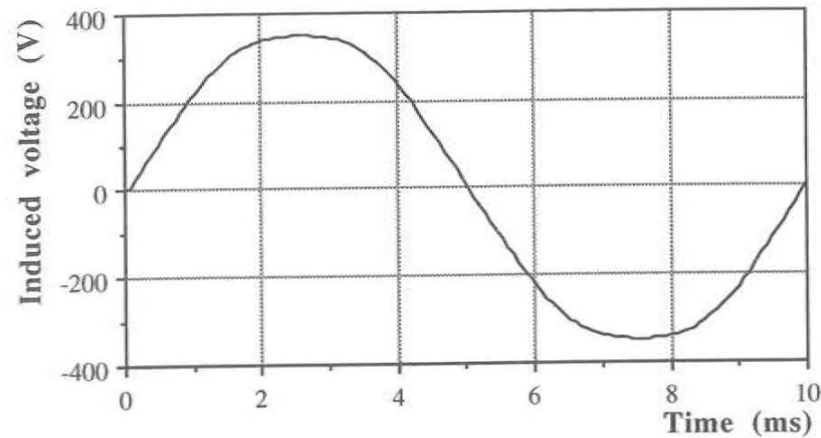


Figure 4.11. Calculated winding voltage.

The inductance of the end turns is added to the leakage inductance. This value is calculated with the FEM-program assuming that the end turn is an infinite conductor situated at a distance of 20 mm from the iron core. The evaluated inductance per meter is multiplied with the length of the end turn. The resulting leakage inductance of the end turns is

$$L_{\lambda e} = 0.96 \text{ mH}$$

The synchronous inductance in the machine is, hence, calculated at

$$L_d = L_\lambda + \frac{3}{2}L_h = L_{\lambda a} + L_{\lambda e} + \frac{3}{2}L_h = 5.0 \text{ mH}$$

The eddy current losses in the winding are calculated using the Fourier components of the flux density in the winding. The width of the conductors in the tangential direction is  $\Delta x_{cu} = 0.8$  mm and in the axial direction the width is  $\Delta y_{cu} = 2.0$  mm, see Figure 4.12. The flux density varies with position but the flux density in the middle of the winding is used as an approximation. The Fourier components in the middle of the winding are displayed in Table 4.4.

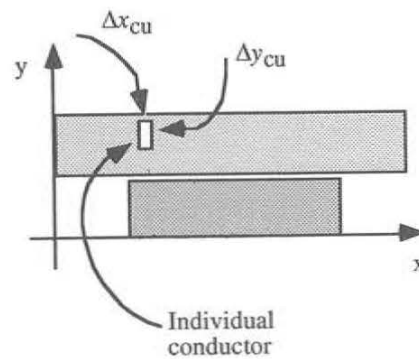


Figure 4.12. Definition of the conductor widths.

Table 4.4. Fourier components of flux density waves.

Order of flux density wave $n$	Axial direction $B_{ypn}$ (T)	Tangential direction $B_{xpn}$ (T)
1	0.62	0.121
3	0.112	0.0196
5	0.0293	0.0284
7	0.0067	0.0244

The power losses per unit length due to eddy currents in the conductor are [37]:

$$P_{nR} = \Delta x_{cu} \Delta y_{cu} n^2 \omega^2 (\Delta y_{cu}^2 B_{xpn}^2 + \Delta x_{cu}^2 B_{ypn}^2) \frac{1}{24\rho} \quad (4.1)$$

where  $n$  is the order of flux density wave  $\Delta x_{cu}$  and  $\Delta y_{cu}$  is the conductor width in  $x$  and  $y$  direction respectively.

The calculated electrical parameters are summarized in Table 4.5.

Table 4.5. Electric data of tested machine.

Resistance (at 20° C)	2.44 Ω/phase
Reactance	3.1 Ω/phase
Nominal current	6.5 A
Mechanical power	5.1 kW
Electric power	4.6 kW
Copper losses	310 W
Iron core losses	18 W
Eddy current losses in conductors	132 W
Efficiency	91 %

#### 4.2.2 Measurements of Machine Parameters

The stator was built in two steps. Some measurements were taken using only one stator winding, called stator No.1. At this time the flux density was measured in the space where the winding of the second stator, stator No.2. would be situated.

When the flux density in the winding was measured the total winding thickness was 1 mm smaller than the final magnetic air gap. The flux density at different radii is shown in Figure 4.13 and Figure 4.14. From Figure 4.13 it is clear that the flux density is not constant with the radius and in this case the 2-dimensional analysis is not sufficient. The error in measuring is in the range of  $\pm 5\%$ .

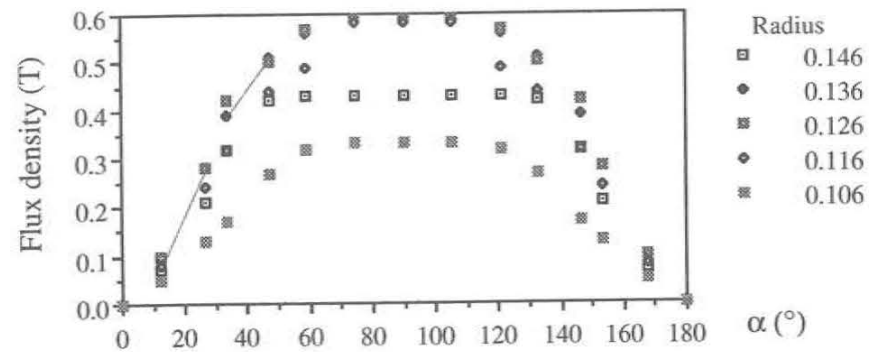


Figure 4.13. Flux density at different radii at the stator iron core.

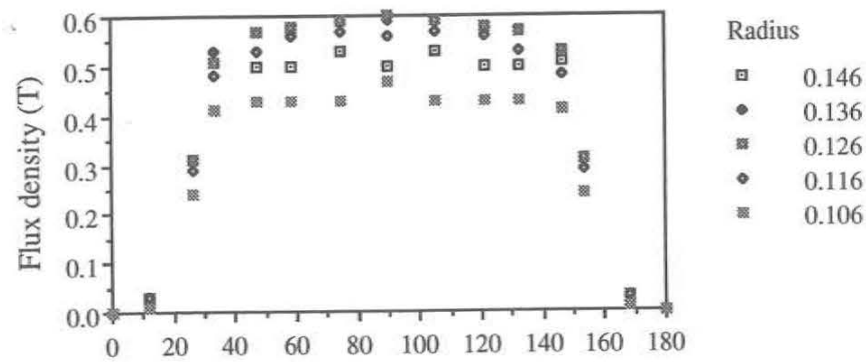


Figure 4.14. Flux density at the magnet

The induced voltage is evaluated with the three-dimensional data as input. The data measured in the space of stator No.2 are used as input into the PERMASYNK-program. Figure 4.15 shows the calculated and measured induced winding voltage, respectively, in the first stator No. 1.

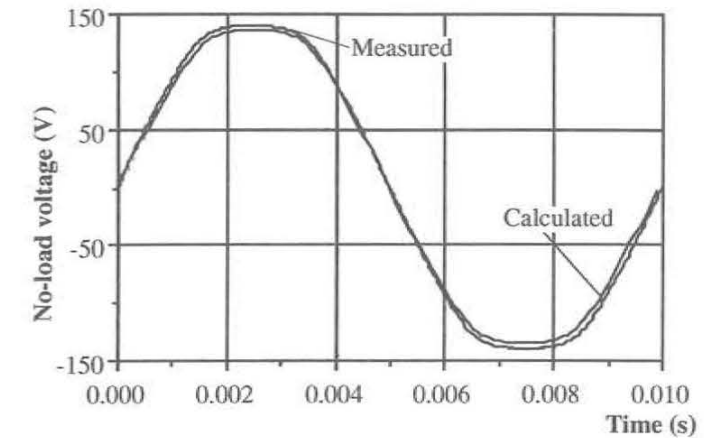


Figure 4.15. Comparison of measured and calculated induced voltage,  $n=1000$  rpm.

This method of calculating induced voltage gives good agreement between calculated and measured voltage. The error is 1 %, which is closer to the measured value than the calculated value of the voltage based on the two-dimensional calculated data.

After assemblance of the whole stator the impedances of the machine were measured. The resistance of the complete machine winding was measured with a DC-current and the inductances were measured using a single-phase AC-current, 50 Hz. The impedances are summarized in Table 4.6.

Table 4.6 Measured impedances

Phase	$R_{dt}$ ( $\Omega, 22^\circ\text{C}$ )	$X_\lambda + X_h$ ( $\Omega$ )
a	2.10	1.42
b	2.08	1.45
c	2.08	1.43

The leakage reactance was measured when all phases were connected in series and the main flux was cancelled. The leakage inductance is  $L_\lambda = 1.2$  mH and the mean winding inductance is  $L_\lambda + L_h = 4.5$  mH, i.e. the main inductance  $L_h = 3.3$  mH. Finally the synchronous reactance,  $X_d$  is:

$$X_d = \omega(L_\lambda + \frac{3}{2}L_h) = 3.86 \Omega$$

$$L_d = 6.1 \text{ mH}$$

The electric frequency is 100 Hz at nominal speed, which means that  $\omega=200\pi$  rad/s. The reactance was also measured by using an inductive load and it is found that  $X_d=3.95 \Omega$ , i.e.  $L_d=6.3$  mH. The measured value of the reactance is 27 % higher than the calculated value, which is not satisfactory. In order to evaluate the leakage flux from the end windings a more accurate three-dimensional method should be used. The equivalent parameters of the machine are summarized as:

$$\begin{aligned} E &= 245 \text{ V} \\ R &= 2.1 \Omega \text{ (0.056 p.u.)} \\ X_d &= 3.95 \Omega \text{ (0.105 p.u.)} \end{aligned}$$

The next step was testing the machine with both stators at no-load. A set-up according to Figure 4.16 was used in the following measurements.

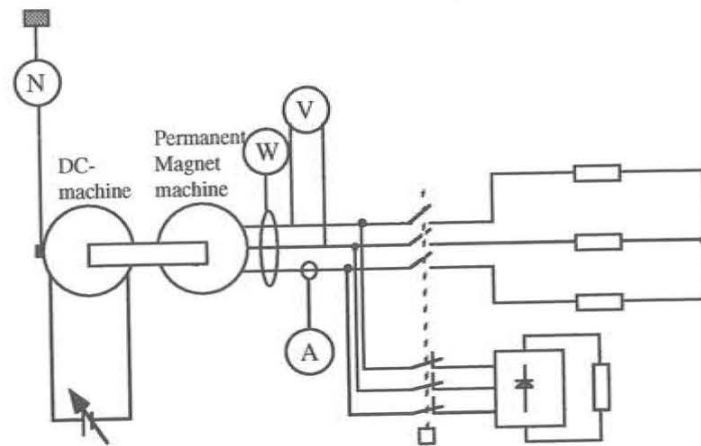


Figure 4.16. Test set-up

The induced no load voltage between the phases is  $E_h=425$  V ( $n=1000$  rpm), which is 5.5 % lower than the calculated value. The necessary torque required to rotate the machine was measured. At 1000 rpm the no-load torque is  $T_0=1.6$  Nm, which corresponds to a no-load power loss of 168 W. These power losses should be compared with the calculated iron core losses and eddy current losses in the conductors. The calculated value is 150 W excluding mechanical losses in the bearing and due to air friction. The calculated value agrees well with the measured value.

#### 4.2.3 Test with Resistive Load

At 1000 rpm, the machine was loaded with different resistive loads. The measured mechanical and electrical power is displayed in Figure 4.17 and the efficiency curve is shown in Figure 4.18. At nominal conditions the efficiency of the machine is  $\eta=91.6$  %.

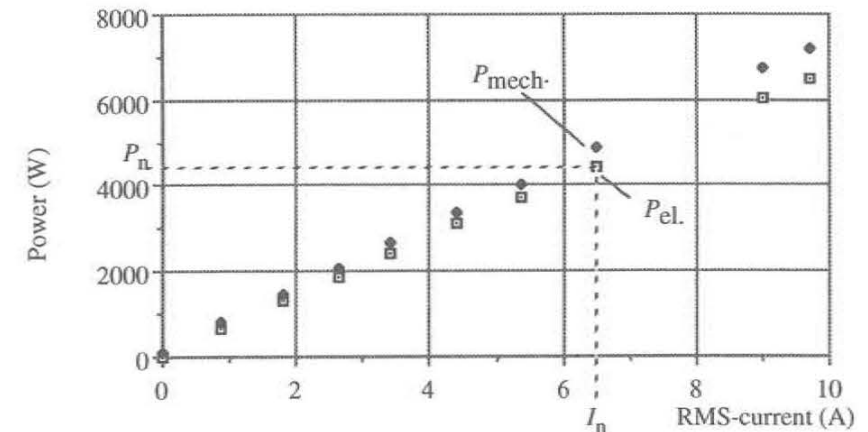


Figure 4.17. Mechanical and electrical power

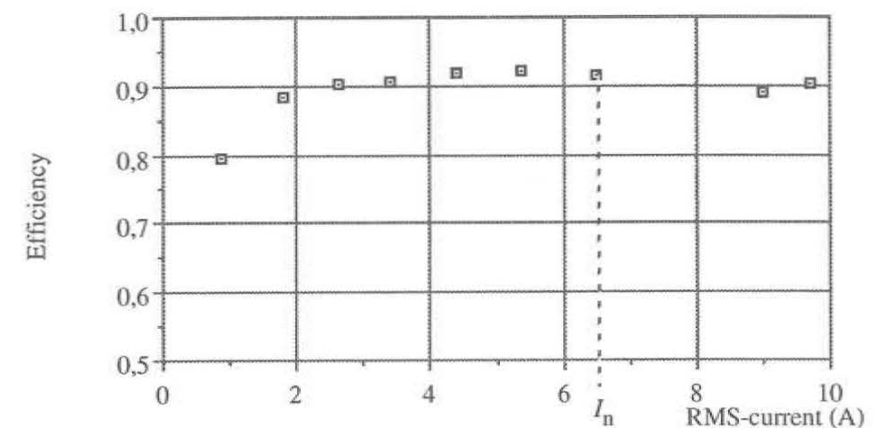


Figure 4.18. Efficiency of the generator with resistive load.

The total losses at 1000 rpm and nominal current are 409 W. Subtracting the measured no-load losses, the current-dependent losses are 241 W. Calculating the ohmic losses using the measured resistance yields the figure of 266 W. This difference can be explained by measurement error or an actual decrease in the losses in the winding. This decrease may be explained by the fact that

flux density decreases slightly in generator operation when current is applied to the winding. This decrease will lower the eddy current losses in the winding. The error corresponds to 0.5 % of the machine power. The measured data are compared with the calculated data in Table 4.7.

Table 4.7. Calculated and measured electric and mechanical data.

	Calculated	Measured
Resistance, $R$ (at 20° C)	2.44 $\Omega$	2.1
Reactance, $X_d$	3.1 $\Omega$ /phase	3.95
Nominal current, $I_n$	6.5 A	6.5 A
Mechanical torque, $T_{mech}$	48.7 Nm	46.4 Nm
Mechanical power, $P_{mech}$	5099 W	4859 W
Electric power, $P_{el}$	4640 W	4450 W
Ohmic losses, $P_{cu}$	310 W	266 W
Iron losses, $P_{fe}$	18 W	
Eddy current losses, $P_{Ft}$	132 W	
No-load losses, $P_{fe}+P_{Ft}$	150 W	
$P_{fe}+P_{Ft}+P_{fric}$		168 W
Efficiency, $\eta$	91 %	91.6 %

#### 4.2.4 Test with Diode Rectifier

The machine performance was measured once again with a diode rectifier loaded by means of resistance. The current at nominal conditions, i.e.  $I=6.5$  A, is shown in Figure 4.19.

The measured overlap angle is 21° and the commutation inductance is, hence, calculated at  $L_k=9.8$  mH, i.e. 78 % of twice the measured synchronous inductance. There are some parts in the machine that conduct eddy currents during the commutations, which lowers the inductance during this transient.

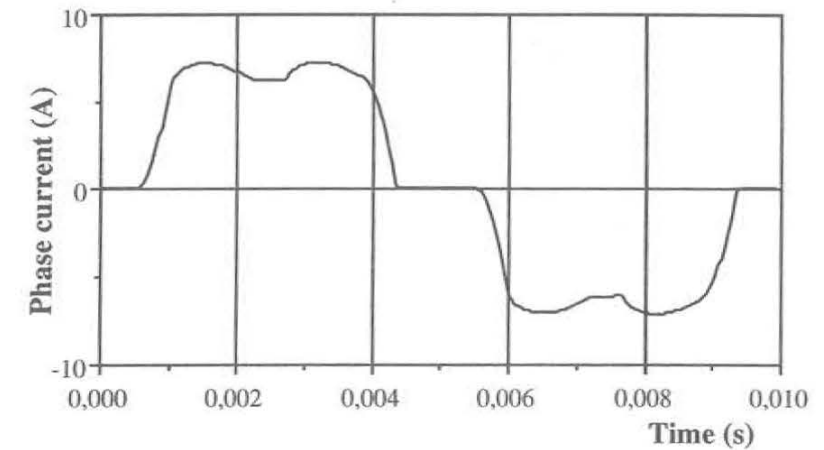


Figure 4.19. Current at rectifier load.

At 1000 rpm the electrical power and mechanical power were measured again. Figure 4.20 shows the measured power, and the efficiency is displayed in Figure 4.21. At rated conditions the efficiency is 91%. In the case of a diode rectifier load, the electric output from the machine is reduced to 4180 W, i.e. 94 % of the output at resistive load. The low inductance of this machine makes it suitable for this type of converter.

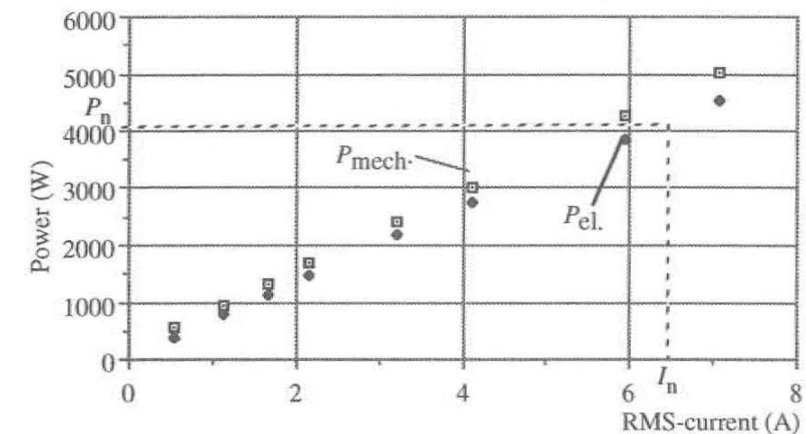


Figure 4.20. Power at rectifier operation. The current is the RMS-value of the machine current.

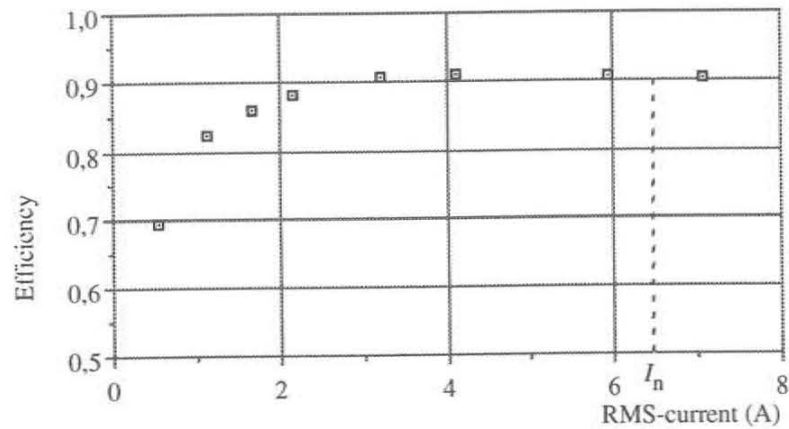


Figure 4.21. Efficiency at rectifier operation.

### 4.3 6-pole Machine for High Speed

As mentioned earlier, a group in Great Britain [3,5] is working on a gas turbine application to a hybrid vehicle. The generator is an axial flux machine with several stators and rotors. The machine used in the reference mentioned, has pieces of permanent magnet material embedded in fiber carbon material. Contrary to this, the machine described in this chapter has a homogeneous rotor magnet that is magnetized in different sections. The stator and rotor parts that are suggested may be used in a multi-rotor machine, according to Figure 2.4. The rotor is displayed in Figure 4.22. A ring of carbon fibre composite material can be placed around the magnet. In the cases in which several rotor and stator parts must be used, the winding can not have crossing end parts if it is not very thin. The lack of space between the two rotor parts, especially at the inner radius  $r_i$ , implies that the end parts must be manufactured in a special way.

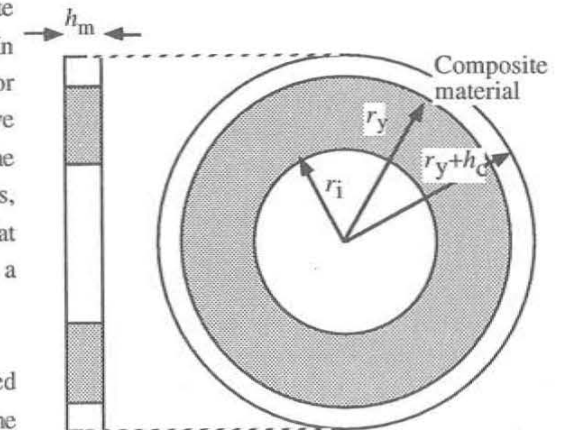


Figure 4.22. Magnet ring to a high speed axial flux machine.

The main data of the machine parts are listed in Table 4.8. According to Chapter 3, the winding thickness should be slightly thinner than the magnet. The winding thickness 3 mm is used.

Table 4.8. Main data of axial flux high speed segment.

Outer radius	$r_y=0.036$ m
Inner radius	$r_i=0.02$ m
Air gap	$h_\delta=0.5$ mm
Axial thickness	$h_m=4$ mm
Fundamental flux density	$B_f=0.62$ T
Current density	$J_{1cu}=6 \times 10^6$ (A/m <sup>2</sup> )
Fill factor	$k_{cu}=0.5$
Magnet weight	$m_{Nd}=83$ g
Number of pole pairs	$p=3$

In this axial flux machine the space for the end turns at the inner radius is limited. For that reason, a special winding must be used. Figure 4.23 shows one coil of a possible winding. The thickness of each coil is 1 mm. Six such coils form one phase and are placed 60° deflected from each other

and coupled in series. The two other phases are deflected 120 electrical degrees from each other and then joined to a unit, see Figure 4.24. The three phases are a unit with the axial thickness of 3 mm. The number of turns in each coil is 8, and the winding is made of a Litz-wire consisting of 60 strands with the individual conductor diameter of 0.1 mm. The complete stator winding is displayed in Figure 4.24.

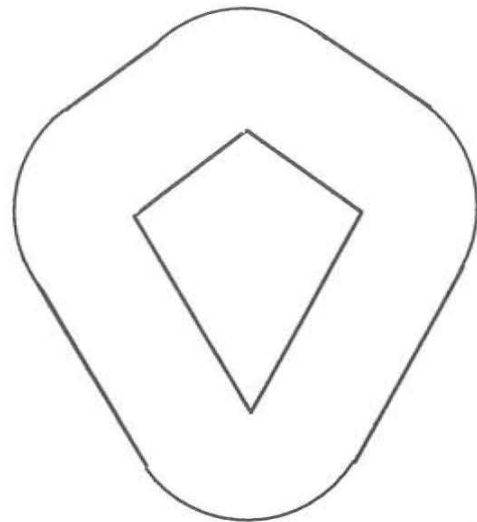


Figure 4.23. One coil of the winding

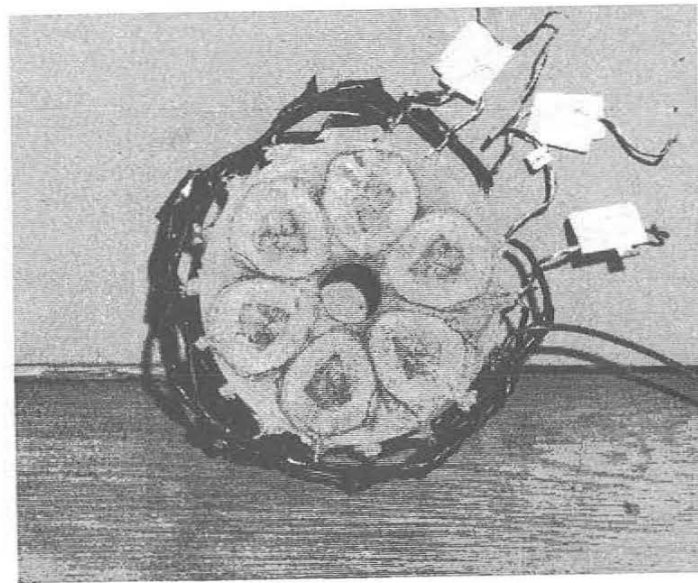


Figure 4.24. Photo of the stator to an axial flux machine

This stator is glued to an iron powder core with a relative permeability of 35. If the winding is used with several stators, the winding should be doubled and placed between two rotors. Figure 4.5 shows the rotor and stator.

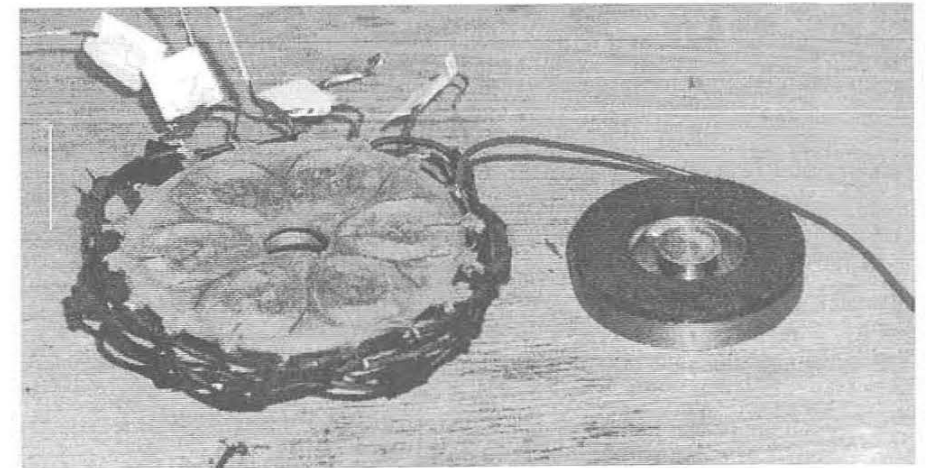


Figure 4.25. Rotor and stator to an axial flux machine.

#### 4.3.1 Magnetisation

The motor has six poles and in order to achieve this the rotor disk is magnetized in a six-pole configuration according to Figure 4.26. The magnet ring is magnetized using the magnetizer shown in Figure 4.27. With this magnetizing equipment the remanent flux density in the middle of the pole is 0.94 T after the first magnetization. After an extra magnetization the remanent flux density increases to 0.97 T. According to the manufacturer this material should have  $B_r=1.1$  T, which implies that the magnet material is not fully magnetized.

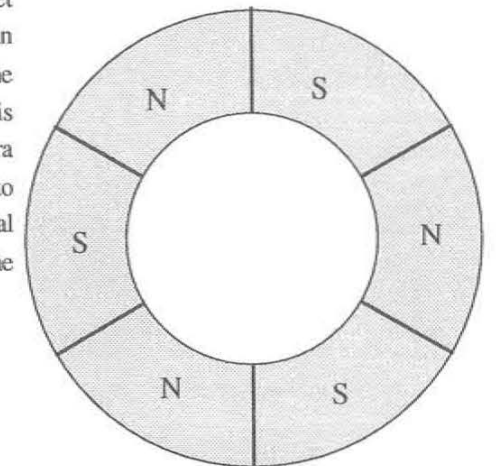


Figure 4.26. The different sections of an axial flux rotor

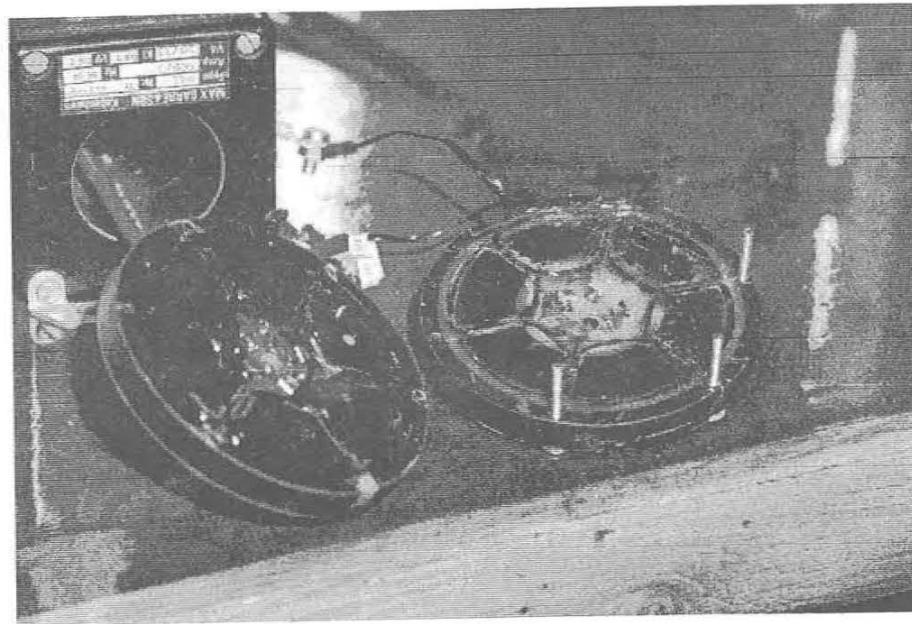


Figure 4.27. The magnetizing winding.

#### 4.3.2 Calculations

The flux density in the winding is evaluated with the FEM-program. The amplitude of the fundamental flux density wave is 0.51 T.

The winding factor of this particular winding is found in Appendix B, Equation (B.11). The dimensions of this machine yield the value of winding factor  $k_w=0.4$ . The value is calculated numerically.

The calculated induced voltage of the machine is:

$$e_{1p} = k_w p N_p \frac{2}{\pi} B_{1p} \omega \frac{\pi}{6} (r_y^2 - r_i^2) \quad (4.2)$$

which yields the induced RMS-voltage of 0.45 V at 695 rpm.

Assuming a constant fundamental flux density amplitude in the whole winding volume, i.e.  $B_{1p}(y)=B_{1p}$ , the torque from an axial flux machine equipped with a winding according to Figure 3.2, may be written as [13]:

$$T = \frac{3}{2} k_{cu} B_{1p} J_{1pcu} r_i h_l (r_y^2 - r_i^2) \quad (4.3)$$

and with the data according to Table 4.8 the torque from this machine size is

$$T=0.21 \text{ Nm}$$

This value should be compared with the results achieved with the special winding.

#### 4.3.3 Measurements

The machine was tested at low speed in order to measure the induced voltage and in order to calculate the possible torque. The induced voltage of the machine was measured at 695 rpm. The induced phase-to-zero voltage in one stator winding is  $E=0.448$  V. The RMS-value of the phase current is 2.8 A at a current density of  $J=6$  A/mm<sup>2</sup>. The calculated value of the torque is  $T=0.05$  Nm if the current is directed in the q-direction. If a better magnetic material,  $B_r=1.3$  T, is used it would be possible to increase the torque to 0.067 Nm. The achievable torque is 32 % of the value calculated using Equation (4.3). The low torque is due to the special winding that is used. The described winding has a low winding factor and the coil has a thickness that is only one third of the whole winding.

#### 4.4 Discussion

The tested radial flux machine with an air-gap winding performs almost the same as the slotted machine. The power losses can be lowered with a better iron core material and there are better permanent magnet materials that can enhance the performance of the slotless machine.

The calculation approach shows good agreement with measured values. In the tested 12-pole axial flux machine the length of the pole in the radial direction is short compared with the winding thickness, which implies a high leakage of magnet flux. This leakage flux should be evaluated by using three-dimensional FEM programs. Using three-dimensional measured flux density data as input to the PERMASYNK-program gives good agreement between the calculated induced voltage and the measured value. In the 12-pole machine with relatively low frequency, the prediction of power losses is adequate.

The tested high-speed axial flux machine with the special winding has a rather low torque compared to what should be possible to achieve with a normal winding. A more normal winding can be used but in such a case it must be thinner in order to cross the end turns.

## 5 Comparison of Radial and Axial Flux Machines

The axial flux machine has been suggested for use in high torque concepts and in high speed applications. It is of great interest to compare the machine with other concepts and especially with the radial flux machine.

The torque production in the axial flux air gap wound machine is analysed and compared with that of the radial flux machine. A small current-carrying element in the vicinity of the outer radius of an axial flux rotor is considered, see Figure 5.1.

The flux density is directed in the axial direction. The conductors are directed radially. The angular force in a small element, situated in a uniform magnetic field, is

$$dF = J \cdot B \cdot r dr d\theta dz \quad (5.1)$$

The torque acting on this small volume is

$$dT = r \cdot dF = r^2 J \cdot B \cdot dr d\theta dz \quad (5.2)$$

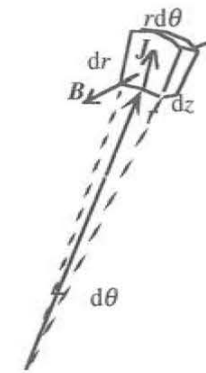
$$r \leq r_y$$

where  $r_y$  is the outer radius of the winding and the magnet.

In the radial flux machine, the current carrying conductor is situated just outside the rotor with a radius approximately equal to the outer radius of the magnet, see Figure 5.2. In the radial flux machine, the magnetic flux is directed in the radial direction and it is assumed that the flux is constant independent of the actual radius. We may assume that the flux density, directed radially, decreases proportionally to the inverse of the radius. In the vicinity of the rotor periphery, we get the following force on the small current carrying element:

$$B(r) = B(r_y) \frac{r_y}{r}; \quad r \geq r_y \Rightarrow \quad (5.3)$$

$$dF = J \cdot B(r_y) \frac{r_y}{r} \cdot r dr d\theta dz$$



Figur 5.1. A small current-carrying element in an axial flux machine.

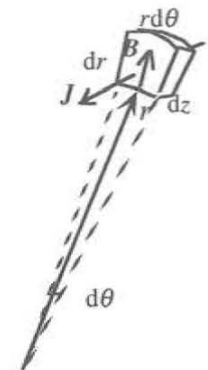


Figure 5.2. Current-carrying element in a radial flux machine.

The torque on this element is :

$$dT = J \cdot B(r_y) r_y r dr d\theta dz \quad (5.4)$$

$$r \geq r_y$$

What is interesting about this minor investigation is that in spite of the decrease of flux density  $B(r)$ , the torque on the element increases when the radius is increased. This increase is due to the increase of the current-carrying element volume with radius, and indicates that we can have a small rotor radius and still have a relatively large radius of the winding and a high torque.

Since the axial flux machine is distributed in the axial direction and approximately half the space is filled with conductors and the rest with permanent magnets, the necessary space in the axial direction is greater than that in the radial flux machine. The radial flux machine is distributed in the radial direction, which makes it shorter but the outer diameter is greater than the diameter of the axial flux machine if the rotor radius is the same. If the different current elements would develop the same torque in the radial and the axial flux machines, the radial flux machine should produce more torque per unit length.

In a case in which the rotor radius of the axial flux machine can be increased to the same value as the outer radius of the radial flux winding,  $r_2$ , the comparison is different. A radial flux machine with four poles is compared with the axial flux machine. The radial flux machine can have the rotor on the outside of the stator or it may be inside the stator, according to Figure 5.3.

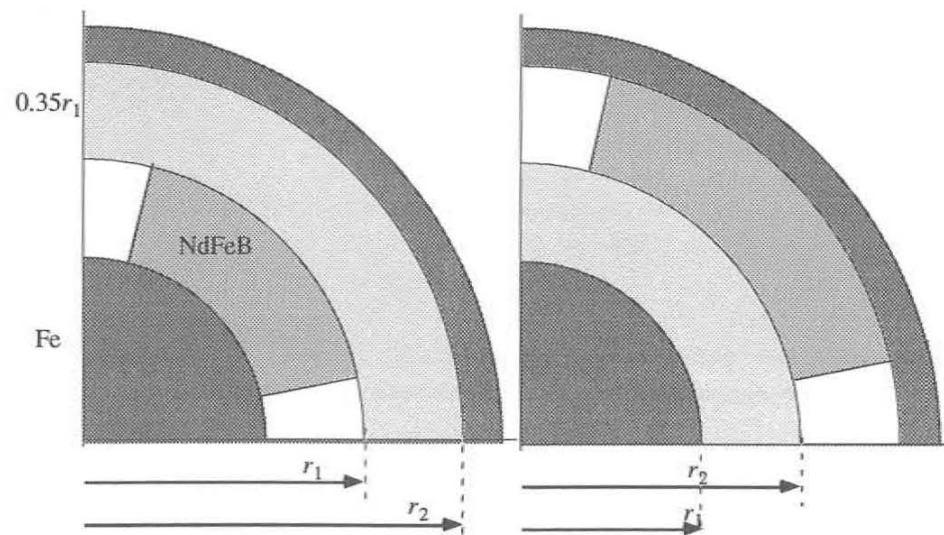


Figure 5.3. Inner rotor radial flux machine and outer rotor radial flux machine.

In the two cases above the thicknesses of the winding and the magnets are equal to  $0.35r_1$ , and the magnet width is 70 % of the pole pitch. The coercive force of the magnet corresponds to a relatively high energy material,  $H_c=920$  kA/m. The relative permeability of the yoke is  $\mu_r=1000$ . The flux density in the winding region is evaluated with the FEM-program. The fundamental flux density at different locations in the winding are displayed in Figure 5.4.

The fundamental wave in the winding of the inner-rotor machine is approximated according to the following formula:

$$B_{1p}(r) = k_1 \left( \frac{r}{r_1} \right)^{-k_2} \quad (5.5)$$

$$k_1 = 0.6309 \text{ T}$$

$$k_2 = 1.596$$

$$r \geq r_1$$

In the outer rotor configuration, the flux density fundamental is approximated as:

$$B_{1pouter}(r) = k_3 - k_4 \left( \frac{r}{r_1} \right) + k_5 \left( \frac{r}{r_1} \right)^2 \quad (5.6)$$

$$k_3 = 1.7347 \text{ T}$$

$$k_4 = 2.447 \text{ T}$$

$$k_5 = 1.382 \text{ T}$$

The approximations are shown in Figure 5.4.

Considering the fundamental waves, the torque is expressed by (3.12), i.e. an integral, current loading and constants. The integral is:

$$g = \int_{r_1}^{r_2} r^2 \cdot B_{1p}(r) dr \quad (5.7)$$

The integral is evaluated numerically for both cases and the resulting values for the inner and outer rotors are:

$$g_{inner} = 0.236r_1^3$$

$$g_{outer} = 0.161r_1^3$$

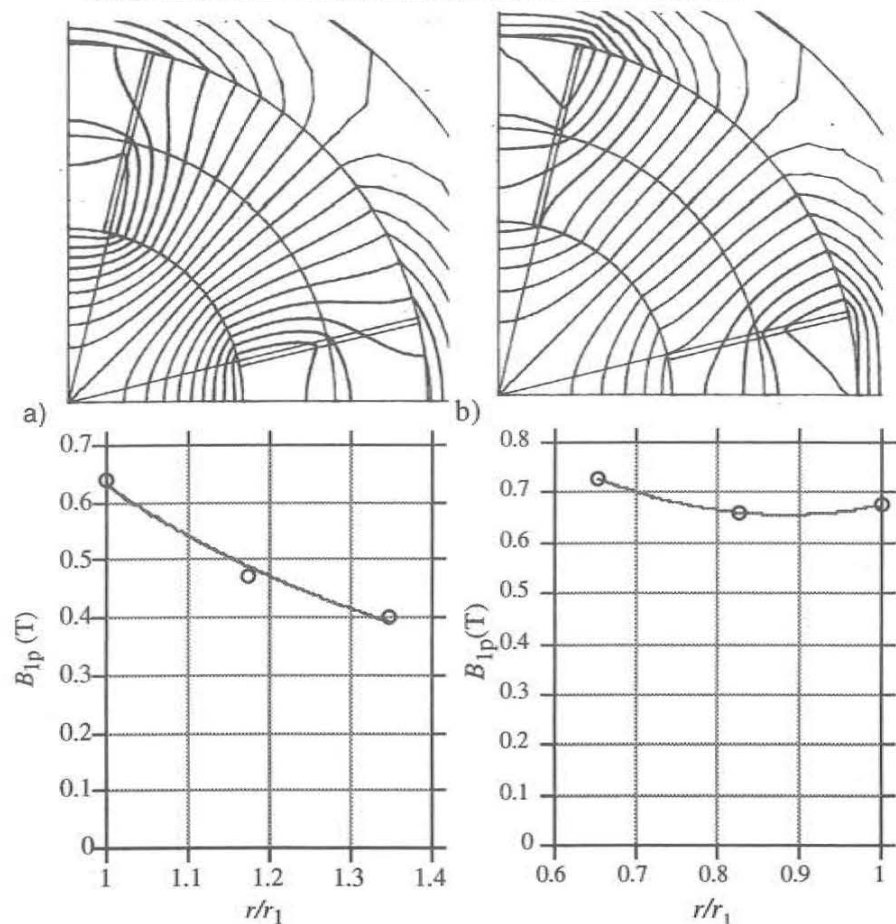


Figure 5.4. Calculated flux density of a) inner rotor construction and b) outer rotor.

The inner rotor configuration produces 46 % more torque, although the amount of magnetic material is 70.4 % of the outer rotor configuration. The outer rotor machine is not suitable for air gap windings, due to a concentration of the magnetic flux for smaller radii. The flux is to converge into the stator which means an increased flux density. The area through which the flux is to flow decreases which means an increased reluctance at small values of the radius and that the flux flows easier along a leakage path that does not penetrate the winding.

An axial flux machine is compared to these radial flux machines. It is assumed that the active materials of the axial flux machine have the same inner and outer radii as the winding of the inner rotor machine. As a first approximation, it is assumed that the flux density is constant with radius and axial positions. The axial flux machine is displayed in Figure 5.5.

In the axial flux machine, the current density is proportional to the inverse of the radius. It is assumed that flux density is constant  $B_{1p}=0.65$  T. According to Figure 3.5 this corresponds to a

magnet thickness of  $h_m=1.2h_1$  and a magnet width of 70 % of the pole pitch and a remanent flux density  $B_r=1.2$  T. The integral of the axial flux machine is:

$$g = \int_{r_1}^{r_2} \frac{1}{r} r^2 \cdot B_{1p}(r) dr = 0.266r_1$$

$$r_y = r_2 = 1.35r_1$$

$$r_i = r_1$$

It should be possible to achieve more torque from this construction in comparison to the radial flux machines. It is however necessary to evaluate the flux that leaks at the inner and outer radii of the magnet. This leakage will lower the figure for the axial flux machine. The figure represents a torque per unit length and in this case the length is the thickness in the axial direction of the machine. The magnet height is  $1.2h_1$ , i.e. the amount of magnetic material is 20 % higher than in the outer rotor construction.

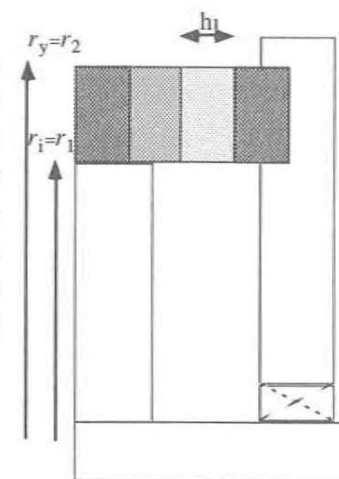


Figure 5.5. Axial flux machine.

### 5.1 High Torque Machine

It has been shown that the axial flux machine must have a high rotor radius in order to be comparable to the radial flux machine. To exemplify this, the tested axial flux machine with air gap winding, according to Section 4.2, is compared to a radial flux machine with the same mean radius. The mean radius is defined as the air gap radius of the radial flux machine and as the mean radius of the active area for the axial flux machine. The fill factor of copper is the same in the two machines.

The axial flux machine achieved the fill factor of copper at the inner radius:

$$k_{cu} = 0.495$$

The current loading, i.e. current per length unit is

$$k_{cu} h_1 J_{1cu} = 22737 \text{ A/m}$$

Neglecting the effect of flux leakage in the radial direction, the flux density of this machine is according to Section 4.2.1 :

$$B_{1p} = 0.62 \text{ T}$$

The corresponding electromagnetic torque may be calculated according to Equation (4.3):

$$T=48.8 \text{ Nm}$$

A radial flux machine with the same fill factor of copper, i.e. current loading, is calculated. The torque of a radial flux machine is approximately:

$$\begin{aligned} T &= 3k_{cu} J_{1pcu} l_{st} \cos(\beta) \int_{r_1}^{r_2} r^2 \cdot B_{1p}(r) dr \approx \\ &\approx 3k_{cu} J_{1pcu} l_{st} h_l r_{12}^2 \cdot B_{1p} \end{aligned} \quad (5.8)$$

where

$$r_{12} = \frac{r_1 + r_2}{2} = 0.134$$

The integral in this example can be simplified, as it has a small pole pitch in relation to the radius. The flux density is evaluated with the FEM-program in the middle of the winding:

$$B_{1p} = 0.59 \text{ T}$$

In order to produce the same torque at the same current density the machine should have the length:

$$l_{st}=72 \text{ mm.}$$

The weights of the active materials are listed in Table 5.1, which does not include the end windings.

Table 5.1. Weight of material in axial flux and radial flux machine

	Axial flux machine	Radial flux machine
Copper weight, $m_{cu}$	2.04 kg	2.23 kg
Magnet weight, $m_{Nd}$	2.71 kg	2.14 kg
Iron weight, $m_{fe}$	6.85 kg	6.28 kg
Total weight	11.6	10.6 kg

The rotor core material should be added to the weight of the radial flux machine. This material can, however, be used as a part of the rotor and it can be solid, which is a cheap solution. It is shown that, in a case where the radial flux machine has the same mean radius, the active material has a lower weight than the active material of the axial flux machine. The amount of magnet material is lower in the radial flux machine.

In the tested machine the length of the pole ( $r_y-r_1$ ) is too small in relation to the winding thickness, which implies a high flux leakage at the inner and outer radii of the magnet. The radial flux machine has longer poles and the amount of leakage flux will be lower.

## 5.2 High-speed Machine

The tested axial flux machine according to Section 4.3 has the following data:

$$T=0.05 \text{ Nm}$$

$$r_y=0.036 \text{ m}$$

$$k_{cui}=0.376 \text{ (fill factor at the inner radius of the machine)}$$

$$l_{ax}=0.0075 \text{ m (axial length of magnet, air gap and winding)}$$

With a better magnetic material,  $B_r=1.3 \text{ T}$ , and full magnetization it should be possible to increase the torque to  $T=0.067 \text{ Nm}$ .

The torque from the radial flux shaft magnet rotor machine according to Section 3.2 is:

$$T=25 \text{ Nm/m (} h_l=15 \text{ mm and } J_{1cu}=6 \text{ A/mm}^2\text{)}$$

Scaling this torque to the same magnet radius, fill factor and better magnetic material, as in the axial flux machine, yields the following figures:

$$T_{\text{radial}}=280 \text{ Nm/m}$$

$$T_{\text{axial}}=8.93 \text{ Nm/m}$$

In this case where the radius is restricted, the radial flux machine has a much higher torque to

length ratio.

If all dimensions are scaled up the torque of the axial flux machine increases with the cube of the radius, which implies that the axial flux machine radius must be:

$$\left(\frac{r_{\text{axial}}}{r_{\text{radial}}}\right)^3 = \frac{280}{8.9} \Rightarrow r_{\text{axial}} = 3.2 r_{\text{radial}} \quad (5.9)$$

The axial flux rotor radius must be 3 times the rotor radius of a radial flux machine. If this can be solved with another mechanical arrangement, the axial flux machine may be an alternative.

The axial flux machine must generally use more active material in comparison with the radial flux machine in order to produce the same torque. The advantage of the axial flux machine is the simple construction with an iron core that is wound to the right dimension.

## 6. Investigation of a Pole with Integrated Teeth

Iron powder material can be formed to an entire stator with slots and teeth, similar to the way in which sheets are punched and stacked to the stator core. Earlier works [21,6,22] have concentrated on iron powder with teeth and winding in the conservative sense. Pressing big stator cores leads to very high forces which limits this method to smaller machines. Recently, a technique for building big stators was developed. Essentially this technique is based on producing smaller pieces that are joined to a bigger stator [2].

As a new approach to winding production it is here assumed that the winding region shall be produced before assemblance in the machine. Iron powder teeth are glued to the conductors before the assemblance. The core is not formed with the teeth attached; instead the teeth are integrated to the winding and mounted together with the conductors. The necessary insulation material between the phases and the yoke are fixed to the winding before mounting it to the yoke.

Before analysing machines with integrated teeth, a simplified flat pole is evaluated, see Figure 6.1. The teeth are made of an iron powder material and magnetized with an NdFeB magnet. The influence of the stator material permeability is evaluated using the FEM-program. The relative permeability was studied earlier by Boules and Weh [6] using analytical formulae. Since their study, the capacity of permanent magnetic material has improved which means that a material with permeability in the medium range may be used with the same flux density in the winding as a SmCo-material and a high permeability material. In their study, the air gap length was constant and the teeth were joined with the yoke. In this case, the influence from insulating parts between the winding and the yoke must be evaluated. There are many ways to choose all the parameters of the pole. Here it is assumed that a slot width that is equal to the tooth width is near the optimal value. Weh and Boules [36] have studied the influence of the slot width to slot pitch and have found that the power is maximized when the slot width is higher than half the slot pitch. Their study did not consider the power losses in the construction, and for other studies they have chosen a slot width equal to tooth width.

The goal is to find a stator that can be used with surface-mounted permanent magnets, producing a high force density. Another aspect is to find the maximal winding thickness, i.e. current loading. As we will see, a relatively long air gap will reduce the flux density ripple on the magnet surface

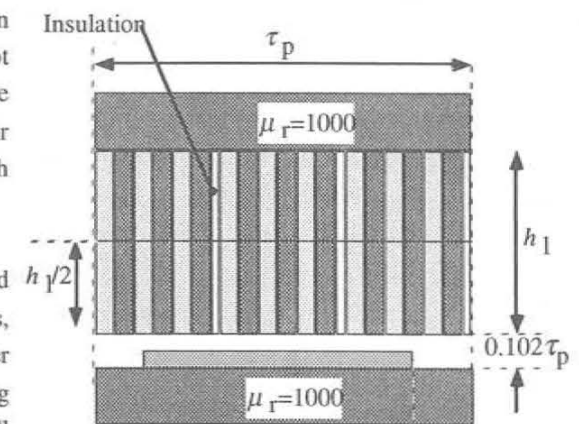


Figure 6.1 Analysed pole equipped with integrated teeth.

and reduce the inductance of the winding. As a start a stator with three slots per pole and phase, (i.e.  $q=3$ ), is studied, see Figure 6.1. The assumed remanent flux density of the magnet is  $B_r=1.3$  T.

### 6.1 Stator with Integrated Teeth

The stator, according to Figure 6.1, is studied and the flux density in the winding is evaluated using the FEM-program. The pole pitch and magnet width are held constant,  $\tau_m/\tau_p=0.7$ , which was found to be a good compromise earlier. The pole pitch of the studied structure is  $\tau_p=19.5$  mm. The mechanical air gap is, as a start, 5.1 % of the pole pitch and the magnet height is equal to the mechanical air gap. Between the phases there is a space for insulation material, with a thickness of 2.6 % of the pole pitch. In this way the space for the winding will be equivalent to the space for the teeth and the amount is 46 % of the winding region. In order to evaluate the armature reaction, current is applied to the winding in the q-direction. The armature reaction is studied at constant current loading and at constant current density in the conductors. The current density is  $J_{icu}=6$  A/mm<sup>2</sup>, which in the studied pole corresponds to a current loading of

$$S_1 = 51 \cdot 10^3 \frac{h_1}{\tau_p} \text{ (A / m)}$$

As a start, the flux density is studied as a function of iron powder permeability and the thickness of winding region. When current is applied to the winding the flux density in critical parts increases which increases the power losses. The limit for what is practical is studied in this first approach. With the flux density from the first study in mind, the influence of varied air gap, thickness of insulating material, tooth permeability with an insulating material between the winding and the yoke and, finally, the pole are evaluated more carefully with an assumed iron powder material, EF6880. In the last calculations, the non-linearity of the material is taken into account.

Under linear conditions the fundamental current and flux may be represented by vectors according to Figure 6.2. It is assumed that the rotor does not have salient poles. Two values of the flux in the q-direction are indicated: one corresponding to a machine with low armature reaction and the other is a case with relatively high armature reaction. The current in the q-direction produces torque with the flux in the d-direction, i.e. with the magnet flux. It is obvious that a machine with low armature reaction produces higher torque at the same total flux compared with a machine with high

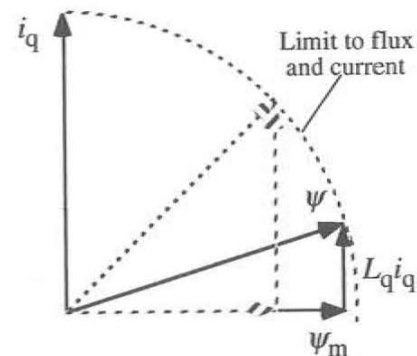


Figure 6.2 Vector representation of the flux.

armature reaction. The current produces a flux in the q-direction that is not useful in torque production but it increases the flux density in the magnetic parts, i.e. if the maximum permissible flux, due to limited power losses, is set, the amount of useful magnet flux will be lowered by the flux in the q-direction. In order to minimize the power losses the flux produced by the winding in this construction must be minimized. The increased flux will also correspond to an increased voltage, i.e. the converter that feeds the machine must feed the machine with reactive power and the converter has to have higher apparent power, which dimensions the converter.

The flux linkage is, according to Equation (2.2):

$$\begin{aligned} \Psi &= \Psi_d + j\Psi_q \\ \Psi_d &= L_d i_d + \Psi_m = \Psi_m \\ \Psi_q &= L_q i_q \end{aligned} \quad (6.1)$$

The current in the d-direction is assumed to be zero. The flux linkage is proportional to the flux density and therefore we can evaluate the fundamental flux density:

$$\begin{aligned} B &= B_{1d} + jB_{1q} \\ B &= |B| = \sqrt{B_{1d}^2 + B_{1q}^2} = \sqrt{B_{1m}^2 + B_{1q}^2} \end{aligned} \quad (6.2)$$

The flux density components  $B_m$  and  $B_q$  depend on the pole geometry and for the component from the magnet is dependent on the permanent magnetic material. The q-component depends on the current loading and the geometry. Finally, the total flux density  $B$  is the absolute value of the vectorial addition of the two components. The flux density is evaluated by means of the FEM-program.

#### 6.1.1 Flux Density at Varied Permeability

The influence of winding thickness,  $h_1$ , and the relative permeability of the teeth are investigated. As a start the relative permeability of the yoke is 1000. The flux density at varied winding thickness is displayed in Figure 6.3. As an approximation of the mean flux in the winding the fundamental flux density is evaluated along the line indicated in Figure 6.1,  $y=h_1/2$ . This simplification causes a negligible error as long as the relative permeability is over 50. Higher winding thickness can be used than with the air gap winding. With a relative permeability of 200 the winding can be as high as the pole pitch and the mean flux density remains at 0.6 T.

Current is applied to the winding and the flux density is evaluated again. The current is applied in the q-direction. Figure 6.4 shows the flux density at constant current loading,  $S_1=51$  kA/m. The mmf from the magnet is, in this case put to zero. For low relative permeability the flux density decreases with increased winding thickness. On the contrary, when the relative permeability is high the flux density is increased with increased winding thickness. At high winding thickness the leakage flux is increased.

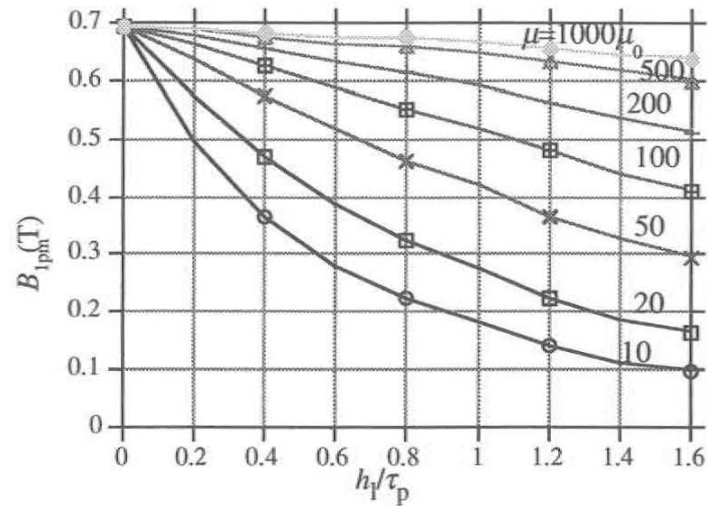


Figure 6.3. Fundamental flux density at different winding thicknesses with relative permeability as a parameter. The current is zero and the magnet thickness is constant.

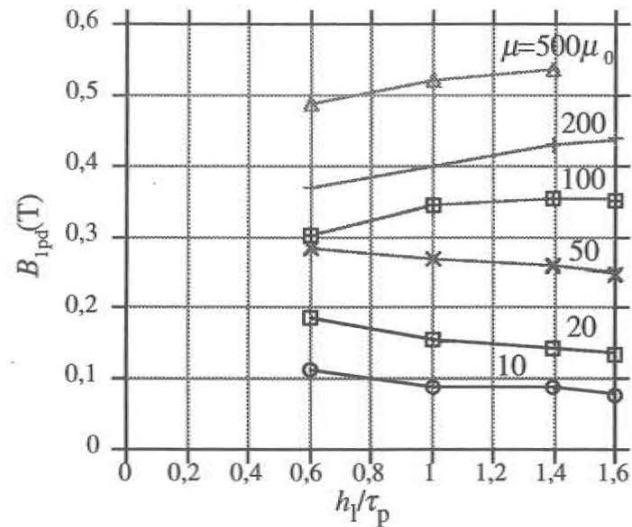
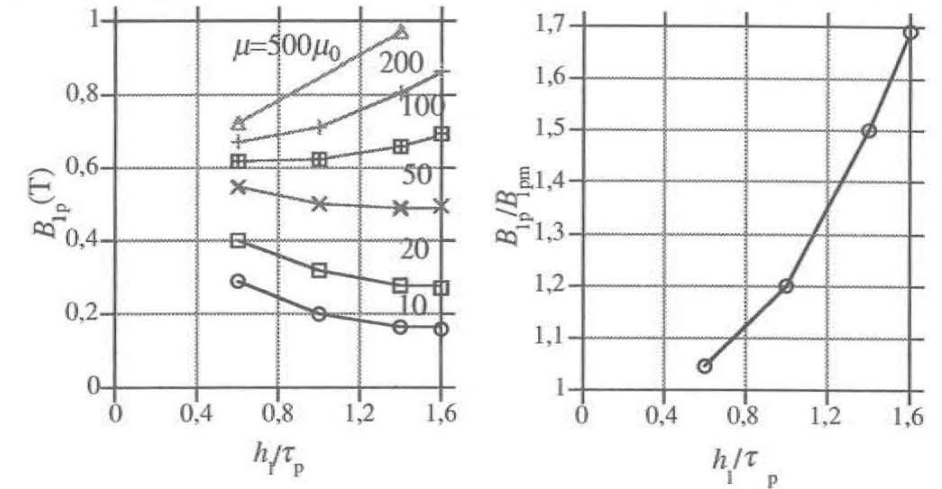


Figure 6.4 Flux density due to the winding and at constant current loading. Relative permeability as a parameter.  $S_1=51$  kA/m.

The power losses per unit volume are not dependent on current loading but on current density. At constant current density  $J=6$  A/mm<sup>2</sup>, the total flux density when current is applied is shown in Figure 6.5.a) The total flux density divided by flux density from the magnet is shown in Figure 6.5.b) The relative increase of flux density is approximately independent of the relative permeability in the studied interval, i.e. the relative per unit impedance does not depend on

permeability when current density is constant. The apparent power compared of the active power to the machine depends on how much the voltage must increase when the machine is loaded.



a) Figure 6.5.a) Total flux density when current is applied to the winding in the q-direction,  $J_{Cu}=6$  A/mm<sup>2</sup> b) Total flux density divided by magnet flux density when current is applied.  $\mu_r=100$ .

As an example it is possible to have a peak air gap flux density of 0.6 T if the iron powder material have a relative permeability of  $\mu_r > 100$  and modern permanent magnet material, With a reasonable current loading of  $S_1=51$  kA/m the increase of flux density corresponds to an apparent power that is 20 % higher than the active power, i.e.

$$\frac{B_{1p}}{B_{1pm}} = 1.2$$

### 6.1.2 Varied Air Gap Length

The air gap is increased in order to decrease the armature reaction of the stator. The winding thickness is fixed at  $h_1/\tau_p=1.4$  and  $h_1/\tau_p=1$ , respectively, and the magnet thickness is increased to 1.5 times the air gap. As the air gap is varied, the magnet thickness also varies. The resulting flux density at no-load is shown in Figure 6.6.

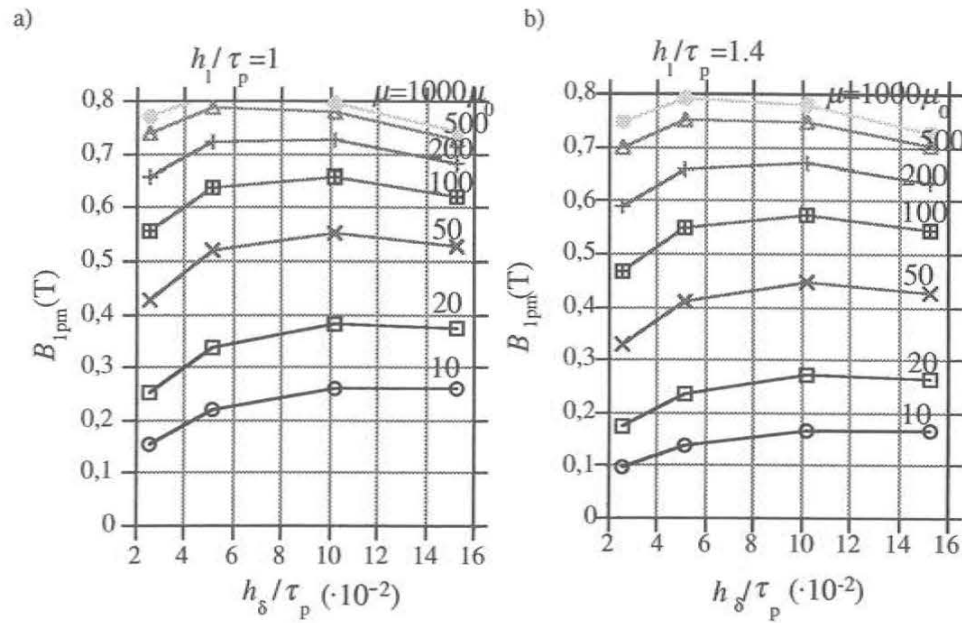


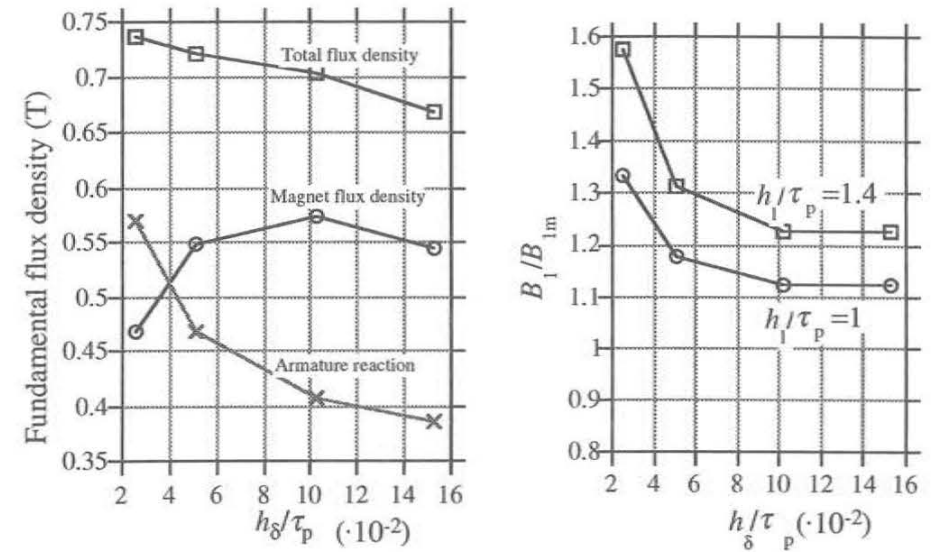
Figure 6.6. Flux density due to the magnet at varied air gap length with relative permeability as a parameter.  $h_m = 1.5 h_\delta$ . a)  $h_1/\tau_p = 1$ . b)  $h_1/\tau_p = 1.4$

For small magnet heights and, consequently, short air gaps the reluctance of the winding region reduces the flux density. The reluctance of the winding region is high in relation to the relatively thin magnet. For high magnets and air gaps, similar effects start as in the air gap wound machine; the magnet flux leaks around the magnet and does not pass the winding region at all. With current applied to the winding in q-direction the flux density is calculated again, and the ratio between the no-load flux density and the flux density in loaded conditions, is shown in Figure 6.7. An increased magnet thickness and air gap length does not decrease the armature reaction when the air gap exceeds 10 % of the pole pitch.

The magnetic vector potential is shown in Figure 6.8, when  $h_1/\tau_p = 1$  and the air gap length  $h_\delta$  is 10 % of the pole pitch. The fundamental flux density from the magnet is, in this case:

$$B_{1pm} = 0.65 \text{ T}$$

It is shown that if the air gap is increased, the armature reaction is decreased. With  $J_{1cu} = 6 \text{ A/mm}^2$ , the air gap is 10 % of the pole pitch and if the winding thickness is equal to the pole pitch, the total flux density will be 12 % higher than the magnet flux density. This increase of flux density seems to be a reasonable value of the armature reaction.



a) Figure 6.7. Flux density with current applied divided by magnet flux density.  $S_1 = 51 \text{ kA/mm}^2$ ,  $\mu_r = 100$ . a) The different components of the flux density,  $h_1/\tau_p = 1$ . b) Total flux density divided by magnet flux density.

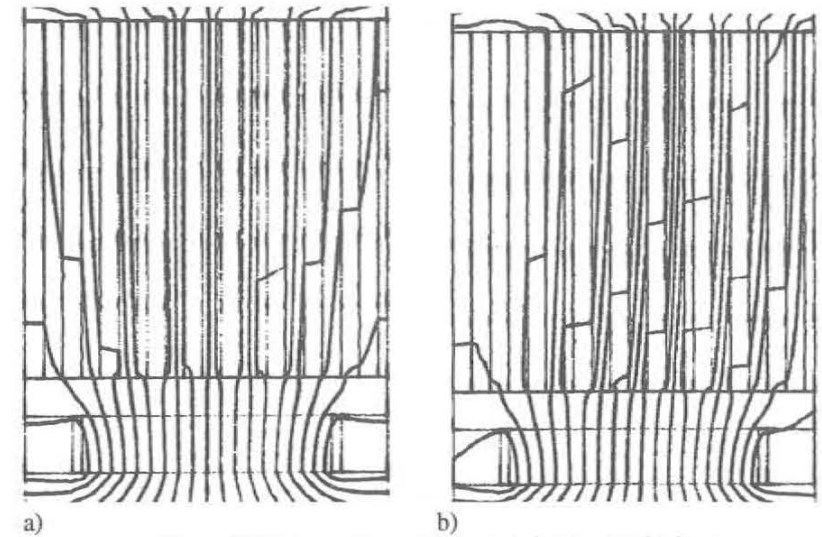


Figure 6.8. Magnetic vector potential of the studied pole. a) No-load. b)  $S_1 = 51 \text{ kA/mm}^2$  q-direction.

### 6.2 Further Investigations of a Pole with $q=2$

In the previous section, it was found that iron powder material may be used in permanent magnet machines with a high winding thickness and relatively high fundamental flux density. The pole, must, however have insulation material between the different phases of the winding and between the winding and the yoke. This thickness of the insulating material must be investigated. It is assumed that the varnish around the conductors is enough to withstand the voltage between adjacent winding turns. There is higher voltage between the phases which is isolated with insulation material. It was earlier assumed that the insulation between the phases occupied 2.6 % of the pole pitch, which corresponds to 0.5 mm with a 19.5 mm pole.

In comparison with a normal stator with punched sheets and round conductors, the main advantage of the integrated teeth stator is the increased fill factor of copper, which is possible to achieve only if the insulation material does not occupy too much space. If a small pole pitch and high copper fill factor are desired, it is necessary to minimize the number of slots. A pole with 2 slots per pole and phase is studied, see Figure 6.9. With the lower number of slots the mean flux density decreases to:

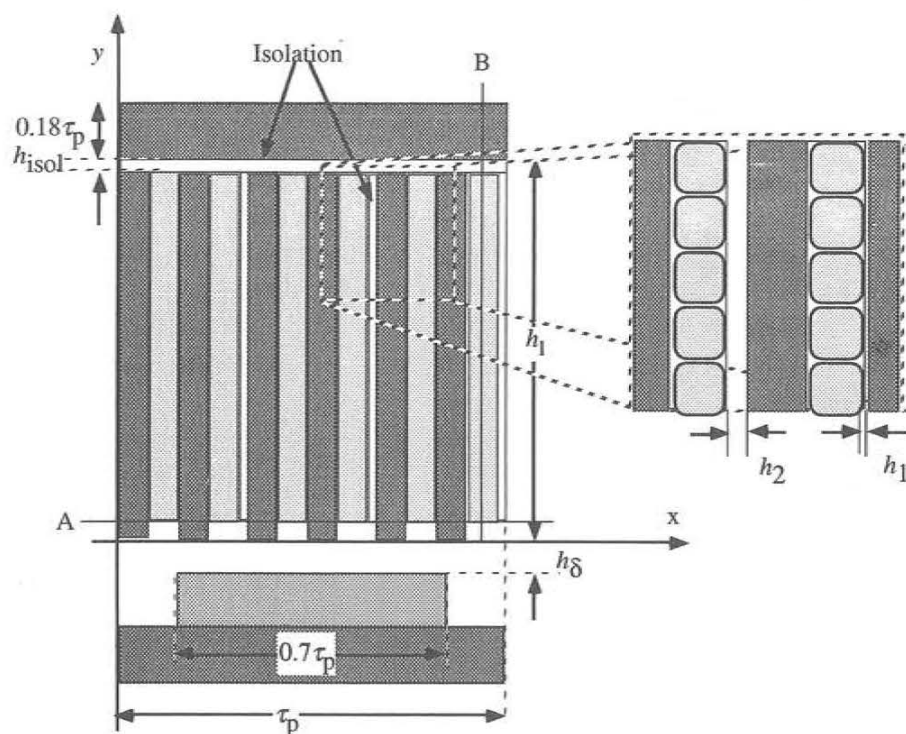


Figure 6.9. Slotted pole with  $q=2$ .

$$B_{1p} = 0.64 \text{ T} \left( \frac{h_1}{\tau_p} = 1, \mu_r = 100 \right)$$

if the same dimensions are used as in the previous section.

In the previous study the relative permeability of the back iron core was high. It is obvious that the yoke surface must be smooth and must fit into the winding with slots. Roughness adds to the distance between the teeth and the core. Of this reason an iron powder yoke, which can be produced with a defined shape and without sharp edges, is investigated. With the relative permeability in the teeth  $\mu_r=100$ , the relative permeability of the yoke is varied. The fundamental flux density in the winding is displayed in Figure 6.10. The relative permeability of the rotor core is assumed to be  $\mu_r=1000$ . According to Figure 6.10 a relative permeability of 100 is necessary in order to achieve more than 90 % of the flux density when the permeability is 1000.

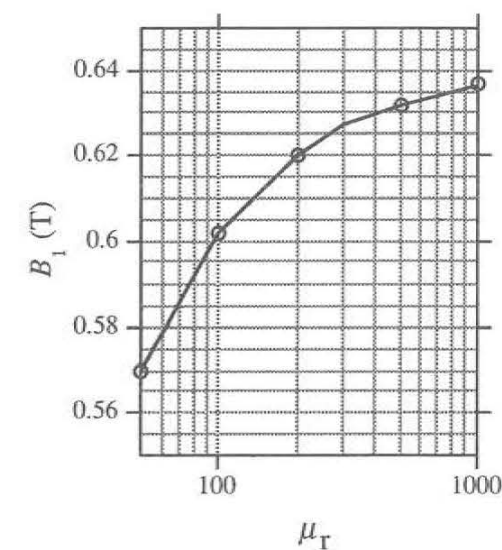


Figure 6.10. Fundamental flux density of the winding,  $\mu_{\text{teeth}}=100$ . Relative permeability of the yoke is varied

The insulating material between teeth and yoke must be thin in order to maintain a high flux density. When this material is inserted, the flux density decreases and, in order to increase the flux density, the air gap length is shortened from 10 % to 9 % of the pole pitch. This shortening of the air gap compensates for the decrease when the insulating material is inserted. Assuming an insulation thickness  $h_{\text{isol}}=0.01\tau_p$  the flux density is:

$$\begin{aligned} B_1 &= 0.569 \text{ T} & \text{relative permeability of the teeth and the yoke is } \mu_r &= 100 \\ B_1 &= 0.628 \text{ T} & \text{relative permeability of the teeth and the yoke is } \mu_r &= 200 \end{aligned}$$

The permeability of the iron powder material is for further studies assumed to be  $\mu_r=200$  both in teeth and core.

One effect that decreases the usable area of the slot, is that the flux density in the slot opening is not zero. This flux density would induce eddy currents in the first conductor of the slot. The flux density decays rapidly and is almost zero at a distance equal to the slot pitch  $y=\tau_s$ . The slot width is not constant due to the assumed insulation material between the phases. The absolute value of the flux density in the widest slot is displayed in Figure 6.11. The slot width is in this case:

$$b_s = 0.092 \tau_p$$

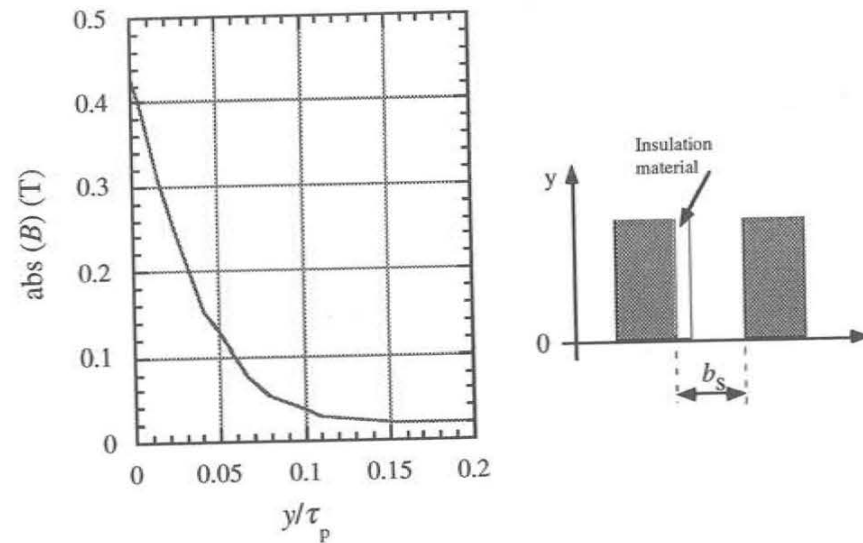


Figure 6.11. Flux density in the slot, absolute value.

The power losses in the conductor that is situated in the slot opening will be high in high frequency applications, which should be taken into account. At  $y=0.05\tau_p$  the flux density decreases to 0.12 T which produces a power loss density of  $0.35 \text{ MW/m}^3$  at  $f=250 \text{ Hz}$  and conductor width  $b_{cu}=2 \text{ mm}$ , i.e. half of the power loss density due to resistance in the conductor at  $J_{1cu}=6 \text{ A/mm}^2$ . For lower frequencies it seems possible to use the slot from  $y=h_3=0.05\tau_p$  to the slot bottom.

The thickness of the varnish around the conductor is assumed to be  $h_1=0.1 \text{ mm}$  and the thickness of the insulation between the phases is  $h_2=0.4 \text{ mm}$ . The total thickness of the insulating material in the x-direction is:

$$h_{isox} = 3 \cdot (h_1 \cdot 4 + h_2) = 2.4 \text{ mm}$$

The teeth material area was earlier assumed to be 46 % of the winding area and hence the copper area is:

$$\begin{aligned} A_{cu} &= (h_1 - h_3)(\tau_p - 0.46\tau_p - h_{isox}) = \\ &= (h_1 - h_3)(0.54\tau_p - 0.0024) \end{aligned} \quad (6.1)$$

where  $h_3=0.05\tau_p$  in a low frequency machine, i.e. in which the frequency is lower than 250 Hz. The fill factor of copper in the winding region is:

$$k_{cu} = \frac{(h_1 - h_3)(0.54\tau_p - 0.0024)}{h_1\tau_p} \quad (6.2)$$

It is important to keep the ripple due to the slots low on the magnet surface. The flux density on the magnet surface is displayed in Figure 6.12. The flux density on the magnet surface is almost unaffected by the slotted stator. The flux density ripple is lower than 0.05 T peak to peak. This result implies that the construction is done in a way that suppresses eddy current losses in the magnet even at high frequency.

The flux density in the x-direction is evaluated in the slots. The resulting flux density of the slot opening, i.e. along line A in Figure 6.9, ( $y=0.05\tau_p$ ) in the x-direction is displayed in Figure 6.13a). The flux density along the line B, i.e. in the slot farthest to the right, is displayed in Figure 6.13b). The flux density is evaluated assuming that the current density is  $6 \text{ A/mm}^2$ . A part of this flux density is due to the magnet but most of it is due to current loading. The maximum flux density in the slot is approximately:

$$B_x(y) = 0.16 \frac{S_1}{S_{10}} + \left( 0.04 \frac{h_1}{\tau_p} - 0.16 \frac{S_1}{S_{10}} \right) \frac{y}{h_1} \quad (6.3)$$

where  $S_{10}$  is the current loading at which Figure 6.13 is displayed, i.e.  $S_{10}=51 \text{ kA/m}$ .

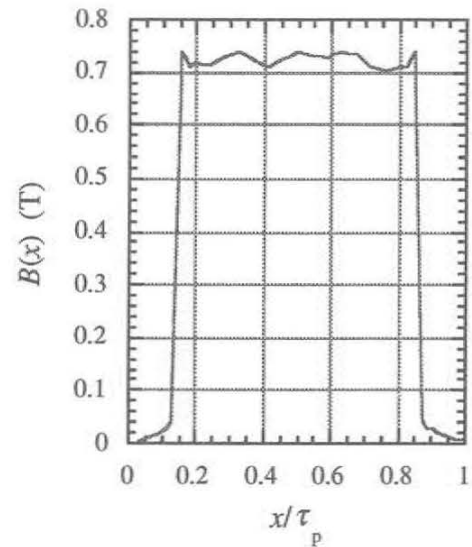


Figure 6.12. Flux density on the rotor surface.

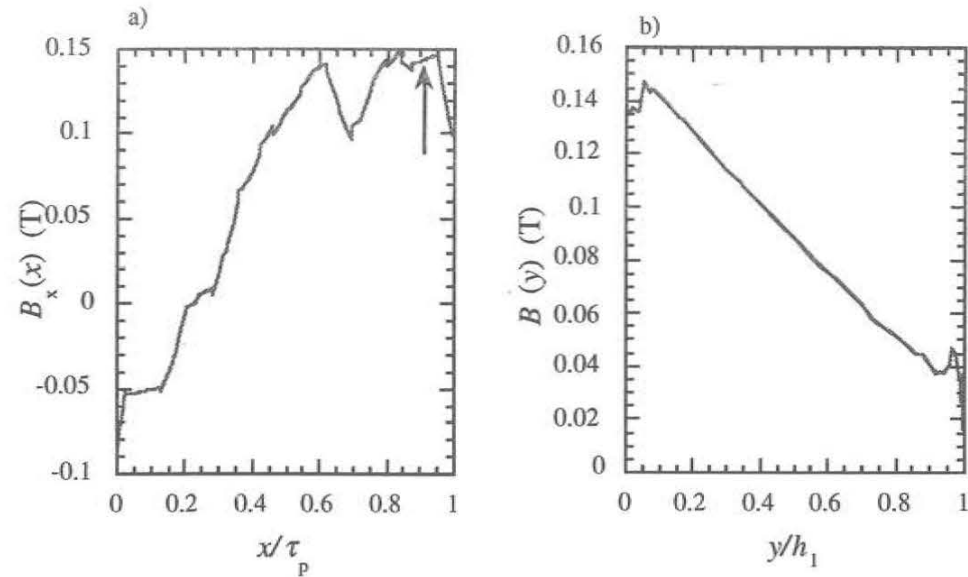


Figure 6.13. a) The x-component of the flux density under loaded conditions, along line A Fig. 6.9. b) The x-component of the flux density in the middle of the 6<sup>th</sup> slot.  $J_{1cu}=6 \text{ A/mm}^2$

The maximum x-component of the flux density, when the machine is loaded, is 0.15 T and it decays to 0.04 T at the bottom of the slot. This flux tries to penetrate the conductors and the

induced eddy current losses in the conductors must be evaluated, see Equation (4.1).

The flux density of the air gap is concentrated into the teeth and therefore the flux density in the teeth is approximately:

$$B_{\text{teeth}} = B_{1p} \frac{1}{k_{po}} = \frac{1}{0.46} \sqrt{B_{1pm}^2 + B_{1pq}^2} \quad (6.4)$$

At no-load the fundamental flux density is 0.62 T and according to Equation (6.4) the flux density in the teeth should be 1.35 T and at loaded conditions the flux density should be 12 % higher, i.e.

$$B_{\text{teeth}}=1.51 \text{ T.}$$

The flux density in the teeth is calculated using the FEM-program. The flux density directed in the y-direction in the middle of the winding region,  $y=0.5\tau_p$  is displayed in Figure 6.14. Figure 6.14a) shows the flux density in the teeth at no-load. Figure 6.14b) shows the flux density when the construction is loaded with  $J_{1cu}=6 \text{ A/mm}^2$ . Under loaded conditions the peak value of the flux density reaches 1.6 T in the teeth, which is higher than predicted by Equation (6.4). It is essential to use the right value of the flux density when we evaluate the power losses in the teeth.

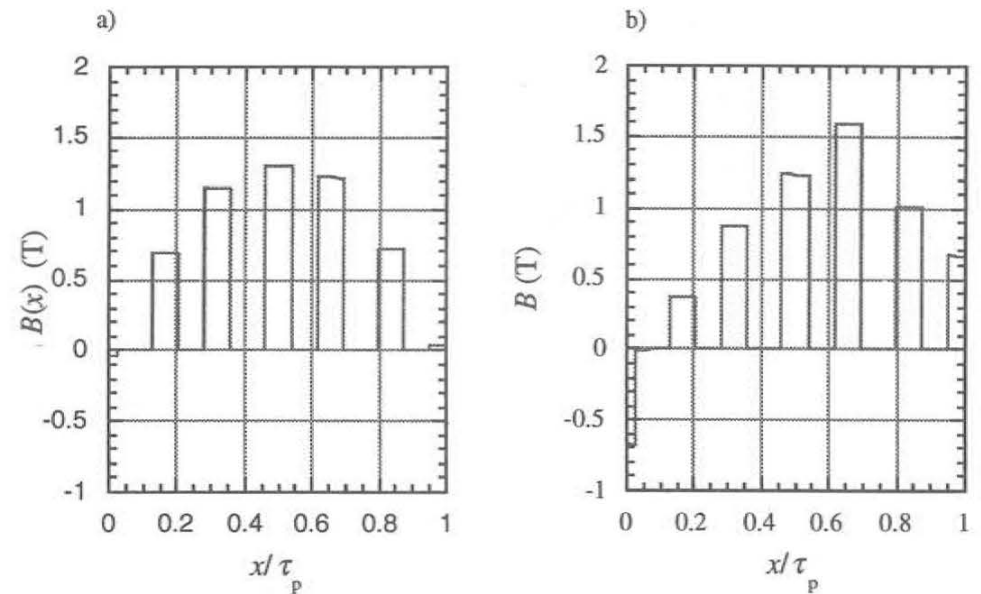


Figure 6.14. Flux density in the middle of the winding.

a) Unloaded  
b) Loaded with  $6 \text{ A/mm}^2$ , equivalent to  $S_1=51 \text{ kA/m}$ .

The inserted insulating material and other changes on the pole decrease the armature reaction of this pole to an 8 % increase in relation to the permanent magnet flux density. Finally, the magnetizing curve of the material EF6880 is used to represent the iron powder material and a new FEM-calculation is done. In this example the program option of non-linear material characteristics, according to Figure 2.15a), is used. The vector potential lines are shown in 6.15. The fundamental flux density is:

$$B_{1p} = 0.626 \text{ T}$$

without current, i.e. almost the same as with a linear material having a relative permeability of  $\mu_r=200$ . With  $6\text{A/mm}^2$  in the winding the flux density increases to:

$$B_{1p} = 0.668 \text{ T}$$

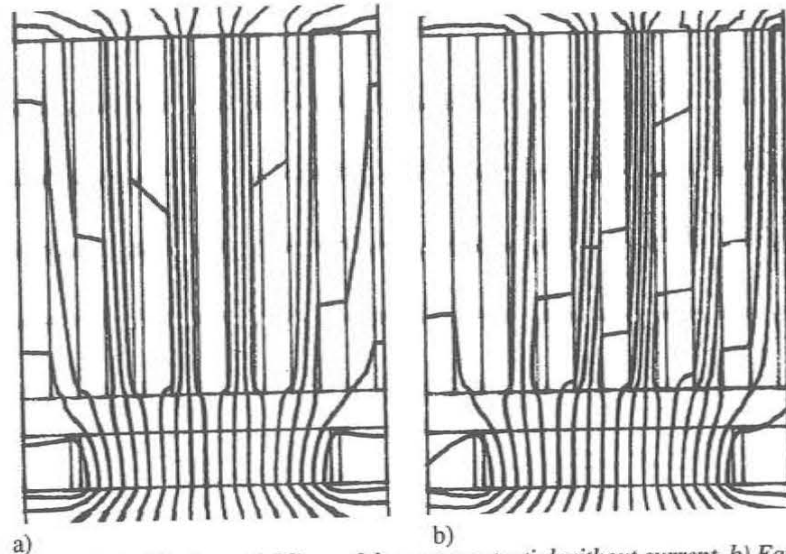


Figure 6.15. a). Equipotential lines of the vectorpotential without current. b) Equipotential lines of the vectorpotential at  $J_{1cu}=6\text{A/mm}^2$ ,  $S_1=51\text{kA/m}$ .

We can conclude that it seems possible to produce a winding with approximately a 40 % fill factor of copper and 0.63 T fundamental wave. The force density of this pole is

$$F_A = 0.301 k_{cu} J_{1cu} \frac{h_1}{\tau_p} \tau_p \quad (6.5)$$

### 6.3 Minimized Power Losses

Just as with the slotless pole the power losses should be minimized with respect to winding thickness. In the following examples the power losses in the teeth are important and their expressions can be found. The flux density from the magnet in the middle of the winding is approximately:

$$B_{1pm} = 0.69 - 0.06 \frac{h_1}{\tau_p} \quad (6.6)$$

The peak flux density in the teeth is approximated according to Equation (6.4) but the value is corrected to the value found in the FEM-analysis:

$$B_{teeth} = \sqrt{B_{t1}^2 + \left( \Delta B_1 \frac{S_1}{S_{10}} \right)^2} \quad (6.7)$$

where  $B_{t1}$  is the flux density in the teeth at no-load,  $\Delta B_1$  is the flux density in the teeth due to current loading,  $S_{10}=51 \text{ kA/m}$ . In the same way, the flux density of the yoke is approximated as:

$$B_{yoke} = \sqrt{B_2^2 + \left( \Delta B_2 \frac{S_1}{S_{10}} \right)^2} \quad (6.8)$$

$\Delta B_2$  is the flux density in the yoke due to current loading.

The force density of the pole is:

$$F_A = \frac{1}{2} \frac{3}{\pi} k_{cu} \cdot h_1 J_{1pcu} B_{1pm} \quad (6.9)$$

Fixing the force density, the necessary current density is evaluated for different winding thicknesses:

$$J_{1pcu} = \frac{2\pi F_A}{3k_{cu} \cdot h_1 B_{1pm}} \quad (6.10)$$

The power losses of the pole are:

$$P = P_{cu} + P_{yoke} + P_{teeth} + P_{Fe}$$

$$P_{cu} = \rho_{cu} f_{tot}^2 k_{cu} \frac{h_l}{\tau_p} \tau_p^2 l_{st} \quad (6.11)$$

$$P_{teeth} = p_{fe50} B_{teeth}^2 k_{po} \frac{h_l}{\tau_p} \tau_p^2 \frac{f}{50} l_{st}$$

$$P_{yoke} = p_{fe50} B_{yoke}^2 h_{fe} \tau_p \frac{f}{50} l_{st}$$

$$p_{fe50} = 55 \text{ (kW / m}^3\text{)}$$

where  $P_{teeth}$  is the power losses in the teeth,  $P_{yoke}$  is the power losses in the yoke.

The power losses due to eddy currents are found through approximating the flux density in the  $x$ -direction according to Equation (6.3). The power losses may be written as:

$$P_{Fe} = 6p \sum_{N_p} \Delta y_{cu} \Delta x_{cu} \frac{\omega^2 \Delta y_{cu}^2 B_x^2(y)}{24\rho} l_{st} \quad (6.12)$$

The minimum conductor width is 1mm and the corresponding pole pitch is as an absolute minimum  $\tau_p=15$  mm. Using this pole pitch, the power losses are calculated and are shown in Figure 6.16 and Figure 6.17. The frequency is the parameter. The power losses are shown for a high force case and for a low force case. At low frequency and high force rating the optimal winding thickness lies above what is reasonable with respect to relative reactance. In cases where power losses in the iron powder material and power losses due to eddy currents in the conductors dominate, i.e. at high frequency or low force ratings the winding thickness is to be limited to lower values. The power losses are distributed according to Figure 6.18 at 500 Hz and  $F_A=15$  kN/m<sup>2</sup>.

It is assumed that the conductors have a quadratic cross-section,  $\Delta y_{cu}=\Delta x_{cu}=1$ mm.

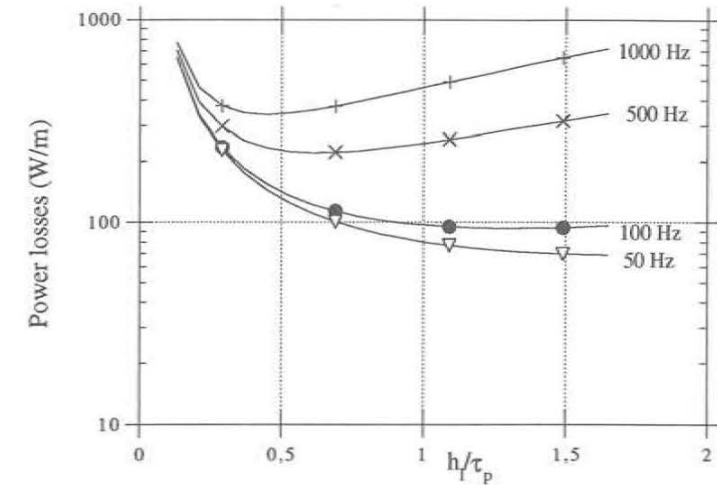


Figure 6.16. Power losses as a function of winding thickness,  $\tau_p=15$  mm. High force density  $F_A=15$  kN/m<sup>2</sup>.

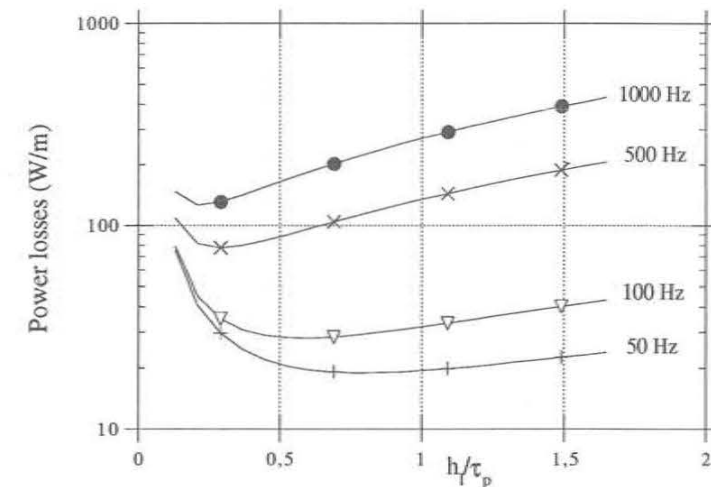


Figure 6.17. Power losses as a function of winding thickness,  $\tau_p=15$  mm. Low force density  $F_A=5$  kN/m<sup>2</sup>.

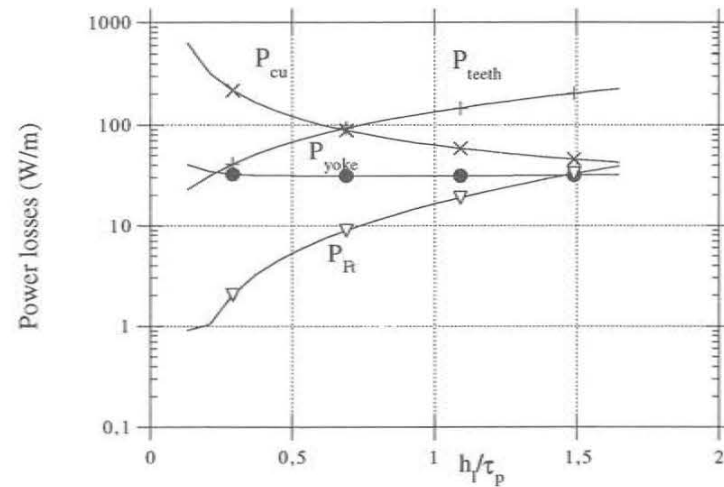


Figure 6.18. Power losses at  $=500$  Hz,  $F_A=15$  kN/m<sup>2</sup>,  $\tau_p=15$  mm.

#### 6.4 Measurements on Iron Powder Parts

The power losses in iron powder material were measured and a simplified pole was tested. The tests were made in order to verify the iron powder data, calculation method and whether the pole construction is possible to produce.

##### 6.4.1 Measurement of Power Losses.

A commercial iron powder toroidal core was used as a test object. The purchaser has no data on the core except that the relative permeability of the material is 100. The core dimensions are shown in Figure 6.19.

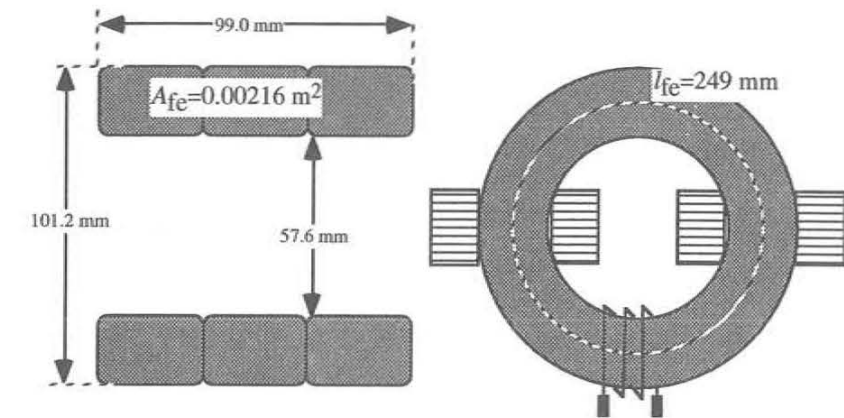


Figure 6.19. Iron powder toroids used as a stator core.

Three cores were put together forming a yoke for a radial flux machine. The volume of the core is 538 cm<sup>3</sup>. The windings are concentrated to two windings on opposite sides of the iron core. The number of turns in each winding is 75. Voltage was applied to the windings and iron losses were measured at different frequencies. The flux was measured by means of a measuring winding. Power losses as a function of the frequency are displayed in Figure 6.20. Iron losses at  $B_{fe}=0.4$  T are approximated by a second-order polynomial:

$$\begin{aligned}
 P &= p_1 f + p_2 f^2 \text{ (W)} \\
 p_1 &= 0.136 \text{ Ws} \\
 p_2 &= 8.686 \cdot 10^{-5} \text{ Ws}^2
 \end{aligned}
 \tag{6.13}$$

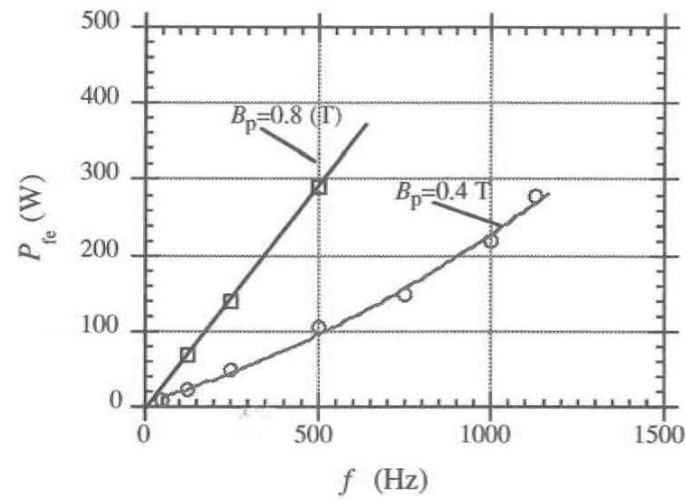


Figure 6.20. Iron losses in the core. Last point at 1500 Hz.

In the studied interval the linear term dominates. At 50 Hz and 0.8 T the iron losses are 32 W, i.e. 59 kW/m<sup>3</sup>. In relation to the data of EF6880 the studied material has rather high losses.

The magnetizing characteristics were measured using a computer measuring system in which the induced voltage in the extra winding is measured and integrated, see Figure 6.21. Integrating the hysteresis loop yields the figure of  $W=1250$  Ws/m<sup>3</sup> at .8 T and 50 Hz, corresponding to power losses of 62.5 kW/m<sup>3</sup>. The value agrees well with what is measured and it can be concluded that power losses are mainly due to the hysteresis. A line corresponding to  $\mu_r=100$ , which is the relative permeability claimed by the distributor, is indicated in Figure 6.21 and it is clear that the relative permeability of the material is higher over the investigated range.

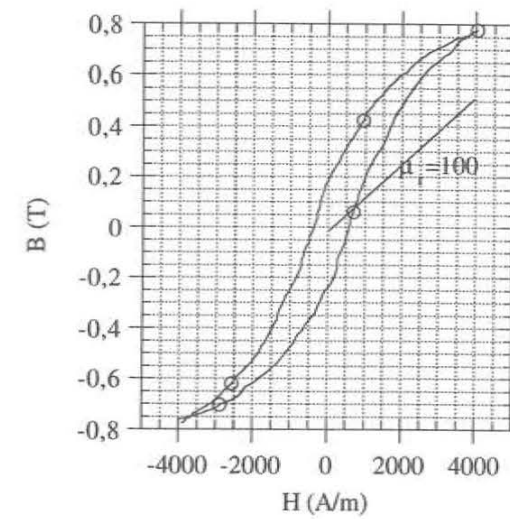


Figure 6.21. Measured hysteresis curve.

#### 6.4.2 Measurements on Iron Powder as Teeth Material

An integrated teeth winding using iron powder pieces cut from a bigger piece was tested. The iron powder material has a relative permeability of 75. The winding is shown in Figure 6.22.

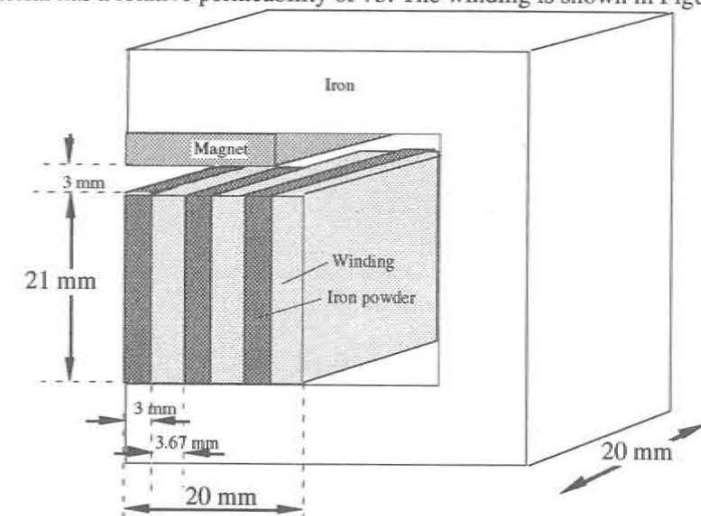


Figure 6.22. Integrated test winding.

The measured peak value of the flux density in the air gap is 0.45 T. The structure is analysed by

means of the FEM-program. The vector potential is displayed in Figure 6.23 and the flux density is shown in Figure 6.24. The calculation of flux density agrees well with the measured value.

The winding is made of rectangular conductors with a width of 2 mm and a thickness of 0.8 mm. The number of conductors per slot is 30. The fill factor of copper in the winding region is:

$$k_{cu} = 0.34$$

The fill factor of iron powder material in the winding region is:

$$k_{po} = 0.45$$

which is almost the same as in the analysed pole in section 6.1. The number of conductors between each iron powder piece is rather high in this example and the varnish takes a relatively large space. The amount of varnish is approximately 15 % of the slot and 76 % of the slot is filled with copper. 10 % of the slot is filled with other material which could be replaced by copper. In order to achieve a high fill factor of copper, bigger conductors should be used. The production of the pole must be improved so that no space is left for material other than the active ones.

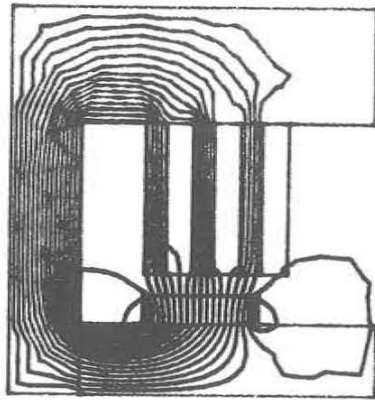


Figure 6.23 Equipotential lines of integrated teeth made of premanufactured iron powder pieces.

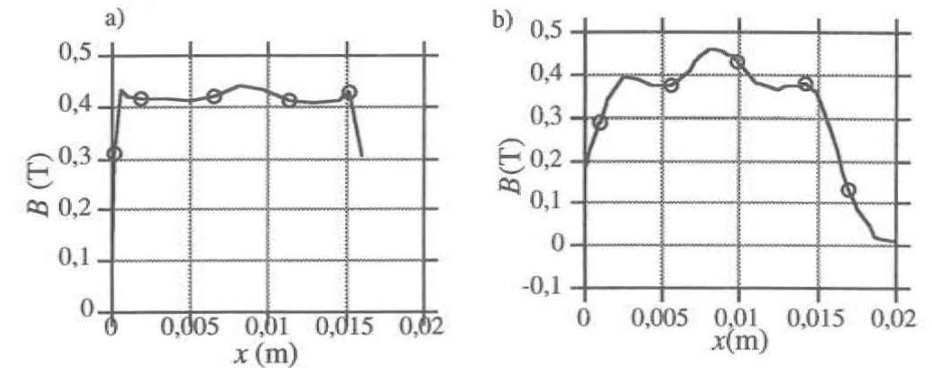


Figure 6.24. a) Flux density on the magnet surface. b) Flux density in the middle of the air gap.

## 6.5 Discussion

A machine part was analysed and some choices were made. One assumption was that slot width is approximately half of slot pitch. Weh and Boules [6] showed that an increase in slot width would increase the power. An increase would decrease the fundamental flux density of the winding and increase power losses in the teeth, something they did not investigate and which was not investigated in this work, either. The reason for this, is that in the case of small pole pitches the minimum rectangular conductor has the same width as the tooth. If the slot is widened, the flux density ripple on the magnet surface will increase and, therefore, it will be necessary to increase the air gap. The increased air gap will decrease the fundamental flux density and the construction will be more sensitive to the high value of the insulating thickness  $h_{isol}$ . An alternative is to partly close the slot opening, which will increase the leakage flux from the winding.

The force density of the integrated teeth winding with  $h_l/\tau_p=1$  is evaluated. In order to minimize armature flux and to minimize flux density variations on the rotor surface, the air gap is set at 9 % of the pole pitch and the magnet thickness is  $h_m=0.15\tau_p$ . If the slots are filled with rectangular conductors the fill factor  $k_{cu}$  will depend on pole pitch. An approximate figure of the fill factor is:

$$k_{cu}=0.4$$

Hence, the force density is

$$F_A = 0.12 J_{1cu} \tau_p \quad (6.13)$$

Due to the long air gap, the construction has relatively low armature reaction. With a current

loading of  $S_{10}=51$  kA/m the increase of flux density in the winding is 8 % in relation to the no-load case.

The weights of the pole parts are displayed in Table 6.1. The weight of the slotted pole is 2.35 times that of the slotless pole, i.e. the force to weight ratio of this pole is better than that of the slotless construction.

Table 6.1. Weight per unit length of the pole.

Magnet mass	$777\tau_p^2$
Copper weight	$3592\tau_p^2$
Teeth weight	$3450\tau_p^2$
Iron yoke weight	$1350\tau_p^2$
Total weight	$9169\tau_p^2$
Force/weight	$13.1 \cdot 10^{-6} J_{1cu}/\tau_p$

The lower limit of the pole pitch is approximately 15 mm due to the minimum dimension of the rectangular conductors, which is 1 mm. According to Vacuumschmelze, it is possible to produce iron powder pieces with a thickness of 1 mm. Handling such thin iron powder parts may be difficult and small pole pitches must have a very thin insulating layer between the winding region and the iron core. The parts must also be produced with low tolerances. Whether or not it is possible to manufacture small poles depends on material and winding machinery. It might be useful to choose poles that are wider, which simplifies the production and increases the fill factor of copper.

The optimal winding thickness depends on force rating and frequency. At low force ratings or at high frequency the power losses in iron powder parts dominate and a low winding thickness yields lower losses.

## 7. Calculated Machines with Integrated Teeth

An approach with integrated teeth is studied for three different machine types. In a direct-driven wind power application, the integrated teeth machine is compared with a transversal flux machine. Secondly the construction is evaluated in high speed operation and is compared with the slotless machine [1]. In this case it is not possible to approximate the pole with the flat pole. Finally the integrated teeth machine is compared with a standard induction machine.

In wind power operation, the machine is to be optimized with respect to cost over its entire lifetime, i.e. the cost for producing the machine must be compared to the produced energy. The machine size is not restricted but a large diameter will be expensive to produce.

The high speed machine has a restricted rotor size due to mechanical stresses. We shall investigate how high power a certain rotor size can produce with the iron powder stator. The frequency and the power losses of the iron powder material are high and the volume of the machine is low. The high power losses in a small volume implies that there is a cooling problem. The temperature of the machine must in all cases, but especially in a high speed machine, be limited to values that do not damage the materials.

In the third case, the outer dimensions of the machine are limited to the same dimensions as a standard induction machine. The possible power rating is evaluated under the assumption that the machine is to have the same power losses as the induction machine.

It is for all machines assumed that the available iron powder material EF6880 and the permanent magnet material VACODYM 362 HR are used.

### 7.1 Direct-driven Wind Power Generator

In a direct-driven wind power generator the stator frequency is rather low and the maximum winding thickness is assumed not to be limited by power losses and temperature. In this study, the winding thickness is fixed at  $h/\tau_p=1$ .

A radial flux machine is calculated and compared with the transversal flux machine reported on by Weh [11]. The nominal power of this machine is 6.4 kW at 195 rpm and the torque is 313 Nm. Firstly, it is assumed that power losses in the radial flux machine are to be the same as in the transversal flux machine,  $P_{loss}=600$  W. Secondly, the most economical machine is found based on assumptions about material costs and the cost of power losses.

Power losses are evaluated according to the equations in Chapter 6 with the difference that the copper losses in the end turns are added. One type of end turns is shown in Figure 7.1. The end turn must be bent upward so that it can pass over the two other phases that come out of the yoke.

Under idealized conditions the length of the end turns is:

$$l_e = \tau_p + \frac{\pi h_1}{2} \quad (7.1)$$

In reality insulating material and tolerances make the end turn longer and, therefore, it is assumed that the length of the end turns is:

$$l_e = \tau_p + 1.7h_1 \quad (7.2)$$

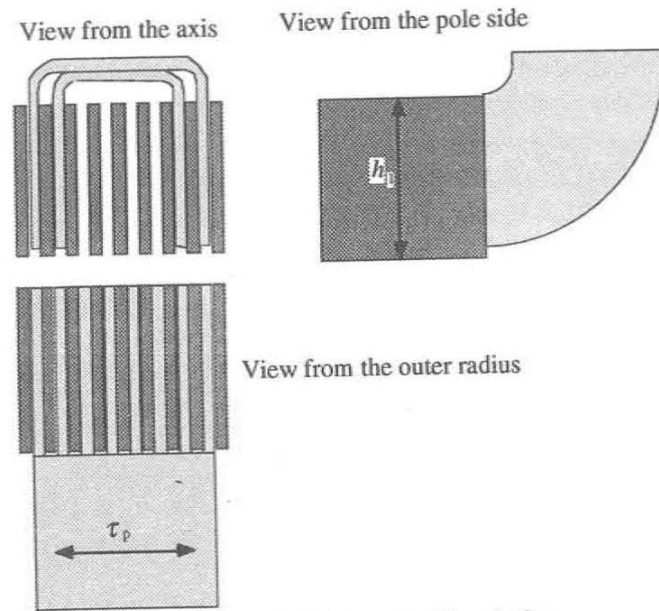


Figure 7.1 End turns of the winding

The copper losses are:

$$P_{cu} = 2p\rho_{cu}J_{in}^2 k_{cu}h_1\tau_p(l_{st} + \tau_p + 1.7h_1) \quad (7.3)$$

Other power losses are calculated according to the Equations (6.11)-(6.12).

The produced torque is derived from the force density, according to Equation (6.9), and the active surface area:

$$T = r_\delta F_A 2\pi r_\delta l_{st} \quad (7.4)$$

where  $r_\delta$  is the radius of the air gap.

The machine length is varied and the radius and current density that corresponds to the specified power losses and torque is calculated. The radius and magnet weights are shown in Figure 7.2a) and b), respectively. Three alternative pole pitches are evaluated. For pole pitches lower than 25 mm it is not possible to achieve a machine with the assumed power losses. As can be seen in Figure 7.2b), the magnet weight increases with pole pitch and, therefore, it is not interesting to investigate higher pole pitches. In fact there are two combinations of length and radius that fulfil the requirements. The combinations that are not shown are longer, have lower radius and higher magnet weight. Due to the higher magnet weight this alternative is not further examined.

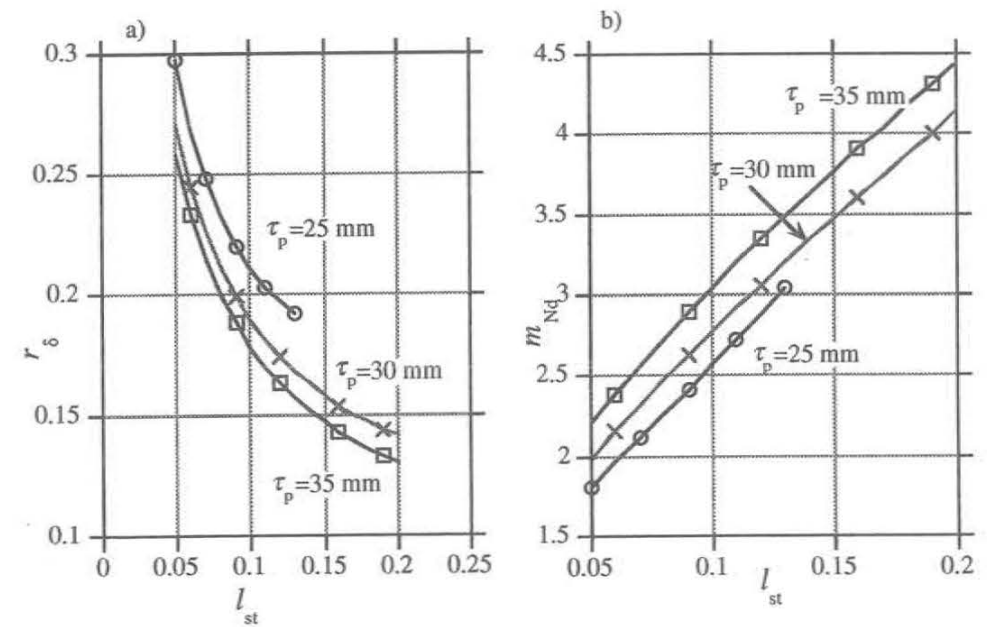


Figure 7.2. a) Air gap radius at varied machine length, pole pitch as a parameter. b) Magnet weight. Power losses are constant.

A machine with nearly the same magnet weight,  $m_{Nd} = 2.1$  kg, as the transversal flux machine is more closely examined:

$$\begin{aligned} \tau_p &= 25 \text{ mm} \\ l_{st} &= 0.07 \text{ m} \\ r_\delta &= 0.25 \text{ m} \end{aligned}$$

The weight and mechanical dimensions of the machine are summarized and compared with the transversal flux machine in Table 7.1. The power losses are:

$$\begin{aligned}
 P_{cu} &= 265 \text{ W} \\
 P_{teeth} &= 271 \text{ W} \\
 P_{yoke} &= 69 \text{ W} \\
 P_{Ft} &= 4 \text{ W} (\Delta y_{cu} = 1 \text{ mm}) \\
 P_{loss} &= 609 \text{ W} (9.5 \%)
 \end{aligned}$$

i.e. the efficiency is 90.5 % excluding mechanical losses and losses due to converter feeding.

Table 7.1. A comparison between transversal and radial flux machines.

	Transversal flux	Radial flux (same magnet weight)
Mech. input power	6.4 kW	6.4 kW
Electric. output power	5.8 kW	5.8 kW
Rated speed	195 rpm	195 rpm
Active diameter	360 mm	494 mm
Pole pitch	7.85 mm	25 mm
Frequency	234 Hz	101 Hz
Efficiency	0.91	0.905 (mech. losses excluded)
Iron mass	20.5 kg	13.4 kg
Copper mass	4.7 kg	20.1 kg
Magnet mass NdFeB	2.0 kg	2.1 kg
Total mass active material	27.2 kg	35.6 kg
Machine diameter	0.5 m	0.59 m
Machine length	0.2 m	appr. 0.15 m

It was earlier assumed that a high winding thickness can be used in this application. Compared to Figure 6.17 the force density is high ( $F_A = 11.4 \text{ kN/m}^2$ ) and the frequency is low ( $f = 101 \text{ Hz}$ ) in this case. It seems correct to use a high winding thickness in this case. Testing the calculation with higher winding thickness yields higher values of radius and magnet weight. For lower winding thicknesses it is not possible to achieve the low power losses. This result implies that the assumed winding thickness is the most favourable. Taking into account that this machine should be possible to control with a diode rectifier, it is of interest to keep the armature reaction low.

It is clear that it is possible to build force dense machines with performance in the same range as this particular transversal flux machine. The weight of the machine is 30 % higher as that of the transversal flux machine, the radius of the machine is higher but the machine is shorter. The optimal machine is, however, to be calculated from an economic point of view.

As an example, the cost of the materials is approximated and with an assumed cost of power losses the most economical solution is evaluated. The material costs are assumed:

$$c_{Nd} = 1000 \text{ SEK/kg (permanent magnet material)}$$

$$\begin{aligned}
 c_{pow} &= 100 \text{ SEK/kg (iron powder material)} \\
 c_{cu} &= 100 \text{ SEK/kg (copper)}
 \end{aligned}$$

The cost of power losses is found by assuming that the machine runs at nominal operation for 10 years and that the income from produced electricity is 0.25 SEK/kWh. Power losses in this case will result in a loss of income. The cost per kW is:

$$c_{ploss} = 21900 \text{ SEK/kW}$$

The cost for housing and other mechanical parts depends on the machine size. It is assumed that 30 % of the machine volume is filled with mechanical supporting material and that this steel material costs 100 SEK/kg. It is, furthermore, assumed that the cost for producing flanges increases with radius:

$$c_{other} = 741700 l_{st} r_{outer}^2 + 10000 r_{outer}$$

where  $r_{outer}$  is the outer radius of the machine. The optimal length and radius are evaluated numerically for different pole pitches. The resulting cost is shown in Figure 7.3.

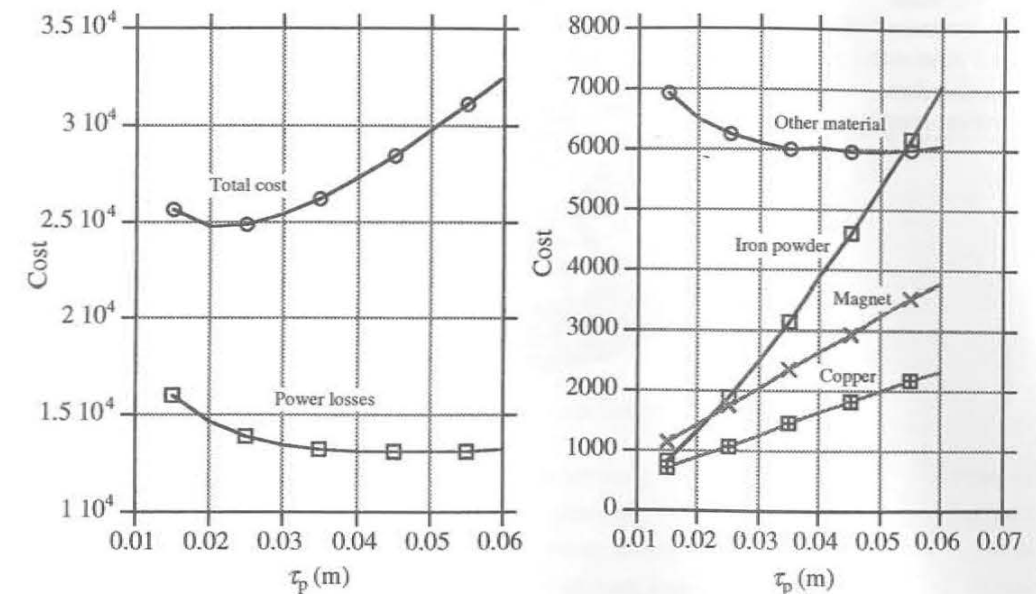


Figure 7.3. Cost for different pole pitches. a) Total cost and cost of power losses. b) Cost of different materials.

The optimal pole pitch is 20 mm in this example. The dominating cost is the cost for power losses as shown in Figure 7.3.a). The material costs are shown in Figure 7.3.b). The data of the optimal pole pitch machine are shown in Table 7.2. The number of pole pairs is corrected to 43.

With the assumed cost factors the optimal machine will have 14 % lower weight than the transversal flux machine, the efficiency of the integrated teeth machine is lower and the overall diameter of the machine will be significantly higher.

Table 7.2. A comparison of transversal and integrated teeth machines. Optimal pole pitch of the integrated teeth machine.

	Transversal flux	Radial flux (optimal pole)
Mech. input power	6.4 kW	6.4 kW
Electric. output power	5.8 kW	5.71 kW
Rated speed	195 rpm	195 rpm
Active diameter	360 mm	546 mm
Length of stator core		52.5 mm
Number of pole pairs		43
Pole pitch	7.85 mm	20 mm
Frequency	234 Hz	140 Hz
Efficiency	0.91	0.89 (mech. losses excluded)
Iron mass	20.5 kg	8.9 kg
Copper mass	4.7 kg	13.1 kg
Magnet mass NdFeB	2.0 kg	1.4 kg
Total mass active material	27.2 kg	23.4 kg
Machine diam	0.5 m	0.65 m
Machine length	0.2 m	appr.0.13 m

## 7.2 High-speed Machine with Integrated Teeth

A high speed machine with integrated teeth is calculated and compared to the shaft magnet slotless machine described in Chapter 3. In high speed operations, power losses in iron powder parts will be high and problems with cooling must be solved. The possible winding thickness and power from the same rotor size as in Section 3.2 are investigated based on the assumption that the core is to be cooled to a housing attached to the outer parts of the yoke.

Chudi and Malmquist [1] showed that a slotted stator will produce high power losses on the rotor surface of a high speed machine. Flux density variations on the rotor surface are, however, cancelled if the air gap has an appropriate length. The slot opening of the integrated teeth winding is small which implies that the air gap can be of reasonable length. The machine is outlined in Figure 7.4 and the common data of the two machines are listed in Table 7.3.

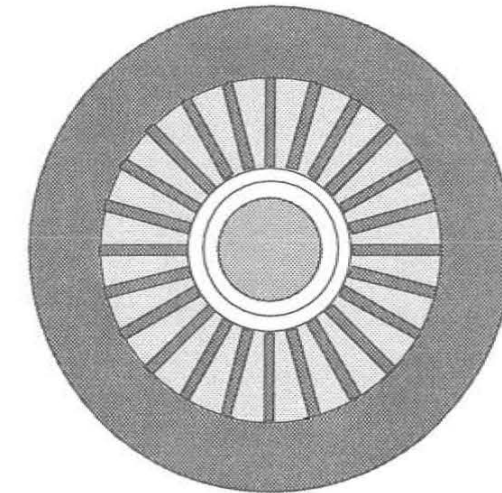


Figure 7.4. High speed machine with integrated teeth. Tooth no. 1.

If the machine voltage is to be in the same range as normal grid-voltage, i.e. 400 V, the number of winding turns is low, i.e. the conductor area is rather large. A single conductor cannot be used due to the skin effect. Instead, a Litz wire must be used and it is assumed that the fill factor of copper in the slots is 50 %. The amplitude of eddy currents that are induced in the Litz-wire is low which means that the whole slot may be filled with conductors.

The number of slots per pole and phase is  $q=4$ . The slot opening is 2.2 mm. Two types of teeth are investigated and shown in Figure 7.5. The first construction has rectangular teeth and the second tooth type has rectangular slots, i.e. the tooth width increases with radius.

Table 7.3. Common data of the two high speed machines.

Magnet radius	$r_m=11.5$ mm
Rotor radius	$r_r=15$ mm
Rotational speed	$n=100\ 000$ rpm
Active length	$l_{sl}=0.1$ m
Magnet material	VACODYM 362 HR
	$B_r=1.33$ T
	$H_c=1020$ kA/m
Magnet weight	$m_{Nd}=307$ g
Iron yoke and teeth material	VACTEK EF6880
Iron yoke thickness	$h_{fe}=15$ mm

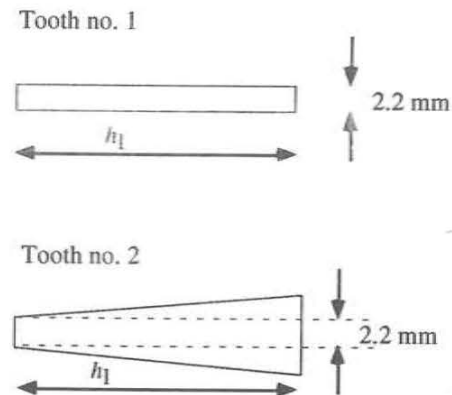


Figure 7.5. Investigated teeth.

The inner radius of the winding is 17 mm, i.e. the air gap is 2 mm. The flux density on the rotor surface is displayed in Figure 7.6. The flux density ripple due to the slots is lower than 0.05 T peak to peak.

It is assumed that the machine operates at 1667 Hz and the power losses in tooth type no. 1 are evaluated. The flux density in this tooth is 1.1 T all the way through the winding region. Assuming a yoke thickness of  $h_{fe}=15$  mm, the flux density in the yoke is  $B_{lyoke}=0.6$  T, i.e. the power loss factors are  $p_{teeth}=2.22$  MW/m<sup>3</sup> and  $p_{yoke}=660$  kW/m<sup>3</sup>.

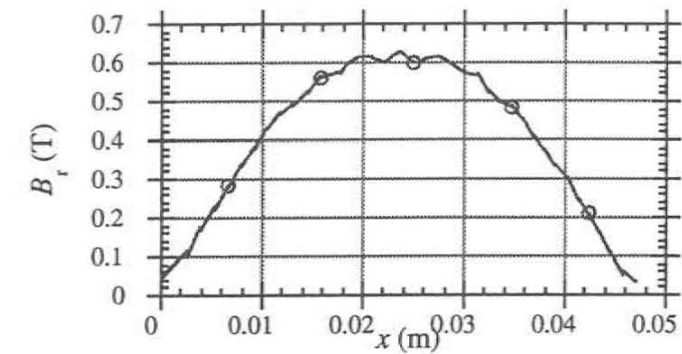


Figure 7.6. Flux density on rotor surface, unloaded.

The temperature is evaluated when the winding thickness is  $h_1=23$  mm. It is assumed that an insulation layer of 0.2 mm with thermal conductivity  $\lambda=0.2$  W/Km is situated between the winding region and the yoke. The current density is  $J_{cu}=5$  A/mm<sup>2</sup> and it is assumed that no heat is transferred to the rotor and that the winding has the equivalent thermal conductivity of three times the thermal conductivity of the impregnating material,  $\lambda_{wind}=0.6$  W/Km, Kylander [39]. The resulting maximum temperature is 168°C, if the yoke outside is held at 60°C. This maximum temperature exceeds the maximum operating temperature of the iron powder material, which means that the design must be altered.

Tooth no. 2 has an increased area for higher radius which lowers the flux density and the cooling area of the tooth bottom is increased. Figure 7.7 shows the absolute value of the flux density in the tooth. The maximum current density at different winding thicknesses is the current density that produces maximum operating temperature in the material.

The FEM-program is used to evaluate the hot spot in the winding area for different winding thicknesses. The current density is adjusted so that the hottest spot reaches 120°C when the outer surface is held at 60°C. For each current density the flux density in the tooth and in the yoke are found and fed into the temperature analysis. When evaluating the temperature, the teeth are divided into several pieces and power losses per unit volume are

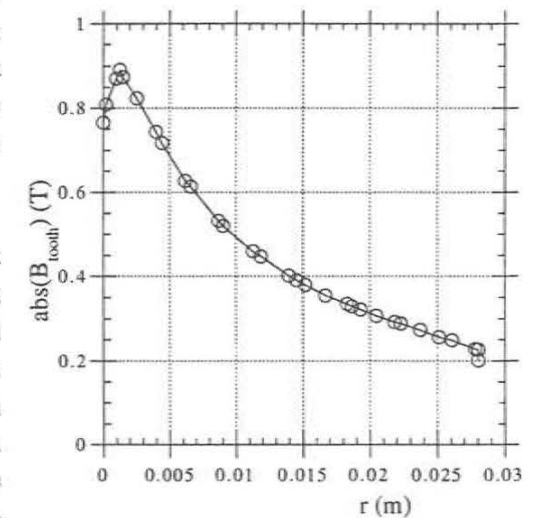


Figure 7.7. Flux density in tooth no. 2.

calculated from the actual flux density in each piece. The maximum temperature at different current densities for various values of  $r_2$  is displayed in Figure 7.8.

The power from the machine corresponding to the current density that produces 120°C in the winding region is shown in Figure 7.9. A peak power of

$$P=44 \text{ kW}$$

is produced with the outer winding radius  $r_2=45 \text{ mm}$ .

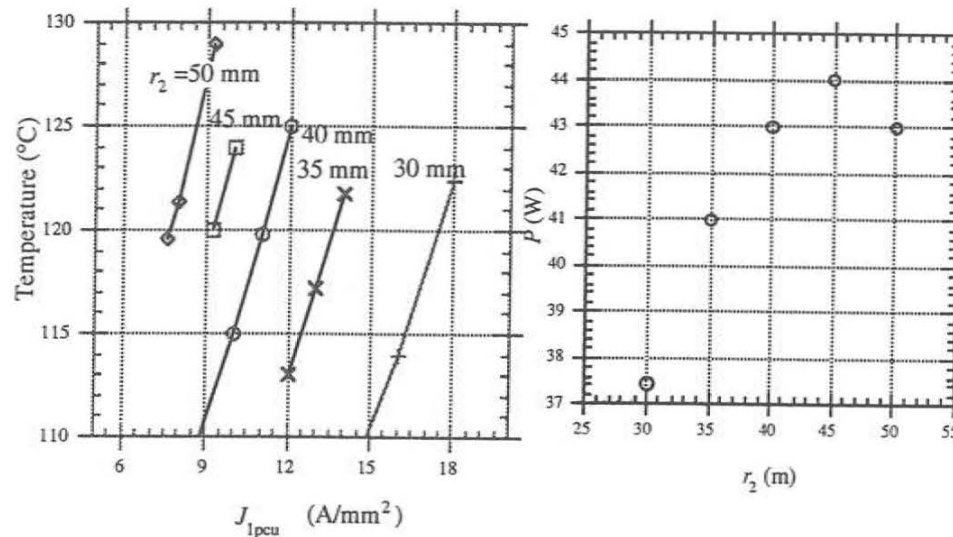


Figure 7.8. Maximum temperature at varied current density, pole pitch as parameter

Figure 7.9. Power at varied outer radius of the winding, hot spot 120 °C.

The equipotential lines of the magnetic vector potential without current and with current are displayed in Figure 7.10. Power losses in the active parts are listed in Table 7.4.

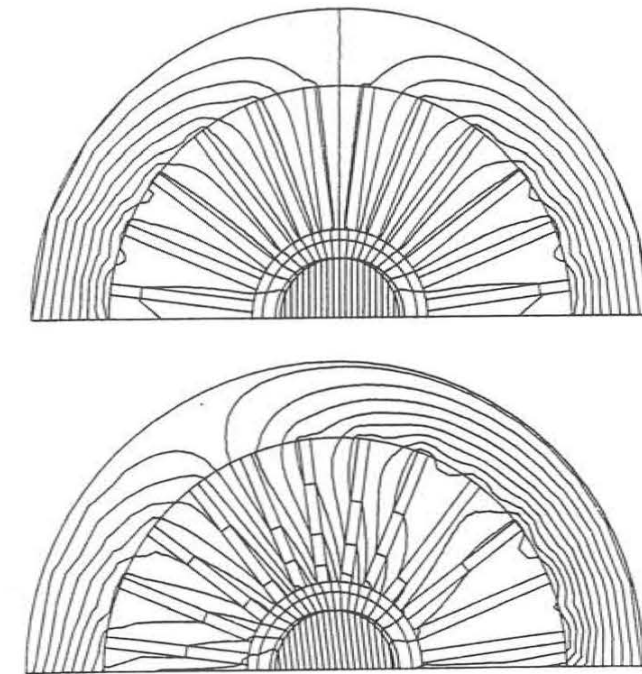


Figure 7.10. Equipotential plot of the vector potential. High speed machine with slots. Without current (upper) and loaded with  $J_{1cu}=6.5 \text{ A/mm}^2$  (lower).

The achievable power in a slotless generator with a shaft-magnet rotor is evaluated in the following. The dimensions of the machine are displayed in Tables 7.3 and 7.4. The machine performance can be calculated with information from Section 3.2.

The ohmic losses of the shaft magnet rotor decrease with winding thickness, as shown in Figure 3.21. This decrease means that a high winding thickness may be used. Chudi and Malmquist [1] chose a winding radius ratio corresponding to the highest torque to volume. This choice has proved to be a useful winding thickness. The corresponding outer radius of the winding is  $r_2=30.5 \text{ mm}$ . The produced power is:

$$P=24 \text{ kW}$$

The losses of the active materials are listed in Table 7.4.

The total power losses in the active region are  $P_{tot}=157 \text{ W}$  (corresponding to 0.65 % of machine

power). The winding temperature of the slotless machine is analysed in the stator region. It is assumed that the heat does not transfer to the air gap and that the outer side of the stator yoke is held at 60°C, i.e. the same conditions as for the integrated teeth machine. The resulting maximum temperature is 118°C which means that we have almost the same hot spot temperature in the two machines.

Table 7.4. Main data of the high-speed radial flux machines

	Slotless machine	Integrated teeth machine
Inner radius of winding	15.5 mm	17 mm
Outer radius of winding	30.5 mm	62 mm
Stator outer radius	45.5 mm	77 mm
Current density in the conductor	6 A/m <sup>2</sup>	6.5 A/m <sup>2</sup>
Fill factor of copper	50 %	50 % in slot
Air gap length	0.5 mm	2 mm
Copper losses	67 W	103 W
Teeth losses		127 W
Yoke losses	80 W	327 W
Eddy current losses	10.3 W	
Total losses	157 W	557 W
Surface area of stator core	0.029 m <sup>2</sup>	0.048 m <sup>2</sup>
Output power	24 kW	44 kW

Power losses are 3.5 times higher in the slotted machine than in the slotless machine. The increase in power losses makes it more difficult not only to transfer the heat to the yoke surface but also from the surface to the ambient. Heat transport from the yoke to the ambient can be described as

$$P' = \alpha(\vartheta_2 - \vartheta_a) \quad (7.3)$$

where  $P'$  is the heat flow density (W/m<sup>2</sup>),  $\alpha$  is the heat transfer coefficient which is multiplied by the temperature difference.  $\vartheta_2$  is the temperature of the yoke, and  $\vartheta_a$  ambient temperature. Normally  $\alpha$  stands for heat transfer from surface to air, but it is here used as a capacity figure of the cooling arrangement:

$$\alpha = \frac{P_{\text{loss}}}{(\vartheta_2 - \vartheta_a)a_{\text{yoke}}} \quad (7.4)$$

where  $P_{\text{loss}}$  is the power losses in the machine, and  $a_{\text{yoke}}$  is the outer area of the yoke.

The necessary heat transfer coefficients of the yoke outer surface, if the ambient temperature 40°C is for the two machines:

$$\alpha = 575 \text{ W/m}^2\text{K (integrated teeth machine)}$$

$$\alpha = 271 \text{ W/m}^2\text{K (slotless machine)}$$

if the temperature difference between yoke and ambient is 20°C. The cooling arrangement in the integrated teeth machine must be 2.1 times as effective as in the air gap machine. Interesting to note is that the highest power losses of the integrated teeth machine are the power losses in the yoke. A better material that would lower these losses to the same range as the yoke losses of the slotless machine, should lower the power losses of the integrated teeth machine to 310 W. Consequently the necessary heat transfer coefficient of this machine should be 322 W/m<sup>2</sup>K. This heat transfer coefficient is close to the same value as in the slotless machine. For instance, Permenorm 5000 H2 has power losses of 10 W/kg at 2 kHz and 0.5 T [1]. In this application, power losses in the yoke would be lowered to 92 W, if Permenorm 5000 H2 is used.

This example shows that a winding with thin and integrated teeth can be used in high-speed machines with low rotor losses if a proper air gap is inserted. The flux density variation due to slots is cancelled if the air gap is bigger than the slot opening. Power losses in the iron parts are high but the thermal conductivity of the iron powder is enough to transport the heat to the yoke surface. The power losses of the iron powder yoke are high, but can be lowered by using another material in the yoke. If a better yoke material is used, the necessary heat transfer coefficient of the machine is in the same range as in the slotless machine and it might be possible to cool this machine with the same methods as used in the slotless machine. If this is possible the produced power with this machine type is 44 kW from the same rotor size as in the slotless machine, which produces 24 kW.

The Litz-wire implies a low copper fill factor, which is not beneficial in this application. The integrated teeth with iron powder parts have high performance when the high fill factor of homogeneous conductors is utilized. If the fill factor is low as with the Litz-wire, higher amounts of iron powder parts must be used and the construction will be bulky. The integrated teeth machine is not better, when compared with machines with other types of soft magnetic material in which the same fill factor may be reached.

### 7.3 PM Machine Compared to a Standard Induction Machine.

The performance of a permanent magnet machine with integrated teeth winding when fit into the dimensions of a 15 kW standard induction machine is evaluated. The data of the induction machine are shown in Table 7.5.

Table 7.5. Data of standard induction machine.

Rotational speed	966 rpm
Number of pole pairs	3
Output power	15 kW
Efficiency	0.87
Stator diameter	291 mm
Stator length	230 mm
Machine weight	145 kg
Air gap diameter	190.2 mm

The stator of the permanent magnet machine is to have the same outer dimensions as the induction machine, which means that the air gap diameter can be increased with a thin yoke and a small winding thickness. The machine is evaluated with the requirement that power losses are 1950 W, i.e. total power losses are approximately equal to power losses in the induction machine. It is further assumed that the mean temperature of the winding is 80 °C. The electric output power is evaluated for different pole pitches and winding thicknesses. The produced power is displayed in Figure 7.11a) and the power to magnet weight ratio is shown in Figure 7.11b).

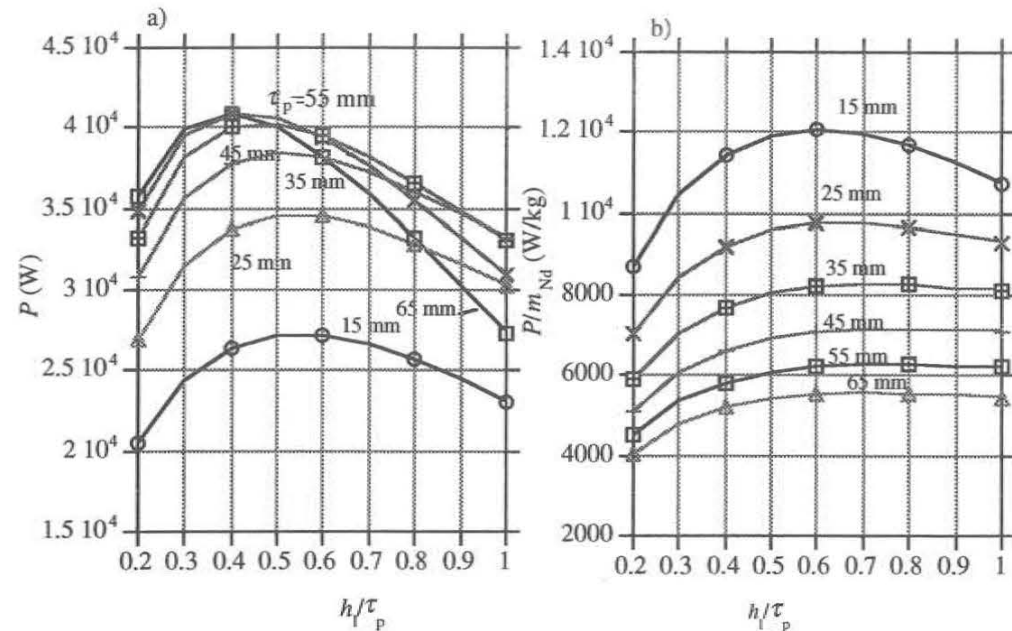


Figure 7.11. a) Produced power as a function of winding thickness, pole pitch as parameter. b) Power to magnet weight ratio.

Electrical power increases with pole pitch with a maximum power of 41 kW for pole pitches 55 and 65 mm. The best winding thickness is in the range 40-60% of the pole pitch. With increased pole pitch the magnet weight also increases, and the best output power divided by magnet weight is achieved with the smallest pole pitch.

With the smallest pole pitches, the stator frequency is rather high, which may be problematic when used in connection with electronic converters. A compromise is to choose  $\tau_p = 35$  mm which yields a produced power of 38 kW and the magnet weight is 4.5 kg, which is 70 % of the magnet weight of the machine with the highest power. Adjusting the number of pole pairs to  $p=10$ , the pole pitch is 36 mm and the air gap radius is:

$$r_g = 20 \cdot \frac{\tau_p}{2\pi} = 0.1146 \text{ m}$$

The winding thickness is

$$r_{outer} = r_g + h_{te} + h_l \Rightarrow h_l = 24.4 \text{ mm}$$

The winding thickness corresponds to 68 % of the pole pitch. In this case, we have a machine with force density  $F_A = 22 \text{ kN/m}^2$  and a stator frequency of 161 Hz. With this force density and frequency it should be possible to use a higher winding thickness, according to Section 6.3. In this application the outer diameter is, however, limited. The limited outer radius means that there is a conflict between high winding thickness and high air gap radius. A high winding thickness decreases the air gap radius and vice versa. The machine is outlined in Figure 7.12.

In this machine, the number of poles is so low that the cylindrical cross-section of the pole must be considered. The previous calculation of Figure 7.11 was made based on the assumption that the cylindrical shape of the machine did not have any effect. The flux density of the machine outlined in Figure 7.12 is calculated by means of the FEM-program and the geometry is defined in Figure 7.13. It is assumed that the slots have the same area as in the flat poles. The non-linearity of the material EF6880 is also taken into account. With an altered geometry, the flux density in the middle of the winding is lowered to 0.59 T. The flux density is lowered but the flux is increased by 10 % in relation to the flat structure. The flux density in the teeth is 1.07 T at no-load and at maximum load the flux density in the teeth is 1.3 T. The power losses of the machine, at nominal operation, are shown in Table 7.6. The adjusted machine has almost the same power losses as the induction machine. The efficiency of the machine is:

$$\eta = 94.8 \%$$

The temperature is evaluated by means of the FEM-program. The resulting temperature in the tooth and in the slot is shown in Figure 7.14. It is assumed that each slot is filled with rectangular conductors and between each conductor there is 0.2 mm of varnish with  $\lambda = 0.2 \text{ W/mK}$ . As can be

seen, the highest temperature drop is over the insulating material between the winding region and the stator yoke.

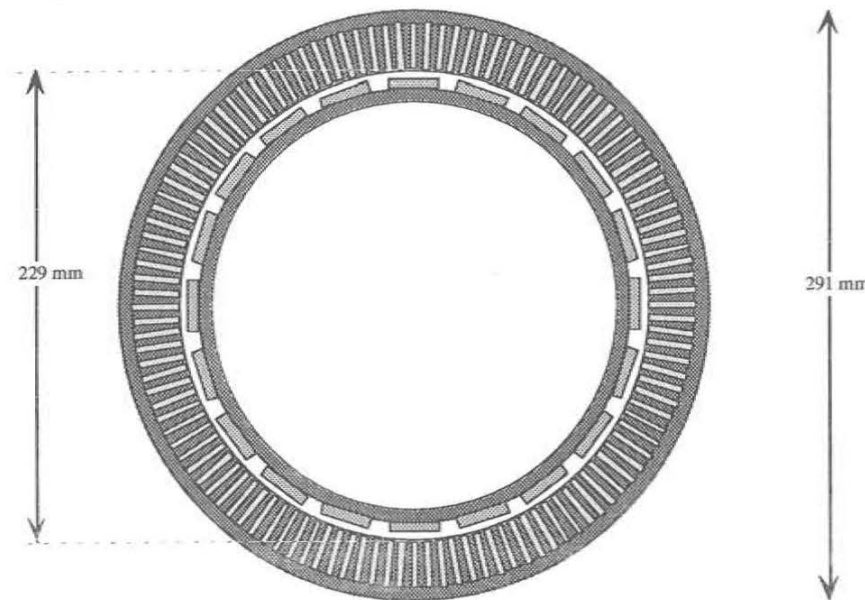


Figure 7.12. A 20-pole machine.

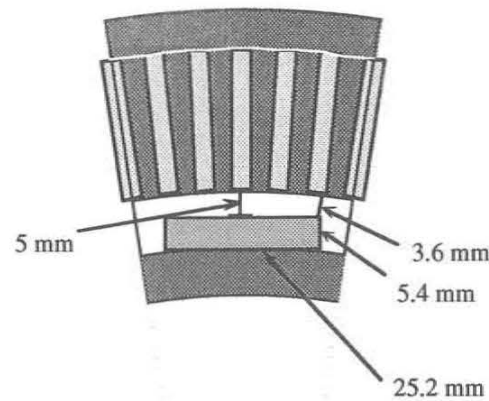


Figure 7.13. Analysed pole.

Table 7.6 Power losses of integrated teeth machine

Copper losses	895 W
Teeth losses	808 W
Yoke losses	230 W
Eddy current losses	39 W (conductor dimension $\Delta y_{cu}=1\text{mm}$ )
Total losses	1973 W

The maximum temperature is 87 °C when the stator surface is held at 60 °C. Power losses due to flux in the tangential direction are, however, calculated assuming the conductor has a thickness of 1 mm. The number of conductors in each slot is 25 and more barriers of varnish are inserted in the winding. Taking this into account, the temperature increases to 93 °C.

Power losses divided by the stator yoke area under the assumption that the temperature is held at 60 °C implies that the heat transfer coefficient of this machine is:

$$\alpha=469 \text{ W/m}^2\text{K}$$

which is rather high.

The amount of active materials in this machine is displayed in Table 7.7.

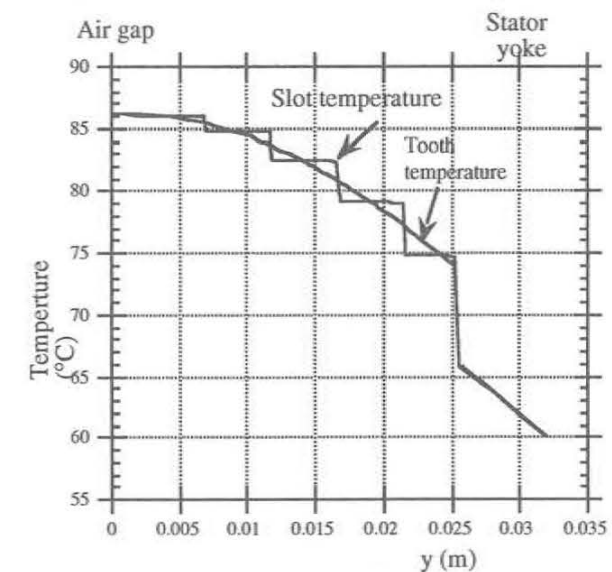


Figure 7.14 Temperature in the slot and in the tooth

Table 7.7 Weight of active material

Magnet weight	4.6 kg
Copper weight	21.3 kg
Powder material	30.0 kg
Rotor core	8.9 kg
Total weight of active material	64.8 kg

The integrated teeth machine can produce high power compared to the induction machine. There are, however, a problem that must be solved. The number of conductors in each slot is high in order to reduce the eddy current losses. The induced voltage exceeds normal line voltage if the coils should be connected in series. This can be solved with a parallel coupling of the coils but there is always a risk for circulating currents between the coils.

## 8. Conclusions

The study of the air gap winding resulted in that the magnet thickness should be in the range of 1-1.2 times the winding thickness if the pole structure can be approximated with a flat pole. It is not recommended that the winding thickness is greater than 20 % of the pole pitch. The magnet width should be in the range of 60-80 % of the pole pitch.

If the number of poles of a radial flux machine is low, then the pole structure cannot be approximated with a flat structure. The winding of such a machine can be thicker. For instance, a four-pole machine has the lowest copper losses if the winding thickness is equal to 30 % of the pole pitch. The winding can also be thicker than the magnets. In the case of a four-pole machine, a semi-radial magnet with one cylindrical surface is recommended. Interior magnets are not recommended for slotless constructions.

Two-pole machines can successfully use a cylindrical magnet inside a hollow non-magnetic shaft. At high speed the magnet is held together by the shaft and a higher winding thickness may be used in relation to a four pole machine. A two-pole machine is better in many respects when compared with a four-pole machine with the exception of the torque-to-magnet-weight ratio.

In order to verify calculations, several machines were built and tested. A four-pole permanent magnet machine with air gap winding is compared with a commercial machine with SmCo-magnets and a slotted winding. With the NdFeB-magnet material, the slotless machine performs approximately the same as the slotted machine. The outer dimensions of the slotless machine are smaller than those of the slotted machine. If the magnetic material of the slotless machine is enhanced, the performance of this machine will exceed that of the slotted machine. The torque from a given rotor dimension of the slotless machine will be higher, while at the same time power losses will be the same.

Two experimental axial flux machines were studied. The tested machines showed that the method of analysis predicts the induced voltage with relatively low error. The 12-pole axial flux machine with a power rating of 4.7 kW reached an efficiency of 92 %. Air gap winding technology can be used in small machines where the cost of permanent magnets is low compared to the cost for producing the machine.

A theoretical comparison of axial flux topology to radial flux topology showed that the torque production of the radial flux machine with the winding on the outside of the rotor is superior to that of the axial flux machine. In most cases where the radius is limited, the radial flux topology is recommended. Especially in high-speed applications, the radial flux machine is better. The advantages of the axial flux machine are its short length and the easily produced iron yoke.

The iron powder material has lower relative permeability than ordinary generator sheets. The power losses of the material are higher as long as the frequency is lower than 1-2 kHz, depending on the material. The major advantage of the material is that it can be formed almost arbitrarily. If the material is glued to the conductors, the fill factor of active material will be high.

In the thesis a so called integrated teeth winding based on iron powder pieces fixed to the winding was studied theoretically. The study shows that the relative permeability should be higher than 100, in which case winding thickness can be equal to the pole pitch. If the air gap is relatively large, two important things are gained: the armature reaction of the pole will be low and the flux density ripple on the rotor surface will be almost zero. The low armature reaction implies high force density and the low flux density ripple implies low power losses on the rotor surface, which is normally sensitive to heat. The force density of a pole with integrated teeth is approximately three times the force density of a slotless pole.

A direct-driven wind power generator of 6.4 kW with integrated teeth can have almost the same power losses and magnet weight as a 6.4 kW transversal flux machine. The machine radius is higher but the machine is shorter, and the overall material weight is higher than that of the transversal flux machine. An optimisation of the machine with assumed cost for material and power losses leads to a machine with a pole pitch of 20 mm. The optimal machine has a higher radius, shorter length, lower magnet weight and lower efficiency. This machine must be regarded as an example. If, for instance, the cost for power losses will be higher, it would be more economical to build the machine with more material and higher efficiency.

The high-speed machine with integrated teeth can produce approximately twice the power of the slotless machine. This high power rating is at the cost of higher power losses and a cooling arrangement that can handle twice as much power per unit area when compared with the slotless machine. In order to limit the temperature in the tooth, the slot is straight and the tooth width increases with radius. With the studied iron powder material, the highest power losses are the yoke losses, which could be lowered with a better material. Using the integrated teeth at extremely high speed is not recommended. Conductors with a high number of strands must be used and the fill factor of copper will be in the same range as that of ordinary machines with punched sheets. There are sheet materials that give a better performance than iron powder material, i.e. an ordinary design should be better than the studied one.

Compared with a standard induction machine, the integrated teeth machine has around 2.5 times the power capability with the same power losses and outer volume. This increased power rating is due to the permanent magnets, which do not produce any power losses in the rotor. The pole pitch of the machine can be lowered, which implies a thinner stator and an increased air gap radius. The high fill factor that is obtained by the integrated teeth winding also increases the force density of this machine type.

## References

1. Chudi, Malmquist, "DEVELOPMENT OF A SMALL GAS TURBINE-DRIVEN HIGH-SPEED PERMANENT MAGNET GENERATOR", Stockholm, Department of Electrical Machines and Power Electronics, Royal Institute of Technology, Report TRITA-EMK-89-3, 1989
2. Huang H., Debruzzi M., Riso T., "A NOVEL STATOR CONSTRUCTION FOR HIGH POWER DENSITY AND HIGH EFFICIENCY PERMANENT MAGNET BRUSHLESS DC MOTORS", SAE 931008, Int., Congress and Exposition Detroit, Michigan March 1-5, 1993, p.77-84.
3. Besant, Pullen, Etemad, Fenocchi, Baines, Ristic, "HYBRID TRACTION-A SOLUTION FOR A NOT TOO DISTANT FUTURE", Mechanical Engineering Department, Imperial College, London SW, Internal Report
4. Chillet C., Brissonneau P., Yonnet J.P., "DEVELOPMENT OF A WATER COOLED PERMANENT MAGNET SYNCHRONOUS MACHINE", SM-100 Conference, 27-29 August 1991, Zürich, p. 1094-1097
5. Pullen K.R., Etemad M.R., Fenocchi A., Eggleston L.W., "AXIAL FIELD ELECTRICAL GENERATOR", European Patent Application No. 0 353 042 A1
6. Weh H., Boules N., "FIELD ANALYSIS FOR A HIGH-POWER, HIGH-SPEED PERMANENT MAGNET SYNCHRONOUS MACHINE OF THE DISC CONSTRUCTION TYPE, Electric Machines and Electromechanics, 5, 1980, p.25-37
7. Weh H., Mayer R., "SYNCHRONOUS MACHINE WITH PERMANENT MAGNET EXCITATION AS A FLEXIBLE PROPULSION MOTOR WITH HIGH EFFICIENCY", ICEM Conference Lausanne, 18-21 September, 1984, p.607-612
8. Weh H., "HOCHAUSGENUTZTE ELEKTRISCHE MASCHINEN MIT PERMANENTERREGUNG", etzArchiv Bd. 4 (1982) H.7, p. 219-224
9. Weh H., "PERMANENT ERREGTE SYNCHRONMASCHINEN HOHER KRAFTDICHTHE NACH DEM TRANSVERSALFLUSSKONZEPT", etzArchiv Bd. 10 (1988) H.5, p.143-149
10. Weh H., "PERMANENTERREGTE SYNCHRONMASCHINE MIT TRANSVERSALFLUSSPFADEN", Patent Offenlegungsschrift DE 36 02 687 A1
11. Weh, Hoffmann, Landrath, Mosebach, Poschadel, "DIRECTLY-DRIVEN PERMANENT-MAGNET EXCITED SYNCHRONOUS GENERATOR FOR VARIABLE SPEED OPERATION", ECWEC 6-10 June 1988, Herning, Denmark, p. 566-572
12. Weh. H., "SYNCHRONOUS MACHINES WITH NEW TOPOLOGIES", Proceedings International Conference on the Evolution and Modern Aspects of Synchronous Machines, Zürich Switzerland 1991, p.C1-C9

13. Caricchi, Crescimbin, Di Napoli, Honorati, Lipo, "DEVELOPMENT OF AN IGBT INVERTER DRIVEN AXIAL-FLUX PM SYNCHRONOUS MOTOR DRIVE", Proc. of the 4th European Conference on Power Electronics and Application, Firenze 1991, p.3/482-3/487
14. Di Napoli, Caricci, Crescimbin, Noia, "DESIGN CRITERIA OF A LOW-SPEED AXIAL-FLUX PM SYNCHRONOUS MACHINE", SM-100, Zürich, 1991, p.1119-1123a.
15. Anderson W.M., Cambier C., "AN ADVANCED ELECTRIC DRIVETRAIN FOR EVs", Proc. EVS-10 Hong Kong 3-5 December 1990, p. 209-221.
16. Consterdine, Hesmondhalgh, Reece, Tipping, "AN ASSESSMENT OF THE POWER AVAILABLE FROM A PERMANENT MAGNET SYNCHRONOUS MOTOR WHICH ROTATES AT 500 000 RPM", ICEM, 15-17 September 1992, Manchester, p. 746-750.
17. Mühlegger W. "FLUX WEAKENING OF PERMANENT MAGNET EXCITED SYNCHRONOUS MACHINES WITH HIGH LEAKAGE REACTANCE", Proceedings International Conference on the Evolution and Modern Aspects of Synchronous Machines, Zürich Switzerland 1991, p. 426-429
18. Ādnanes, Sulkowski, Aga, Norum, "A FULLY DIGITAL PERMANENT MAGNET SYNCHRONOUS MOTOR DRIVE WITH FLUX WEAKENING", IEE 5th Int. Conf. on Electrical Machines and Drives (Conf. Publ. No. 341), 1991, p. 227-231.
19. Ādnanes A.K., "HIGH EFFICIENCY, HIGH PERFORMANCE PERMANENT MAGNET SYNCHRONOUS MOTOR DRIVES", Doctor thesis, Institutt for Elkraftteknik, Trondheim 1991:60
20. Schiferl R., "DESIGN CONSIDERATIONS FOR SALIENT POLE, PERMANENT MAGNET SYNCHRONOUS MOTORS IN VARIABLE SPEED DRIVE APPLICATIONS", UMI Dissertation Services Order No. 8727256, Univ. of Wisconsin-Madison 1987
21. Weh H., Wahlen H.-J., "EISSENPRESSTEILE ALS STATORMATERIAL FÜR ELECTRISCHE MASCHINEN", ETG-Fachber.8. Berlin und Offenbach: VDE VERLAG 1981
22. Campbell P., Nafisi A., "COMPOSITE IRON POWDER MATERIALS FOR THE ARMATURE OF AXIAL FIELD PERMANENT MAGNET MACHINES", IEEE Transactions on Magnetics, vol. MAG-21, No.5, September 1985
23. Jensen C.C., Profumo F., Lipo A.T., "A LOW LOSS PERMANENT MAGNET BRUSHLESS DC MOTOR UTILIZING TAPE WOUND AMORPHOUS IRON, IEEE Proceedings on Industry Application, 1990, p. 281-286.

24. Zwegbergk S., "PERMANENTMAGNETISERAD SYNKRONMASKIN UTFORMAD ENLIGT TRANSVERSALFLÖDESPRINCIPEN", Swedish patent no. 463 061,8903876-4, 1990
25. Spooner E., Williamson A.C., "PERMANENT-MAGNET GENERATORS FOR WIND POWER APPLICATIONS", ICEM' 92, Manchester 1992, p. 1048-1052
26. Parker Rollin J. "ADVANCES IN PERMANENT MAGNETISM", John Wiley & Sons Inc. New York 1990
27. Data sheets from VACUUMSCHMELZE
28. Kovacs P.K. "TRANSIENT PHENOMENA IN ELECTRICAL MACHINES", ELSEVIER Amsterdam 1984, (Vol.9)
29. Alatalo M., Svensson T. "VARIABLE SPEED DIRECT-DRIVEN PM-GENERATOR WITH A PWM CONTROLLED CURRENT SOURCE INVERTER", Conf. Proc. ECWEC, Lübeck-Travemünde, 1993,
30. Thorborg K., "POWER ELECTRONICS", Prentice Hall, Cambridge, 1988
31. Svensson T., "ON MODULATION AND CONTROL OF ELECTRONIC POWER CONVERTORS", Chalmers University of Technology, Technical Report No. 186 1988
32. Takano, Ito, Mori, Sakuta, Hirasa, "OPTIMUM VALUES FOR MAGNET AND ARMATURE WINDING THICKNESS FOR AXIAL-FIELD PERMANENT MAGNET BRUSHLESS DC MOTORS", IEEE Proceedings on Industry Applications 1990, Vol. 5, p. 157-162.
33. Brauer J.R., Larkin L.A., Overbye V.D., "FINITE ELEMENT MODELLING OF PERMANENT MAGNET DEVICES", J. Appl. Phys. 55(6) 15 March 1984, p. 2183-2185
34. Druzynski P., "KONSTRUKTIONSSTUDIE AV STORA SYNKRON-MASKINER", Chalmers University of Technology, Technical Report No. 186 1988
35. De Fang, Miraoui, Phut, Kauffmann, "INVESTIGATION OF OPTIMAL MAGNETIC CIRCUITS OF PERMANENT MAGNET SYNCHRONOUS MACHINES", Proceedings International Conference on the Evolution and Modern Aspects of Synchronous Machines, Zürich Switzerland 1991, p.1098-1103.
36. Weh H., Boules N., "MACHINE CONSTANTS AND DESIGN CONSIDERATIONS OF A HIGH-POWER, HIGH-SPEED PERMANENT MAGNET DISC TYPE SYNCHRONOUS MACHINE", Electric Machines and Electromechanics, 5, 1980, p.113-123
37. Arkadan A.A., Vyas R., Vaidya J.G., Shah M.J., "EFFECT OF TOOTHLESS STATOR DESIGN ON CORE AND STATOR CONDUCTORS EDDY CURRENT LOSSES IN PERMANENT MAGNET GENERATORS", IEE Trans. on Energy conversion Vol 7, No. 1, March 1992, p.231-237

38. Popovic B. D., "INTRODUCTORY ENGINEERING ELECTROMAGNETICS", Addison-Wesley, United States of America, 1971
39. Kylander G., "MODELLERING OCH MÄTNING AV TEMPERATUR OCH FÖRLUSTER I MINDRE ASYNKRONMASKINER", Chalmers University of Technology, Technical Report No. 147 L, 1993

### Appendix A. Torque and Force in a PM-machine

The torque in an electric machine may be described with the flux and current, [28].

$$T = \psi_d i_q - \psi_q i_d \quad (\text{A.1})$$

The flux can be expressed in terms of inductances:

$$\begin{aligned} \psi_d &= \psi_m + L_d i_d \\ \psi_q &= L_q i_q \\ T &= (\psi_m + L_d i_d) i_q - L_q i_q i_d = \psi_m i_q + (L_d - L_q) i_q i_d \end{aligned} \quad (\text{A.2})$$

When calculating the torque in an air gap winding, the torque is the force on the conductors times the radius. The force may be expressed according to [38]

$$\mathbf{F} = \int_V \mathbf{J} \times \mathbf{B} \, dV \quad (\text{A.3})$$

where  $\mathbf{J}$  is the current density,  $\mathbf{B}$  is the flux density and  $V$  is the volume that is carrying current density.

Assuming a sinusoidal distribution of current and flux density according to Figure A.1, the force is:

$$\begin{aligned} \mathbf{J} &= \hat{z} \cdot J_{1p}(y) \sin\left(\pi \frac{x}{\tau_p} - \beta\right) \\ \mathbf{B} &= \hat{y} \cdot B_{1p}(y) \sin\left(\pi \frac{x}{\tau_p}\right) \end{aligned} \quad (\text{A.4})$$

where  $\beta$  is the angle between the current density and flux density waves.

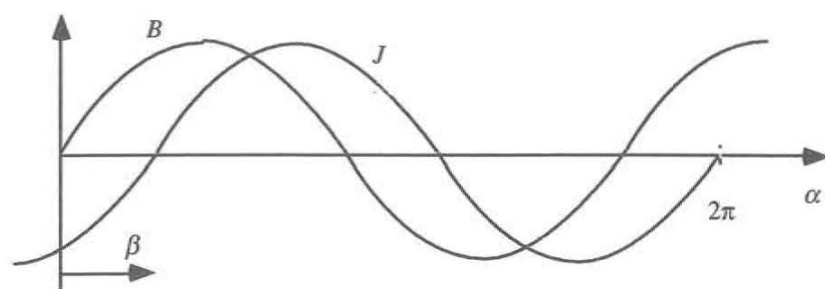


Figure A.1. Fundamental waves of flux density and current density.

If the current density is constant, the Equation (A.4) may be rewritten:

$$\begin{aligned}
 F &= -\hat{x} \int_0^{\tau_p} dx \int_0^{h_l} dy \int_0^{l_p} dz \cdot J_{1p} \sin\left(\pi \frac{x}{\tau_p}\right) \cdot B_{1p} \sin\left(\pi \frac{x}{\tau_p} - \beta\right) \\
 &= -\hat{x} l_{st} \frac{\tau_p}{2} \cos(\beta) J_{1p} \int_0^{h_l} B_{1p}(y) \cdot dy
 \end{aligned}
 \tag{A.5}$$

In many cases the flux density can be assumed constant and (A.5) may be simplified to:

$$|F| = \frac{1}{2} \tau_p l_{st} S_{1p} B_{1p} \cos(\beta) \tag{A.6}$$

where  $S_{1p} = J_{1p} h_l$ . The force density is the force divided by pole area:

$$F_A = \frac{|F|}{\tau_p l_{st}} = \frac{1}{2} S_{1p} B_{1p} \cos(\beta) \tag{A.7}$$

In a case where the stator is slotted the forces act on the teeth, i.e. equation (A.3) cannot be used directly. However, the force density of a slotted construction can be expressed in the same way if we consider that the current loading of such a pole is:

$$S_{1p} = k_w k_{cu} J_{1pcu} h_l \tag{A.8}$$

where  $J_{1pcu}$  is the current density in the conductor.

## B. Winding Factors

The winding is displayed in Figure B.1. The winding factor  $k_w$  is:

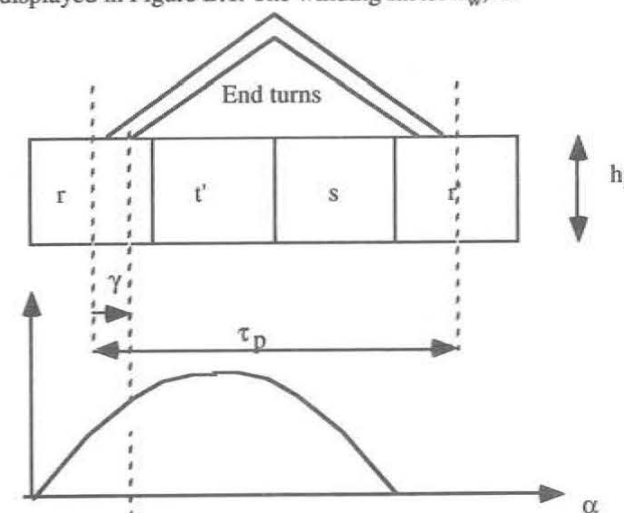


Figure B.1. Winding

$$k_w = \frac{e_{1p}}{N_p \omega \phi_{1p}} \tag{B.1}$$

where  $\phi$  is the flux that flows through a full pitch winding. The denominator in Equation (B.1) is the induced voltage in a concentrated winding. It is assumed that the conductors are very small and distributed evenly in the pole. The number of conductors per length unit is

$$\begin{aligned}
 \frac{dN}{d\alpha} &= \frac{N_p}{\pi/3} \\
 \alpha &= \frac{\pi x}{\tau_p}
 \end{aligned}
 \tag{B.2}$$

The peak induced voltage of each individual turn in the coil is:

$$e_{1p\gamma} = \frac{N_p}{\pi/3} d\gamma \cdot \omega \tau_p B_{1p} \frac{2}{\pi} \cos(\gamma) \tag{B.3}$$

The induced voltage in the whole winding is:

$$\begin{aligned}
 e_{1p} &= \int_{-\frac{\pi}{6}}^{\frac{\pi}{6}} e_{1r} d\gamma = \frac{N_p}{\pi/3} d\gamma \cdot \omega \tau_p B_{1p} \frac{2}{\pi} \int_{-\frac{\pi}{6}}^{\frac{\pi}{6}} \cos(\gamma) d\gamma = \\
 &= \frac{3N_p}{\pi} \cdot \omega \tau_p B_{1p} \frac{2}{\pi}
 \end{aligned} \tag{B.4}$$

Finally the winding factor is:

$$k_w = \frac{3}{\pi} \tag{B.5}$$

The high-speed machine in Section 4.3 has a special winding and, hence, the winding factor of this machine is evaluated. The winding is shown in Figure B.2.

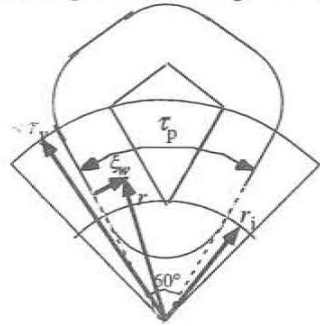


Figure B.2. Winding of the high speed machine.

The flux through the winding turn at position  $r$ ,  $\xi_w$  is:

$$d\phi_{1p} = dr \int_{\xi_w}^{\tau_r - \xi_w} B_{1p} \sin\left(\frac{\xi_w \pi}{\tau_p}\right) d\xi_w = dr \frac{2\tau_p B_{1p}}{\pi} \cos\left(\frac{\xi_w \pi}{\tau_p}\right) \tag{B.6}$$

The number of turns in a small section  $d\xi_w$  is:

$$\Delta N = \frac{N_p}{\tau_{pi}} d\xi_w \tag{B.7}$$

where  $\tau_{pi}$  is the pole pitch at the inner radius. The flux linkage per pole is evaluated. We must integrate the flux density over the whole pole:

$$\begin{aligned}
 \psi_p &= \Delta N \int_{r_i}^{r_y} \int_0^{\tau_{pi}/2} d\phi_{1p} = \\
 &= \frac{N_p}{\tau_{pi}} \frac{2}{\pi} B_{1p} \int_{r_i}^{r_y} dr \frac{\tau_p^2}{\pi} \sin\left(\frac{\tau_{pi} \pi}{2\tau_p}\right)
 \end{aligned} \tag{B.8}$$

The pole pitch is:

$$\tau_p = \frac{\pi r}{3} \tag{B.9}$$

The linked flux is:

$$\begin{aligned}
 \psi_{1p} &= \frac{N_p}{\tau_{pi}} \frac{2}{\pi} B_{1p} \int_{r_i}^{r_y} \frac{\pi r^2}{9} \sin\left(\frac{r_i \pi}{2r}\right) dr = \\
 &= \frac{N_p}{\tau_{pi}} \frac{2}{9} B_{1p} \int_{r_i}^{r_y} r^2 \sin\left(\frac{r_i \pi}{2r}\right) dr
 \end{aligned} \tag{B.10}$$

Dividing Equation (B.10) with the expression of the induced voltage of a concentrated winding, Equation (B.1), yields the winding factor:

$$k_w = \frac{2 \frac{1}{\pi r_i} \int_{r_i}^{r_y} r^2 \sin\left(\frac{r_i \pi}{2r}\right) dr}{(r_y^2 - r_i^2)} \tag{B.11}$$

### C. Representation of Magnets in the FEM-program

The FEM-program used cannot represent material with a remanent flux density, i.e. material data cannot be specified in the second quadrant of the BH-curve. However, current can be applied to materials and this is used to describe the permanent magnetic material.

The method used is described in [33]. The method is based on the fact that at the edges of the magnets we have a difference in the coercive force vector. In order to describe this difference, current density is applied at the edges of the magnet:

$$\mathbf{J}_{pm} = \nabla \times \mathbf{H}_c \tag{C.1}$$

In a simple case where the magnetization direction is in the y-direction the current density is:

$$J_{pm} = \Delta H_c / \Delta x \quad (C.2)$$

Magnetization is more difficult in a case where the magnet is curved. The diametrically magnetized magnet is used to exemplify this. A current layer according to figure C.1. is used and the current density is constant over the surface.

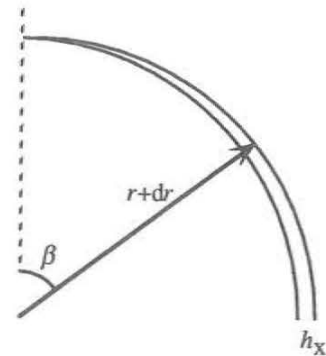


Figure C.1. Diametrically magnetized magnet half pole.

The thickness of the current carrying layer in the  $x$ -direction is constant but the thickness in the radial direction varies sinusoidally with the angle  $\beta$ :

$$dr = h_x \sin(\beta) \quad (C.3)$$

The current density is:

$$J = H_c / h_x \quad (C.4)$$

The total current is:

$$I = \int_S J dS = H_c / h_x \int_0^{\pi/2} r \cdot d\beta \cdot dr = H_c r \int_0^{\pi/2} \sin(\beta) d\beta = H_c r \quad (C.5)$$

## Appendix D. Measuring Instruments

This appendix reveals the main data of the measuring devices used during the tests.

### Flux Density Meter

For measuring flux density a Bell incremental Gauss meter is used.

MODEL 240	
Probe linearity error	+1%
Instrument error	+1%

For various reasons the measuring of flux density has been tricky and the probable error in the measurements is estimated to  $\pm 5\%$ .

### Oscilloscope

For transient measuring of currents and voltages a Philips PM97 scopemeter is used. An optical RS232 link is used to transmit the measured data to a Macintosh computer system.

Vertical resolution	8 bits
DC accuracy	2 %
Bandwidth	50 MHz
Nonlinearity	<2 %
Horizontal resolution	512 points
Accuracy	+0.1 % +1 LSB

**High Frequency Power Meter**

Measuring power has been performed with a power meter 'Erich Marek', which measures signals with frequency components up to 20 kHz

MODEL Integra 6

Error 1.5 % 0-20 kHz

Error 0.5 % 0-10 kHz

**Inductance Meter**

Inductances are measured using an inductance bridge, Philips PM6303 RCL meter. The instrument measures impedances at 1000 Hz.

The inductance is also evaluated using the grid frequency, 50 Hz, and measuring the current and voltage.